Novel Innovative Therapeutic Approaches for the Treatment of Osteosarcoma

---

Dissertation

zur

Erlangung der naturwissenschaftlichen Doktorwürde

(Dr. sc. nat.)

vorgelegt der

Mathematisch-naturwissenschaftlichen Fakultät

der

Universität Zürich

von

Daniela Meier

von

Würenlingen, AG

Promotionskomitee

Prof. Dr. Beat Schäfer (Vorsitz)

Prof. Dr. Dr. Bruno Fuchs

Prof. Dr. Dario Neri

Prof. Dr. Caroline Maake

Zürich, 2016

To my family

and to my love

Contents

1 Summary

Osteosarcoma (OS) is the most common malignant bone tumor in children and adolescents. Although the survival for OS patients increased remarkably over the past decades due to novel surgical techniques and multi-agent neoadjuvant chemotherapy, patients with metastatic disease, however, remain to have a poor 5-year survival rate of approximately 30 %. Unfortunately, the aggressive chemotherapeutic treatment of OS is associated with severe side effects and chemoresistance. Consequently, there is an urgent need for a better understanding of the mechanisms of OS progression for the development of novel more effective therapies that improve the survival and the quality of life of OS patients. The bone microenvironment was shown to have a crucial role in OS development and metastasis. Therefore, in this thesis, we studied, on one hand, the potential benefit of the inhibition of a key regulator of bone remodeling on OS progression and, on the other hand, a low toxic therapeutic approach using photodynamic therapy (PDT).

Bone affecting tumors are supposed to elicit a `vicious cycle` of bone remodeling by stimulating the bone microenvironment to provide a fertile soil for tumor growth. Bone remodeling is normally strictly regulated, but in patients with cancer affecting the bone, these processes get out of balance and promote tumor progression. For tumors metastasizing to the bone, such as multiple myeloma, breast or prostate cancer, activin A has been identified as an important regulator of this vicious cycle. Activin A inhibition exhibited therapeutic potential by suppressing tumor-associated bone remodeling and disease progression in those cancers, however, the role of activin A in OS and its bone microenvironment remains to be unraveled. Therefore, the first aim of this thesis was to investigate the therapeutic potential of activin A inhibition in OS by using two different inhibitors (FST_{315}ΔHBS-hFC and ActRIIA-mFC). Effects of activin A and its inhibitors in combination with the gold-standard inhibitor of pathological bone remodeling, zoledronic acid, on OS progression, bone remodeling and metastatic burden were investigated here. The experimental systems included *in vitro* OS cell lines and osteoclasts and *in vivo* a highly metastatic intratibial OS mouse model. Although both activin A inhibitors showed no inhibitory effects on OS cell viability and migration *in vitro*, they effectively inhibited intratibial tumor growth and associated bone remodeling *in vivo*, via the uncoupling of osteoclastogenesis and the effects of key factors involved in osteoblast activity. In addition, the combination of activin A inhibitors with zoledronic acid further reduced OS progression and suggests a promising combinational therapeutic approach.

In the second aim we evaluated the OS suppressive efficacy of PDT *in vitro* and *in vivo* in intratibial metastasizing OS mouse models in immune-deficient and immune-competent mice. PDT is a locally applied, low-toxic therapy, reported to be effective in a variety of tumor types. One of the most potent photosensitizers, 10,15,20-tetrakis (meta-hydroxyphenyl) chlorine (mTHPC, Foscan), was used for this study, in addition with two novel mTHPC formulation; a liposomal formulation (Foslip) and lipid nanoparticles (LNP). *In vitro* results showed an efficient cellular uptake and effective photo-toxicity of all formulations in different OS cell lines. In view of these promising results, mTHPC uptake and PDT efficacy was determined in two highly metastatic orthotopic OS mouse models, using both immunocompromised and immunocompetent mice. *In vivo* measurements revealed a significantly higher uptake of the different mTHPC formulations by tumor than by healthy tissue, with a significant higher uptake of Foslip and of LNP than of Foscan. Upon these promising results, the treatment efficacy was determined for Foscan, Foslip and LNP *in vivo*. Foslip-based PDT was most effective in inhibiting OS tumor growth in immunocompromised mice, whereas the LNP-based PDT, unexpectedly, showed no treatment effect. In the immunocompetent OS mouse model, a more pronounced tumor- and lung metastasis-suppressive effect than in immunocompromised mice was observed in response to PDT with both Foscan and Foslip.

In conclusion, a more detailed understanding of the role of the bone microenvironment on OS progression, revealing novel treatment modalities with bone remodeling inhibitors such as activin A inhibitors and bisphosphonates, and the application of low toxicity PDT turned out to be promising strategies for the development of novel effective OS treatment modalities, with the potential to improve the quality of life of OS patients in the future.

2 Zusammenfassung

Osteosarkome (OS) sind aggressive Knochentumore, welche vor allem bei Kindern und Jugendlichen auftreten. Die stetige Verbesserung der chirurgischen Techniken zur Entfernung des Primärtumors und die Optimierung neoadjuvanter Chemotherapie hat die 5-Jahre Überlebensrate von Patienten mit einem lokal begrenzten Tumor stark erhöht. Im Unterschied dazu haben sich die Überlebenschancen von OS Patienten mit Metastasen in den letzten Jahrzehnten nicht verbessert und die 5-Jahre Überlebensrate liegt nach wie vor bei ca. 30 %. Zudem werden bei der Osteosarkomtherapie leider oft auch schwerwiegende Nebenwirkungen und Therapieresistenzen beobachtet. Oberstes Ziel der OS Forschung ist es deshalb, neue Therapien zu entwickeln, die auch die Lebensqualität und die Lebenserwartung von Patienten mit metastasierendem OS wesentlich verbessern. Voraussetzung dafür ist ein wesentlich verbessertes Verständnis der molekularen, pathophysiologischen Mechanismen, die bei der Pathogenese und Metastasierung des OS von zentraler Bedeutung sind. Entsprechend wurde der Interaktion der Mikroumgebung mit dem Primärtumor im Knochen in letzter Zeit immer mehr Beachtung geschenkt. Zudem werden intensiv neue, möglichst tumorselektive Therapieansätze gesucht und entwickelt, um toxische Nebenwirkungen in gesundem Gewebe zu verhindern. In dieser Dissertation wurde daher die Wirkung der Hemmung eines wichtigen Faktors in der Regulation des tumorassoziierten Knochenumbaus auf das Osteosarcomwachstum in einem experimentellen intratibialen OS Mausmodell untersucht. In vergleichbaren Modellen in immundefekten und immunkompetenten Mäusen wurden zudem die Tumor- und Metastasierung-hemmenden Effekte einer lokalen, tumorselektiven Behandlung von intratibialen OS mittels photodynamischer Therapie (PDT) untersucht.

In den letzten Jahren wurde nachgewiesen, dass in Krebsarten, die den Knochen befallen, die Interaktionen zwischen dem Tumor und der pathologisch umgebauten Knochenumgebung im sogenannten „Vicious Cycle“, wesentlich zur Entwicklung der Tumore beitragen. Der in gesundem Knochen strikt regulierte Knochenumbau gerät in Knochentumorpatienten in ein Ungleichgewicht zu Gunsten eines erhöhten Tumorwachstums. Bei Tumoren, die in den Knochen metastasieren, wie z.B. das multiple Myelom, oder bei Brust- und Prostatatumoren, wurde Activin A als zentraler Effektor im „Vicious Cycle“ identifiziert. Präklinische Studien haben gezeigt, dass die gezielte Hemmung von Activin A den tumorinduzierten Knochenabbau und das Fortschreiten der Tumorerkrankung

unterdrückt. Erstaunlicherweise sind die genauen Funktionen und das therapeutische Potential von Activin A beim OS noch weitgehend nicht untersucht. Daher war es das erste Ziel dieser Arbeit, das tumorhemmende Potential verschiedener Activin A-Inhibitoren (FST_{315}ΔHBS-hFC und ActRIIA-mFC) zu untersuchen. Zusätzlich wurde die Wirkung einer Kombination von Activin A-Inhibitoren mit dem Bisphosphonat Zoledronsäure auf das Tumorwachstum und die Tumormetastasierung analysiert. Die Wirksamkeit der Activin A Inhibitoren und der Zoledronsäure wurde sowohl *in vitro* in OS- und Knochenzellen, als auch *in vivo* in einem intratibialen, Maus Osteosarkommodell erforscht. Obwohl *in vitro* kein direkter Effekt auf das Überleben und die Migrationsrate der Osteosarkomzellen beobachtet wurde, konnte *in vivo* das Wachstum des intratibialen Tumors und der damit assoziierte Knochenumbau effizient gehemmt werden. Zudem war die Kombination von Activin A-Inhibitoren und Zoledronsäure am wirksamsten.

Im zweiten Projekt wurden die Tumor- und Metastasen-hemmende Wirkung der PDT *in vitro* und in intratibialen OS Modellen in immundefekten und immunkompetenten Mäusen untersucht. PDT erwies sich als effiziente Therapie in verschiedenen Arten von Tumoren, und sie hat den Vorteil einer lokalen Anwendung mit geringen, systemischen Nebeneffekten. Einer der aktuell potentesten Photosensitizer, 0,15,20-tetrakis (meta-hydroxyphenyl) chlorine (mTHPC, Foscan) wurde für diese Studie verwendet. Zusätzlich wurden zwei Träger für mTHPC getestet, eine liposomale Formulierung (Foslip) und lipid-Nanopartikel (LNP). Die *in vitro*-Resultate zeigten eine hohe Aufnahme und Phototoxizität aller mTHPC-Formulierungen in verschiedenen Osteosarkomzellen. Basierend auf diesen vielversprechenden Resultaten wurde die PDT-Wirksamkeit aller mTHPC-Formulierungen in den zwei stark metastasierenden, intratibialen OS Modellen in immundefekten und immunkompetenten Mäusen untersucht. Foscan und Foslip-basierende PDT zeigte eine signifikante Hemmung des Wachstums der intratibialen Primärtumoren, wobei unerwartet, die LNP-basierende PDT keinen therapeutischen Effekt zeigte. In den immunokompetenten Mäusen war der Tumor-hemmende Effekt noch ausgeprägter als in immundefektien Mäusen und zudem wurde ebenfalls die Bildung von Lungenmetastasen gehemmt.

Die Ergebnisse der in dieser Dissertation gemachten Untersuchungen können wie folgt zusammengefasst werden: die Hemmung der biologischen Effekte von ActivinA in der Osteosarkommikroumgebung mittels Activin A Inhibitoren und Bisphosphonaten sowie die Primärtumor-selektive lokale PDT mit zusätzlich Metastasen-hemmender Wirkung in immunkompetenten Mäusen erwiesen sich in den hier verwendeten klinisch relevanten OS Modellen als vielversprechende Strategien für eine wirksame Therapie des metastasierenden

OS mit geringen Nebenwirkungen und, im Falle der PDT, mit der Möglichkeit der repetitiven Anwendung.

3 Abbreviations

ACE-011	activin receptor type II and human IgG fusion protein
ActRIIA	activin receptor type II
ALP	alkaline phosphatase23
APR	acute phase response
BMP	bone morphogenetic protein
BP	bisphosphonate
CatK	cathepsin K
CXCR4	C-X-C chemokine receptor type 4
DAMP	damage associated molecular patterns
Fc	fragment crystallizable region
FST	follistatin
GAPDH	glyceraldehyde 3-phosphate dehydrogenase
ΔHBS	heparin binding site deletion
IgG	immunoglobulin G
IL	interleukin
I-Smad	inhibitory Smad
i.t.	intratibial
i.v.	intravenous
LED	light emitting diodes
LNP	lipid nanoparticles
MAPK	,itogen-activated protein kinases
MH	mad homology
m-CSF	macrophage colony-stimulating factor
MDM2	mouse double minute 2 homolog (E2 ubiquitin-protein ligase)
MM	multiple myeloma
MMP	matrix metalloproteinase
mTHPC	m-tetrahydroxyphenylchlorin

NES	nuclear export signals
NIR	near infrared
OS	osteosarcoma
PBMC	peripheral blood mononuclear cells
PBS	phosphate-buffered saline
PDT	photodynamic therapy
PS	photosensitizer
PTHrP	parathyroid hormone-related protein
RANKL	receptor activator nuclear factor κB ligand
ROS	reactive oxygen species
s.c.	subcutaneously
SCID	severe combined immunodeficiency
Smad	small mothers against decapentaplegic
Smurf	smad-ubiquitination-regulatory factor
TCI	tumor cell injection
TGF	transforming growth factor
TRAP	tartrate resistant acid phosphatase
WHO	World Health Organisation
X-GAL	5-bromo-4-chloro-indolyl-β-D-galactopyranoside

4 Introduction

4.1 Osteosarcoma

4.1.1 Epidemiology and clinical characteristics

Osteosarcoma (OS) is a high grade primary bone neoplasm and one of the deadliest cancers in children and young adolescents (Ward, DeSantis et al. 2014). OS accounts for 35 % of all primary bone cancers, followed by chondrosarcoma (25%), Ewing Sarcoma (16%), Chordoma (8%) and undifferentiated pleomorphic sarcoma (5%).

The overall incidence is 8 - 11 patients per 1`000`000 adolescents between 15-19 years of age, and an overall incidence of 3 per 1`000`000 people per year. OS has a bimodal age distribution with a first peak in the second decade of life and a smaller peak between 60 and 80 years of age (Hogendoorn, Athanasou et al. 2010; Ritter and Bielack 2010). Males are more frequently affected than females with a ratio of 1.43 to 1, with, however, earlier peaks in female than in male subjects (Geller and Gorlick 2010).

Typical symptoms reported for OS patients are local pain and swelling in the affected region, lasting often for several months before diagnosis (Marina, Gebhardt et al. 2004). OS is commonly located in close proximity to the metaphyseal growth plates of long bones, most frequently in the femur (43 %), followed by the tibia (19 %), the humerus (10-11 %) and it rarely occurs in the axial skeleton such as the skull, and pelvis (Longhi, Errani et al. 2006; Ottaviani and Jaffe 2009).

Approximately 15-20 % of the OS patients have detectable metastases at the time of diagnosis, and 80 % present with microscopic metastases. The most common site for metastatic spread is the lungs followed by other bones.

Characteristic bone lesions detected by radiography include osteoblastic, osteolytic and mixed lesions. Typical characteristics for OS are the so called `sunburst` pattern, showing radial ossification in the soft tissue around the bone or the `Codman triangle`, which shows periosteal new bone formation and lifting of the cortex and mostly the mixed osteolytic-osteoblastic lesions are observed (Figure 1) (Miller 2008).

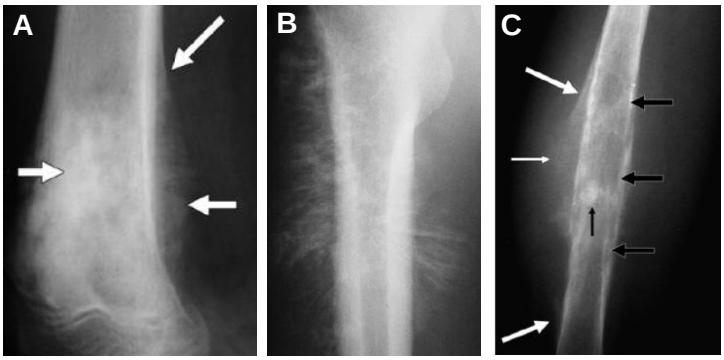

Figure 1 Radio graphical appearance of osteosarcoma. (A) Codman triangle showing the elevated periosteum (large white arrows). (B) Proximal femur, with radial (sunburst) with periosteal reaction. (C) Mixed osteoblastic (small black arrow) /osteolytic (long black arrows) osteosarcoma with a Codman triangle (large white arrows)adapted from (Miller 2008).

4.1.2 Types of Osteosarcoma

Form the cellular aspect, OS is thought to be of mesenchymal origin, but proof for pre-osteoblasts as precursor cells is still missing (Klein and Siegal 2006). OS has a wide variety of histological appearances and, according to the world health organization (WHO), OS is classified into different subgroups. Conventional OS is the most common histological subtype; The tumor cells have a spindle or polyhedral shape and produce extracellular matrix (osseous, cartilaginous or fibrous), and according to the cellular predominance, three main subtypes are distinguished: osteoblastic, chondroblastic, and fibroblastic, which radiographically show extremely variable appearances with lytic, osteoblastic or mixed lesions. Telangiectatic OS is characterized by lytic destruction with large blood filled empty spaces and has similar histological features as an aneurysmal bone cyst. It is a rare subtype, accounting for less than 4% of all OS, with prognostic factors similar to conventional OS. Small cell OS only represents around 1.5 % of all OS, characterized by small cells with a round, hyperchromatic nuclei with low nuclear pleomorphism. Additional rare OS subtypes are low grade central (< 1%), parosteal and periosteal surface (~ 2 - 4 %) OS. Last, secondary OS arises in bones with preexistent aberrations such as radiation or Paget disease. High grade OS predominate, with a better 5-year survival rate in patients with extremity (68.2 %) compared to axial OS (27.3 %) (Klein and Siegal 2006; Fletcher C.D.M. Lyon 2002).

4.1.2.1 Staging

Different staging for sarcomas and carcinomas, first described by Enneking et al., is nowadays widely accepted (Wolf and Enneking 1996; Fletcher C.D.M. Lyon 2002). Staging depends on the histological grading, the primary tumor size and distant metastasis. However,

because patients with metastasis fare so much worse than those without metastasis, it is not that widely used or useful.

4.1.3 Metastasis

Metastases remain the main cause of death in OS patients. A hallmark of malignant tumors, such as OS, is their ability to metastasize to other organs via a multi-step process. This process includes local invasion of the surrounding tissue, intravasation, survival in the circulation, transport to the target organ, extravasation into parenchyma, and colonization of the target organ (Chambers, Groom et al. 2002). Preceding this process is the preparation of the tumors to metastasize, including angiogenesis for sufficient nutrient supply and access to a transportation system for metastasizing tumor cells. Equally important is the preparation of a `pre-metastatic` niche in the target organ, which also defines the sites for metastatic spread, e.g. the lungs and other bones in OS. Stephen Paget published this theory in 1889 and called it the `seed and soil` hypothesis, a proposal that metastatic spread depends on a cross-talk between the cancer cells (seeds) and the specific organ microenvironment (soil) (Paget 1989). A few years later, James Ewing added also the anatomical architecture of the vascular system as an important determinant of organ-specific metastasis, explaining the metastatic spread into the lungs but not the high propensity for bone metastases (Ewing 1928). Although not yet well understood, also organ-specific metastatic traits in primary tumors play an important role in priming tumor cells to metastasize into specific organs. A study performed by Zhang, *et. al*., reported that the mesenchymal signals CXCL12 and IGF, within the primary tumor stroma, prime breast cancer cells for the bone metastatic microenvironment (Zhang, Jin et al. 2013).

Additionally, intrinsic features of cancer cells play an important role in the process of metastases formation. Several classes of genes involved in metastases initiation, progressions and virulence have been identified. Genes involved in the initiation of metastases regulate key processes such as the epithelial-mesenchymal transition (EMT), degradation of extracellular matrix, angiogenesis, intravasation (Nguyen, Bos et al. 2009; Valastyan and Weinberg 2011). For the progression of the metastasis, genes that promote survival during circulation, extravasation of the circulating tumor cell and proliferation in the new microenvironment, such as MMPs, angiopoietin-like 4 or COX2, are essential (Minn, Gupta et al. 2005). Virulence genes on the other hand, do not participate in the growth of the primary tumor, but are essential only at the metastatic site, such as interleukin 11 (IL11) and parathyroid hormone-related protein (PTHRP) facilitated bone metastasis (Mundy 2002).

Furthermore, cells within the tumor microenvironment, such as osteoclasts and macrophages, induce progression and metastasis development in OS. Cells in the tumor stroma can release growth factors and induce inflammation, angiogenesis and tissue remodeling, promoting metastatic spread (Endo-Munoz, Evdokiou et al. 2012). Receptor activator nuclear factor κB ligand (RANKL), an important regulatory factor in osteoclastogenesis, is expressed on a variety of cells in the bone microenvironment (osteoblasts, osteocytes, bone marrow stromal cells) and high RANKL expression in bone metastases was shown to correlate with poor survival of OS patients (Lee, Jung et al. 2011; Nakashima and Takayanagi 2011). The expression of RANKL is also associated with increased cell mobility and anchorage-independent growth, important processes in metastatic spread (Beristain, Narala et al. 2012). Denosumab, a human monoclonal RANKL antibody, is currently under investigation for the treatment of metastatic OS (Cathomas, Rothermundt et al. 2015). A vicious cycle between the primary tumor and the bone microenvironment is thought to drive OS progression, and is described in more detail in the next chapter (Lamoureux, Richard et al. 2007; Endo-Munoz, Evdokiou et al. 2012).

All in all, the metastatic process in OS is complex and dependent on intrinsic characteristics of the tumor cells and on a complex interplay between the tumor, its microenvironment and the target tissue.

4.1.4 Etiology

Despite progress in OS treatment regimens, the etiology of OS remains largely obscure. Proven risk factors for the development of OS are the exposure to radiation, with a risk of 0.03 - 0.8 % in an irradiated bone, but only account for 2 % of all OS (Fletcher C.D.M. Lyon 2002). A number of inherited genetic predispositions are associated with a high risk for OS. These include: heritable germline mutations in the retinoblastoma gene (RB1), a tumor suppressor gene and negative regulator of cell cycle progression, lead to an up to 1000 times higher risk for OS than that observed in the normal population; the Li- Fraumeni syndrome, a rare autosomal dominant disorder caused by germline mutations of the tumor suppressor and guardian of the genome, TP53; autosomal recessive syndromes caused by a mutation in the RecQ DNA helicase family, which are essential for DNA repair and genomic stability. The Rothmund-Thompson syndrome is caused by a germline-line mutation in the helicase RecQ protein –like 4 (RECQL4) and up to 32 % of affected persons develop OS. Werner's syndrome is caused by a mutation in the WRN helicase RECQL2 causing an abnormal telomere length and chromosomal alterations (~10 % of the affected persons develop OS).

Blooms syndrome is caused by mutation in the BLM DNA helicase causing striking genomic instability and OS in 2 % of the affected individuals (Fuchs and Pritchard 2002; Martin, Squire et al. 2012; Kansara, Teng et al. 2014). Also Paget`s disease, a bone disease characterized by disordered bone metabolism, causing an excessive bone remodeling; with abnormal osteoclast function can cause OS formation. The incidence is less than 1 % and occurs usually in individuals older than 50 years (Hansen, Seton et al. 2006).

Chromosomal abnormalities and genomic instability are common in OS. Chromothripsis, a massive genomic rearrangement is shown in approximately a third of primary OS tumors, causing a considerable diversity of genetic alterations. Chromothripsis is particularly high in bone cancer (approx. 25%) compared to other cancers (2-3 %) (Stephens, Greenman et al. 2011).

Somatic mutations of the RB1 gene and TP53 are detected in 35 % and 80 %, respectively, of examined OS tumors and also overexpression of oncogenes, such as the p53 tumor suppressor negative regulator MDM2 or cyclin dependent kinase 4 (CDK4) are observed. In addition, alterations in the glutamate signaling, regulating normal bone physiology, and changes in the glutamate receptor metabotropic 4 (GRM4) expression have been attributed to OS tumorigenesis (Kansara, Teng et al. 2014).

4.1.5 Prognosis and Treatment

Complete surgical resection of the primary tumor is important, and advanced novel surgical techniques allows limb-salvage procedures in many patients (Bacci, Ferrari et al. 2002). Despite the importance of surgery, before the introduction of chemotherapy, the 6-year survival rate was 11 % compared to 61% after the introduction of adjuvant chemotherapy (Link, Goorin et al. 1991). Current state-of-the art OS therapy includes therefore a multi-agent chemotherapeutic approach, including neoadjuvant (before surgery), surgery and adjuvant chemotherapy. This treatment yields cure rates of approx. 90 % for patients who are good-responders to the neoadjuvant chemotherapy (> 90 % of necrosis), but patients with a poor histological response have a cure rate of 50 - 60 % (Isakoff, Bielack et al. 2015).

Although rare, patients with pathological fractures at diagnosis show a lower 5- year survival (34%) than patients with no fractures (58%), thus fractures are apparently a sign for more aggressive tumors (Bramer, Abudu et al. 2007).

Likewise the anatomical location is an important factor for the prognosis. Tumors in the distal femur, proximal tibia, humerus and the radius have a better prognosis. A worse prognosis have patients with OS in the pelvis, with 27 - 47 % 5 year-survival rate and those

with tumors in the spine with a medium survival rate of only 1- 2 years (Bielack, Kempf-Bielack et al. 2002; Clark, Dass et al. 2008). The most reliable prognostic finding is the detection of metastatic spread at time of diagnosis, reducing long-term outcome to less than 20 %. Lung metastases are the most frequent metastases followed by other bone metastases and skip metastases. Patients with bone metastases have a worse survival than those with lung metastases. Skip metastases are rare, but lead to a patients overall survival of only 27.2 months from diagnosis (Clark, Dass et al. 2008).

The most effective chemotherapeutic drugs used so far include doxorubicin, cisplatin and high-dose methotrexate (MAP). Treatment usually starts by the administration of the multi-agent chemotherapeutics for 10 weeks, followed by surgery and another 29 weeks of adjuvant chemotherapy. To improve current therapy, especially for patients with a poor histological response after neoadjuvant chemotherapy (<90% necrosis), effects of ifosfamide and etoposide were studied in the very recent international randomized EUROAMOS-1 study. Patients with a respectable tumor received the MAP regimen as a neo-adjuvant therapy. Poor responders received in addition post-operatively ifosfamide and etoposide, whereas good responders received MAP with or without interferon α. The molecular mechanism behind the different treatment regimens are shown in **Table 1**. Because OS is a rare disease, international collaboration is crucial and current published data from the EURAMOS study show the feasibility of such a collaboration and reports on the patient data, side effects and its successful execution. Unfortunately, the results did not support adding interferon to the standard treatment for OS patients, but treatment benefits for the addition of ifosfamide and etoposide for poor responders are still awaited (Whelan, Bielack et al. 2015).

4.1.5.1 Treatment induced Side Effects and Chemoresistance

Although standard OS therapy considerably increased patient survival, severe side effects are common and affect the quality of life over years. In addition to mild reported side effects such as skin rashes, emesis, alopecia, gastrointestinal problems, also severe toxicities with permanent damage are regularly reported and range from inflammation, neutropenia, cardiotoxicity, nephrotoxicity, neurotoxicity, infertility and even death (Table 1) (Janeway and Grier 2010; Whelan, Bielack et al. 2015).

Drug	Mechanism of action	Side effect
Doxorubicin	DNA and RNA intercalating agents.	Emesis, alopecia, myelosuppression, cardiotoxicity, infection of the bowel, chemotherapy-induced acral erythema

Cisplatin	Binding to DNA, causing crosslinking of DNA strands	Nephrotoxicity, ototoxicity, emesis, myelosuppression, hemolytic anemia, infertility
Methotrexate	Antimetabolite, inhibits synthesis of purine and thymidine by inhibiting the metabolism of folic acid via dihydrofolate reductase	Neurotoxicity, nephrotoxicity, myelosuppression, mucositis
Ifosfamide	Binding to DNA, causing crosslinking of DNA strands	Emesis, hemorrhagic cystitis, nephrotoxicity, neurotoxicity
Etoposide	Topoisomerase inhibitor	Hypotension, emesis, skin reactions, neurotoxicity, myelosuppression, acute myeloid leukemia

Table 1 Chemotherapeutic drugs used in osteosarcoma treatment, their mechanism of action and side effects.

OS patients are often under 20 years of age and effects on the development and long term adverse outcome of OS patients have to be carefully considered. Patients who were treated with multi-agent chemotherapy are nowadays in middle age, making it possible to assess the treatment-induced long term side effects. Subsequent primary neoplasms are reported to cause 34.7 % of all deaths in OS patients (**Figure 2**), showing a significant difference to the expected number of deaths in the general population at the age of 72 (Fidler, Frobisher et al. 2015). Reported second primary neoplasms were most frequently breast cancer, gliomas, leukemia, bladder and digestive cancer, leiomyosarcoma, fibrosarcoma. OS survivors are also reported to have more severe limitations in health status, especially physical function and pain than healthy persons (Aung, Gorlick et al. 2002; Klein, Michaelis et al. 2003; Fidler, Frobisher et al. 2015).

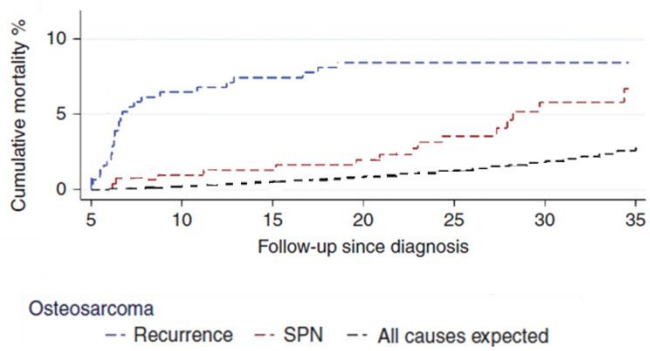

Figure 2: Recurrence and second primary neoplasms in osteosarcoma survivors (adapted from Fidler, Frobisher et al. 2015).

Chemoresistance is also one of the major reasons of failure in OS therapy. Up to 35 - 45% of patients become nonresponsive to chemotherapeutic agents during treatment (Luetke, Meyers et al. 2014). The molecular mechanism inducing chemoresistance are not yet completely known. Mechanisms that play a role include decreased intracellular drug

accumulation (e.g. upregulation of efflux pump P-glycoprotein), drug inactivation (e.g. overexpression of glutathione S-transferase P1), enhanced DNA repair (e.g. overexpression of apurinic endonuclease 1, excision repair, cross-complementing proteins), changes in cell cycle related gene expression (e.g. downregulation of Rb and p53, overexpression of CDK4), inhibition of apoptosis (e.g. upregulation of anti-apoptotic proteins e.g. Bcl-2, downregulation of pro-apoptotic protein e.g. Bax, Bak, Bad), and abnormal regulation of signaling transduction pathways (e.g. activation of MAPK, PI3K) (He, Ni et al. 2014).

Despite the aggressive treatment regimens, survival rates of OS patients have plateaued or remain still very low in patients with recurrent and metastatic disease. Numerous side effects and chemoresistance to current drugs ask for novel more tumor specific and personalized therapies.

4.2 The Vicious cycle of Bone Remodeling in Osteosarcoma and the Role of Activin

Bone is a dynamic tissue, which is constantly remodeled and tightly controlled to maintain its structural integrity. The bone microenvironment plays an important role in primary bone tumors such as OS, chondrosarcoma or Ewing's sarcoma (David, Blanchard et al. 2011; Alfranca, Martinez-Cruzado et al. 2015; Redini and Heymann 2015). The bone is also the most common organ affected by metastatic spread of many other tumor types with prostate, breast, and lung cancer having the highest prevalence for metastatic spread to the bone (Li, Peng et al. 2012). Primary bone tumors and bone metastases are both associated with a high morbidity (Coleman 2006) .

Tumor cells and bone interact with each other in a `vicious cycle`, causing pathological tumor-driven bone remodeling (**Figure 3**). Tumors are reported to produce a variety of factors such as PTHrP, IL-1, IL-6, IL-8, IL-11, TGFβ that stimulate pathological bone remodeling through interaction with osteoblasts and osteoclasts (Guise 2002; Akiyama, Dass et al. 2008). Osteoclasts play an important pro-tumorigenic role in cancer metastasizing to the bone, by generating skeletal lesions. Upon the resorption of the bone, the tumor gains access to these stored growth factors, calcium and phosphate within the bone, which promote the growth of tumor cells (Hauschka, Mavrakos et al. 1986; Mundy 2002; Yoneda and Hiraga 2005).

A recent study performed by Garimella R. *et al*., described the bone microenvironment as a central part in OS-associated bone remodeling. Extracellular membrane vesicles from OS cells were shown to be mediators of communication between the tumor cells and the bone. These extracellular membrane vesicles contain osteoclastogenic cargo, inducing a dysregulated bone remodeling in OS (Garimella, Washington et al. 2014). Another study by Avent S. *et al*., pointed out the interdependence of OS lesions and the bone by demonstrating that osteoclast activity is associated with the aggressiveness of the tumor (Avnet, Longhi et al. 2008). Therefore the finding of novel agents blocking the vicious cycle is an attracting field of research in OS.

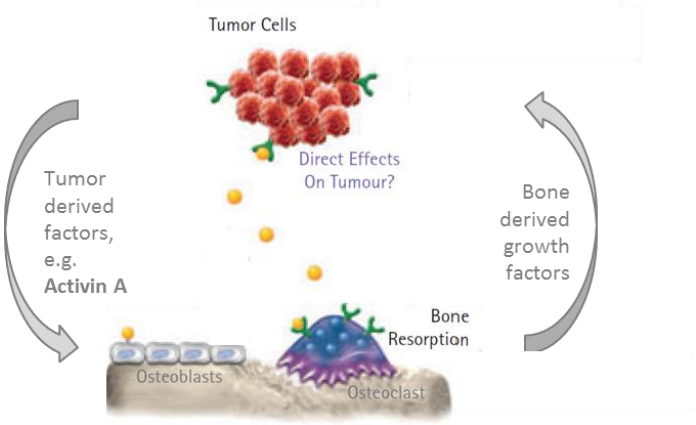

Figure 3: The vicious cycle of tumor and bone interaction *(apapted from Ferrari S, Webinar: Mechanisms of Bone Remodeling as Therapeutic Targets, BoneKey Webinar, 14 April 2012)*

4.2.1 The Balance of Bone Remodeling

Bone remodeling is regulated by the activity of specialized cells; osteoblasts, the bone forming cells that produce the bone matrix and induce its mineralization, and the bone-resorbing osteoclasts, which resorb bone and degrade its extracellular matrix. Osteocytes, a third type of bone cells, derived from osteoblast, are embedded in the bone matrix and regulate mineralization (Bonewald 2011) and bone lining cells coordinate remodeling processes (Everts, Delaisse et al. 2002).

Osteoclasts are huge multinucleated cells from mononuclear precursors of the hematopoietic lineage. Osteoclastogenesis is dependent on the hematopoietic factors, such as the receptor activator of nuclear factor kappa-B ligand (RANKL) and the colony-stimulating factor (m-CSF). RANKL and m-CSF induce signaling regulating genes important for osteoclastogenesis that mediate activation of the precursor cells and cell fusion. Functional osteoclasts polarize, and form a resorption pit (Howship`s lacunae), a sealed compartment between the cell membrane and the bone surface RANKL and m-CSF also stimulate the expression of e.g. cathepsin K (CatK) and tartrate resistant acid phosphatase (TRAP). CatK and TRAP are enzymes secreted into the resorption pit that acidify the resorption area for resorption of the underlying bone (reviewed in (Boyle, Simonet et al. 2003)).

Osteoblast are cells of mesenchymal origin that promote hydroxyapatite crystal formation and delivery to the bone surface via membrane matrix vesicles forming new bone (osteoid) (Anderson 1995). Osteoblastogenesis is tightly regulated by transcription factors, including runt-related transcription factor 2 (Runx2) and distal-less homeobox 5 (DLX5), which induce the production of the key enzyme alkaline phosphatase (ALP) and the secretion of collagen I. The exact function of ALP is not known, but it’s assumed that ALP removes

pyrophosphate, an inhibitor of hydroxyapatite crystallization, from the bone microenvironment, (Hessle, Johnson et al. 2002). Osteoblast differentiation is also regulated by bone morphogenetic protein (BMP), another member of the TGFβ family, which controls local bone formation tightly coupled to bone resorption (Cao and Chen 2005)

Osteoblasts and osteoclasts communicate via different mechanism. Both cell types can secrete paracrine factors but also make direct contact allowing membrane ligands and receptors to interact with each other or form gap junctions to allow interaction between the two cell types. As an example, osteoblasts express RANKL on their surface, which interacts with its receptor RANK on osteoclast, and thereby induce osteoclastogenesis (Karsenty, Kronenberg et al. 2009). Likewise the release of growth factors by osteoclast-mediated bone matrix resorption is important for the activation of osteoblastic bone formation (reviewed in (Matsuo and Irie 2008)). Other factors affecting bone remodeling include physical activity triggering mechanical signals, hormones (calcitonin, PTH, vitamin D3 (1,25 Vit D3) and oestrogen) and, as outlined above, tumor-driven processes.

Altogether, bone remodeling is regulated on many levels and a more detailed description is beyond the scope for this introduction.

4.2.2 Therapeutics targeting Tumor-Associated Bone Remodeling

Standard therapeutics for the inhibition of excessive bone remodeling are bisphosphonates (BP). BP have structural similarities to pyrophosphate enabling them to accumulate in the bone by binding to hydroxyapatite. There are two types of BP, the non-nitrogen and nitrogen containing BP, with the nitrogen-containing compounds having a higher bone resorption inhibiting potency than the non-nitrogen containing BP. Third-generation BP such as zoledronic acid or risedronate have additionally two heterocyclic nitrogen ring as a side chain, which increases their affinity for bone compared to the other BP (De Rosa, Misso et al. 2013). Third-generation BP`s promote osteoclast apoptosis by inhibiting farnesyl pyrophosphate synthase, a key enzyme in the mevalonate pathway, which is important for protein prenylation and the production of isoprenoids (e.g. cholesterol, vitamin K) (Luckman, Hughes et al. 1998). Central for osteoclast activity is the process of membrane polarization via vesicular trafficking, regulated by small GTPase, like Rho, Rab, Rac. These proteins require post-translational isoprenylation by the mevalonate pathway to induce stress fiber assembly, membrane ruffling and osteoclast survival (Coxon and Taylor 2008). Thus, third generation BP inhibit these processes.

BP are most commonly used to treat osteoporosis (Black, Delmas et al. 2007; Drake, Clarke et al. 2008), but BP do not only induce osteoclast apoptosis, they also revealed anti-tumor efficacy via different mechanisms (**Figure 4**). Zoledronic acid was shown to reduce bone pain and skeletal related events in breast cancer, prostate cancer and multiple myeloma (MM) patients (Berenson, Rosen et al. 2001; Rosen, Gordon et al. 2004; Saad, Gleason et al. 2004). Numerous preclinical studies in animal models including MM, breast cancer and prostate cancer demonstrate tumor-suppressing effects of ZOL (Green 2004).

The efficacy of BP in breast cancer patients to reduce tumor burden is still under discussion. The ZO-FAST study, in which postmenopausal woman with early breast cancer received letrozole and zoledronic acid, revealed a reduced risk for local and distant recurrences (-34%) in patients treated from the beginning of the study with zoledronic acid compared to patients obtaining the treatment only upon the appearance of clinical symptoms (Coleman, de Boer et al. 2013). On the other side, a study in early-stage breast cancer patients didn't support the use of ZOL in adjuvant therapy (Coleman, Marshall et al. 2011). A clinical trial in multiple myeloma patients (MM) reported improved progression-free survival and overall survival in patients undergoing high-dose chemotherapy and stem-cell transplantation together with ZOL treatment of MM (Aviles, Neri et al. 2013).

In addition to its ability to inhibit tumor-associated bone resorption, ZOL showed direct effects on SaOS-2 OS cell viability, invasion and differentiation (Dass and Choong 2007). ZOL is also reported to induce cell cycle arrest in POS-1 OS cells (Ory, Heymann et al. 2005), and a study with the OS cell lines HOS, MG-63, SAOS-2, and U2OS showed significant cytotoxicity mediated by the blocking of DNA synthesis and by provoking cell cycle arrest, microfilament breakdown and apoptosis (Kubista, Trieb et al. 2006). Preclinical studies in OS mouse models reported an inhibition of tumor growth, metastatic spread and prolonged overall survival (Ory, Heymann et al. 2005; Dass and Choong 2007). As mentioned above, chemoresistance in OS treatment is p53, Rb and caspase dependent; cytotoxic ZOL effects were shown to be independent of these key genes in several OS cell lines (Ory, Blanchard et al. 2007).

ZOL is commonly well tolerated with mild adverse effects; only rarely, severe side effects such as osteonecrosis of the jaw, pathologic fractures mainly in the proximal femur, and an increased incidence of atrial fibrillation are reported (Berenson, Rosen et al. 2001; Powell, Bowler et al. 2012; Sharma, Chatterjee et al. 2013).

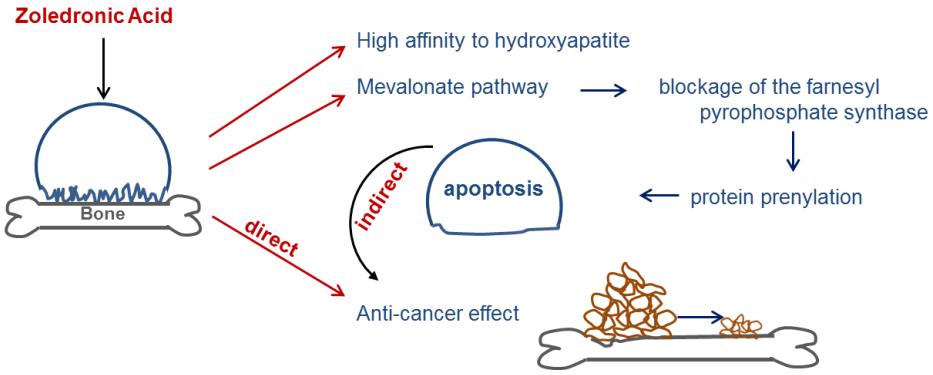

Figure 4: Mechanism of action of zoledronic acid on osteoclasts and OS tumor growth

The demonstration of anti-tumor efficacy by bone remodeling inhibiting agents opened up a novel direction in the pursuit of therapies against OS. A rather novel agent investigated in the context of bone remodeling is activin A, a member of the TGFβ superfamily, influencing osteoclastogenesis, osteoblastogenesis and tumorigenesis.

4.2.3 Activin A and its Role in Bone Remodeling

Activin is the most abundant member of the TGFβ superfamily in the bone and it is secreted by different types of cells in the bone microenvironment, such as bone marrow stromal cells, osteoblast and osteoclasts (Ogawa, Schmidt et al. 1992; Vallet, Mukherjee et al. 2010). Bone tissue contains high levels of activin A (Eijken, Swagemakers et al. 2007). Activin A knockout mice die within 24 hours due to craniofacial defects, indicating its important role in the bone remodeling (Matzuk, Kumar et al. 1995). Activin A is a known inducer of osteoclastogenesis. *In vitro* studies revealed an enhanced osteoclast formation in bone marrow cell cultures incubated with activin A, without any effect on osteoclast activation (Sakai, Eto et al. 1993). Later on, activin A was discovered as an essential co-factor for RANKL in osteoclast differentiation, increasing the induction of osteoclast-like cells from precursor cells (Fuller, Bayley et al. 2000).

The role of activin A in bone formation is more controversial. Matrix mineralization in human osteoblast cultures was shown to be inhibited by activin A, by changing matrix composition to reduced mineralizing capacity (Eijken, Swagemakers et al. 2007). Another study confirmed the inhibitory effects of activin A on osteoblast-mediated mineralization by decreasing ALP activity (Alves, Eijken et al. 2013). Mice overexpressing inhibin A (an activin A inhibitor) showed increased bone formation (Perrien, Akel et al. 2007). In contrast

several studies state stimulatory effects of activin A on osteoblast differentiation and bone mineralization. Osteoblast differentiation is enhanced by activin A in bone marrow cultures (Gaddy-Kurten, Coker et al. 2002) and local administration of activin in bone induced bone formation and fracture healing (Sakai, Miwa et al. 1999).

These different observations might in the end just reflect the complexity of activin A signaling and species-dependent differences.

4.2.4 Activin A and its Role in the Vicious Cycle

In recent years the focus in cancer research was on TGFβ and its involvement in tumorigenesis. TGFβ was shown to have important tumor suppressive characteristics, but it was also shown to induce tumor formation and progression (Massague 2008). Although activin A and TGFβ show structural similarity and share some downstream signaling mechanisms, there are distinct differences in their function (Loomans and Andl 2014). Activin A is involved in the regulation of tissue repair (Antsiferova and Werner 2012) and inflammation (Werner and Alzheimer 2006), processes closely related to cancer (Schafer and Werner 2008; Trinchieri 2012), implying a role of activin A in cancer. Activin A, like TGFβ, has also a dual role in cancer biology. Different studies over the last years revealed a tumor inhibiting function of activin A in a variety of tumours. Activin is shown to have growth inhibitory effects e.g. on liver, prostate and pancreatic cancer cells (Risbridger, Schmitt et al. 2001; Antsiferova and Werner 2012). In contrast, Activin A has also been shown to have direct effects on tumor cells, inducing tumorigenesis.

Different researchers in recent years described activin A as an important regulator in the `vicious cycle` of tumor and bone microenvironment interaction. Activin A is involved in the growth and progression of tumors metastasizing into the bone, such as breast cancer, lung cancer, prostate cancer and MM. Activin A enhances prostate cancer cell migration and it is overexpressed in metastatic prostate cancer (Kang, Huang et al. 2009). In breast cancer, activin A signaling induces epithelial-mesenchymal transition, invasion and metastatic growth (Bashir, Damineni et al. 2015). In a MM mouse model, activin A inhibition exerts anti-tumor effects by inhibition of tumor-associated bone remodeling (Vallet, Mukherjee et al. 2010). The overexpression of the activin A inhibitor Follistatin (FST) reduces tumor progression in small cell lung cancer by inhibiting angiogenesis (Ogino, Yano et al. 2008).

Several studies in patients relate activin A to cancer progression. Circulating levels of activin A were shown to correlate with advanced stage disease, inferior survival and increased bone involvement in patients with advanced MM (Terpos, Kastritis et al. 2012). Patients with

breast or prostate cancers showed increased activin A serum concentration. Activin A levels were also higher in patients with bone metastases and correlated with the Gleason score in prostate cancer patients. (Leto, Incorvaia et al. 2006)

These findings implicate the importance of activin A in the pathogenesis of bone cancers and make it an interesting target for OS research.

4.2.5 Activin A and its Signaling

Activin A is a glycoprotein and a member of the TGF beta superfamily, characterized by six conserved cysteine residues (Lander, Linton et al. 2001). First discovered in 1980, it was purified from gonadal fluids and shown to stimulate the follicle stimulating hormone (FSH) release from the pituitary gonadotropes (Vale, Rivier et al. 1986). Its more detailed characterization lead to the discovery of diverse regulatory functions, including cell proliferation and differentiation, wound repair, inflammation, glucose metabolism and immune response (Yu, Shao et al. 1987; Florio, Luisi et al. 2000; Werner and Alzheimer 2006; Kreidl, Ozturk et al. 2009; Xia and Schneyer 2009).

Members of the TGF beta superfamily include additionally activins, inhibins, TGFβ, bone morphogenetic proteins (BMPs), growth and differentiation factor (GDF), Nodal, myostatin and others. Activins are dimers of two β subunits linked with a single covalent disulfide bond. Four different genes INHBA, INHBB, INHBC, INHBE code for different hetero- and homodimers such as activin A, activin AB, activin B, activin C, activin AC, activin AE, activin CE, and activin BC, where only the first 3 are characterized in their function (Burger and Igarashi 1988; Mason, Berkemeier et al. 1989; Massague 1998).

Activin A is made of to two βA subunits (each around 13kDa) giving rise to a 26 kDa dimeric protein. The βA subunit is produced from a precursor molecule with 425 amino acids. The pro-βA domain is separated from the mature βA subunit via a polyarginine cleavage site, giving rise to a 116 amino acid protein. The pro-βA domain is important for activin folding, dimerization and secretion (Gray and Mason 1990). The monomers are linked via a disulfide bridge between two highly conserved cysteine residues located in the C-terminus of the tow monomers, known as the cysteine knot (Sun and Davies 1995; Makanji, Zhu et al. 2014). Crystallization of activin A alone was not yet achieved. Recent activin structural studies revealed highly flexible conformations, depending on the binding partner of activin. The structure of Activin A contains β-sheets forming a finger domain and an α-helical wrist domain (Thompson, Lerch et al. 2005; Harrington, Morris-Triggs et al. 2006).

There are twelve members of TGFβ receptors in humans, seven type 1 (also called ALKs) and five type 2 receptors and all of them have serine/threonine kinase activity in the cytoplasm (Manning, Whyte et al. 2002). Similar to other TGFβ superfamily members, activin A signals via two types of transmembrane receptors, activin receptor type 1 and 2 with serine/threonine kinase activity. Activin A receptors have a short extracellular domain, a single transmembrane region and a large intracellular domain with N-glycosylation sites and the serine/threonine kinase domain. Type 2 receptors ActRIIA and ActRIIB are constitutively active kinases and act as the primary activin binding receptors.

Crystal structure analyses with binding partners revealed that activin A differs from other TGFβ ligand structures and has a compact folded-back conformation. It binds to its receptors with the outer finger region (Thompson, Woodruff et al. 2003). Upon ligand binding, activin receptor type 1 (ALK4) heterodimerizes with type 2 receptors. Type 2 receptors then phosphorylate type 1 receptors in their juxtamembrane glycine- and serine-rich (GS)-domain. Type 1 receptors contain a conserved GS domain, shown to be important for signal transduction (Franzen, Heldin et al. 1995) and additionally a nine-amino acid sequence, called the L45 loop, shown to be a critical regulator of interactions with Smad isoforms (Persson, Izumi et al. 1998). Phosphorylation of the GS domain of the type 1 receptor by the type 2 receptor in type 1/activin A/type 2 receptor heterodimers activates the kinase domain in the type 1 receptor, which then activates intracellular signaling through the phosphorylation of intracellular mediators, known as the Smad proteins (reviewed in (Abe, Minegishi et al. 2004; Weiss and Attisano 2013)).

4.2.5.1 Smad-dependent Signaling

Smad proteins are transcription factors classified into three groups; receptor regulated Smads (R-Smads, Smad1, 2, 3, 5, 8), common mediator Smads (co-Smads, Smad4) and inhibitory Smads (I-Smads, Smad6, 7) (reviewed in (Shi and Massague 2003; Abe, Minegishi et al. 2004)). Smad2 and Smad3 are mainly activated by activins and TGFβ, whereas Smad1, Smad5 and Smad8 are activated by BMPs. R-Smads and Co-Smads have similar structural domains, the conserved N-terminal Mad homology 1 (MH1) domain and the C-terminal MH2 domain. The interaction of the L3 MH2 domain of the Smad2/3 proteins with the L45 loop within the kinase domain of the Activin type 1 receptor regulate binding specificity. Smad6 and -7 contain MH2 domains, but lack many other homologies with R-Smad and Co-Smad. (Abe, Minegishi et al. 2004)

Type 1 receptors activate R-Smad (e.g. Smad 2 and Smad 3) by phosphorylation of distal serines (SSXS motif) in the C-terminal domain. Co-Smads contain also a conserved MH2 domain but miss the SSXS motif. Upon their activation, R-Smad form a heterodimeric complex with Smad 4, via their L3 loop region, and the heterodimers are then translocated into the nucleus. In the inactive state Smads are constantly shuttling between the nucleus and the cytoplasm. R-Smads are localized mostly in the cytoplasm while Smad4 can be found in the cytoplasm and the nucleus. R-Smad/Smad4 complexes need a nuclear import and export system, which is regulated by importins (into the nucleus), exportins (out of the nucleus), and nucleoporins (part of the nuclear pore complex) (Fornerod, Ohno et al. 1997; Hill 2009). Smads contain in their MH1 domain a conserved nuclear localization sequence (NLS). Smad1 and Smad3 were shown to use the NLS sequence for the classical importin pathway (Chai, Wu et al. 2003). Smad2, on the other hand, has intrinsic shuttling activity in its MH2 domain, binding directly to the nuclear pore complex (Xu, Kang et al. 2002). Nuclear export is guided be nuclear export signals (NES), which are localized in the MH2 domain of the R-Smads or the linker domain of Co-Smads (Smad4) (Hill 2009).

In the nucleus, activated Smads bind to consensus DNA sequences and other binding partners to activate transcription. The Smads (despite Smad2) have a DNA binding sequence in their MH1 domain which binds to the Smad binding element (SBE) (Zawel, Dai et al. 1998). However, the affinity of the Smads for their SBE is weak and co-factors are therefore needed to increase the DNA binding affinity (Schmierer and Hill 2007).

The R-Smad/Smad4 complex interacts with sequence specific transcription factors that bind to their cognate DNA sequences and thereby induce transcription of numerous target genes (Massague, Seoane et al. 2005).

4.2.5.2 Smad independent Signaling

Although activin A signaling is mainly mediated by Smad-dependent signaling, non-Smad dependent pathways are also activated that amplify the biological effects of the TGFβ superfamily.

Activin A ligand binding was shown to activate the p38-mitogen-activated protein kinase (p38MAPK), ERK and JNK pathways, which regulate cell proliferation, migration and differentiation (Cocolakis, Lemay et al. 2001; Bao, Tsuchida et al. 2005; Vallet, Mukherjee et al. 2010). Activation and abnormalities in the signaling by the MAPK pathway play important roles in the development and progression of cancer. In OS, MAPK signaling induces cell proliferation, invasion, metastases in preclinical OS models, and inhibitors for different MAP

kinases demonstrated clinical benefit in OS patients (Sasaki, Hitora et al. 2011; Chandhanayingyong, Kim et al. 2012).

Another non-canonical pathway activates phosphatidylinositol-3-kinase (PI3K), which acts via the phosphorylation of Akt. (Zhang 2009). Phosphorylated Akt acts on mammalian target of rapamycin (mTOR), which regulates protein synthesis via phosphorylation of S6 kinase. The PI3K/Akt signaling is involved in OS tumorigenesis by increasing proliferation and invasion (Zhang, Yu et al. 2015).

4.2.6 Regulation of Activin Signaling

Activin A signaling is regulated at different levels; on the nuclear, cytoplasmic, membrane and extracellular level (**Figure 5**). Its regulation is a dynamic process, broadening the field of action for activin A.

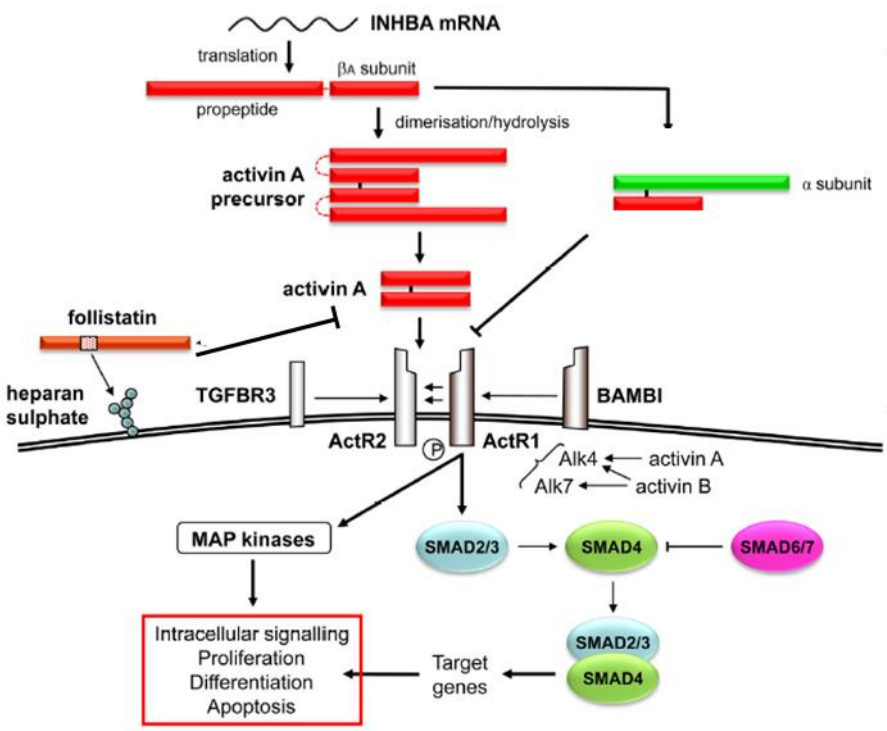

Figure 5: Activin A signaling pathway (*adapted from Hedger M.P. Vitam Horm. 2011;85:255-97. doi: 10.1016/B978-0-12-385961-7.00013-5. (Hedger, Winnall et al. 2011)*)

4.2.6.1 Follistatin

Follistatin (FST) is a soluble extracellular glycoprotein expressed in a wide range of tissues, including the bone microenvironment. FST binds activin with high affinity and with lower affinity it binds to myostatin, inhibin and BMPs (Welt, Sidis et al. 2002; Uhlen, Fagerberg et al. 2015).

FST was first isolated form follicular fluid, shown to inhibit FSH secretion. Located on chromosome 5, the FST gene consists of 6 exons, which, upon alternative splicing, form transcripts encoding the three FST isoforms, FST288, FST315 and a gonadal isoform FST303. FST is made up of five domains, an N-terminal domain, three FST modules (FS1, FS2, FS3) and an FST-isoform dependent C-terminal domain. Two FST molecules bind one activin molecule, building a ternary complex that shield both type1 and type2 receptor binding sites and thereby block receptor binding (Thompson, Lerch et al. 2005). The N-terminal domain and FS domains of FST is associated with the binding to the wrist region of activin (Harrington, Morris-Triggs et al. 2006). Both FST288 and FST315 were shown to have almost identical activin A binding affinities, whereas the C-terminal truncated form FST288 shows much higher affinity for heparin sulfate proteoglycans (Sugino, Kurosawa et al. 1993). FST315 is thought to be the predominant circulating isoform, whereas the FST288 is bound to cell surface proteins. The binding site for heparin sulfate is located in both isoforms in the FS1 domain (Gajos-Michniewicz, Piastowska et al. 2010). FST288/activin A complexes are taken up by cells with the help of cell surface glycoproteins and are degraded by lysosomes. FST315 gains glycoprotein binding affinities after activin A binding, thereby promoting activing A degradation (Lerch, Shimasaki et al. 2007). FST knockout mice die during embryonic development, due to growth retardation, musculoskeletal defects, failure of breathing (Lin, Craythorn et al. 2008).

Follistatin-related protein (FSTL/FSRP) is a homolog of Follistatin, encoded by the FLRG gene: FLRG is an additional regulator of activin with a lower affinity for activin and BMPs than for Follistatin. FLRG possesses only two FST domains, but shares a conserved key residue (R192) with FST, important for activin binding (Tortoriello, Sidis et al. 2001).

4.2.6.2 Additional Regulatory Mechanisms of Activin A Signaling

As outlined above, activin A signaling is regulated on different levels, ranging from intracellular, membranous and extracellular regulatory mechanisms.

Like activin, inhibins are dimeric proteins belonging to the TGFβ superfamily. They consist of βA or βB subunit and a inhibinα subunit linked by a disulfide bond (Risbridger, Schmitt et al. 2001). Inhibin antagonizes activin signaling via the availability of α-subunits which preferentially assembly of αβ heterodimers (inhibins) over ββ dimers (activins) and by competition with activin type I receptor binding. Type III receptor (Betaglycan), a co-receptor and a known binding partner of inhibin, potentiates its binding activity to activin receptors (Makanji, Zhu et al. 2014).

Other regulators of activin signaling are the membrane bound BMP and activin receptor membrane bound inhibitor (BAMBI) and Cripto (glycosylphosphatidylinositol membrane-anchored receptor) (**Figure 5**). BAMBI is transmembrane glycoprotein with sequence similarities to activin A type I receptors, but without a functional intracellular kinase domain (Onichtchouk, Chen et al. 1999), while Cripto forms a complex with activin type II receptors, that blocks activin signaling (Gray, Harrison et al. 2003).

Intracellular regulators are Smad anchor for receptor activation (SARA) binding to Smad2 and Smad3 proteins. The resulting complex facilitates their recruitment to activin receptor type I, and thereby activates activin A signaling. Activin receptor activity is furthermore regulated intracellularly by I-Smads, such as Smad7 and Smad6 (Smad 6 is favorably involved in BMP signaling). Ubiquitin guided proteasome degradation also controls activin receptor and R-Smad levels in the cytoplasm and the nucleus via the E3 ubiquitin ligases called Smurf proteins (Zhang, Chang et al. 2001; Murakami, Watabe et al. 2003).

4.2.7 Activin in Osteosarcoma

Surprisingly, research unravelling activin A inhibition in OS is still in its very infancy. 20 years ago, a follistatin-like protein with activin binding activity, called mac25, was shown to suppress growth of OS cells via cell cycle arrest (Kato, Sato et al. 1996; Kato 2000). A few years later, Matsuyama *et al.* reported that the inhibitor SB-431542 of the activin type I receptor (ALK4) suppressed proliferation of the OS cell line MG63 (Matsuyama, Iwadate et al. 2003). A recent study investigated the effect of knock-down and overexpression of activin A in MG63 cells. Activin A overexpression activated and activing A depletion suppressed proliferation, invasion and migration (Zhu, Liu et al. 2015).

For tumors metastasizing to the bone, a tumorigenic role of activin A in bone metastasis was described (Chapter 4.2.4). *In vitro* data and preclinical studies revealed activin A as a crucial regulator of the `vicious cycle` between tumor growth and associated pathological bone remodeling in the tumor microenvironment. Activin A inhibition exhibited therapeutic potential by suppressing tumor-associated bone remodeling and disease progression in tumors metastasizing to the bone. The common ground of primary bone tumors, such as OS, and tumors metastasizing to the bone, is their bone microenvironment, the disruption of the bone homeostasis and the associated tumor growth. Preliminary results of the above mentioned *in vitro* studies in OS strengthen the involvement of activin A in osteosarcomagenesis. Therefore, the role of activin A and a potential therapeutic benefit of targeting activing A in OS needs to be further investigated.

4.2.8 Activin A Inhibition as a Therapeutic Approach

Based on the novel knowledge on the biological role of activin A and its function in bone remodeling, tumor development and progression, blocking its signaling with antagonists has great potential for the development of new strategies for the treatment of OS, even more so since existing inhibitors of activin A revealed promising therapeutic effects in other cancers affecting the bone.

There are several clinical studies investigating ACE-011 for the treatment of different types of cancers. ACE-011 (Sotatercept, Acceleron Pharma Inc, Cambridge USA, Celgeme Corporation, Summit USA) is a soluble activin receptor type IIA IgG-Fc fusion protein (A murine analogue is called RAP-011) (Ruckle, Jacobs et al. 2009). A completed phase IIA study examined safety, tolerability and efficacy of ACE-011 in osteolytic lesions of multiple myeloma (ClinicalTrials.gov Identifier: NCT00747123). Results displayed higher bone mineral density, increase in bone formation as well as anti-tumor efficacy in treated patients. ACE-011 displayed high tolerability and safety (Abdulkadyrov, Salogub et al. 2014). Currently two additional clinical studies are ongoing in multiple myeloma patients. The first phase IIA study investigates its effect on bone mass and turnover (ClinicalTrials.gov Identifier: NCT02230917). The second phase I study examines the combination of lenalidomide, dexamethasone with ACE 011 with the purpose to reduce or prevent the growth of cancer cells along with improving anemia and bone lesions (ClinicalTrials.gov Identifier: NCT01562405).

Due to the tight regulation of the activin signaling, different approaches are promising to inhibit activin A signaling.

4.3 Photodynamic Therapy, an Introduction

Photodynamic therapy (PDT) and its medical application dates back to ancient times in Egypt, Greece and India, where plant extracts were applied on the skin that, upon exposure to the sun, caused skin reactions and changes of pigmentation (Castano, Demidova et al. 2005). PDT became in the last decades a new treatment option for a variety of neoplastic diseases. It involves the uptake of a so called photosensitizer (PS) in a tissue, followed by illumination, of the area of interest with laser light of a specific wavelength. Upon illumination the PS, in the presence of oxygen, generates cytotoxic reactive oxygen species (ROS) in the tissue. PDT is an attractive treatment modality, since neither the PS, light and oxygen are toxic on their own; only in combination they elicit toxicity. In addition, PDT has high tissue selectivity, because the laser light can be applied locally.

PDT is a multi-staged process; relevant aspects are the way of light absorption and the production of cytotoxic molecules (**Figure 6**). The PS is normally in a low energetic state. Following light absorption, the PS is transformed into a higher energetic state. Usually this energetic state is short-lived, but via intersystem crossing, changing the spin of the electrons, the PS enters a more stable triple-state. The PS then transfers excess energy on tissue-molecules producing radicals, which further react with oxygen producing ROS in a so called type 1 reaction. In a type 2 reaction the excited PS transfers its energy directly on ground-state oxygen, giving rise to ROS. Both processes are occurring during PDT, with the type 2 reaction being assumed to be the predominant one. The PS has a short lifetime, reacting with molecules only in its proximity, and the produced ROS have a diffusion capacity of up to 300 nm, limiting the area of ROS production (Castano, Demidova et al. 2004; Josefsen and Boyle 2008; Robertson, Evans et al. 2009). Consequently, PDT can be applied locally, limiting its effect on surrounding healthy tissue and overall side effects. This may offer PDT an advantage over other therapies such as chemotherapy, where not only the tumor is a target but the drug is distributed through the entire body, often causing severe side effects. This specificity of PDT, on the other hand, has also disadvantages, because many OS patients are diagnosed with metastases.

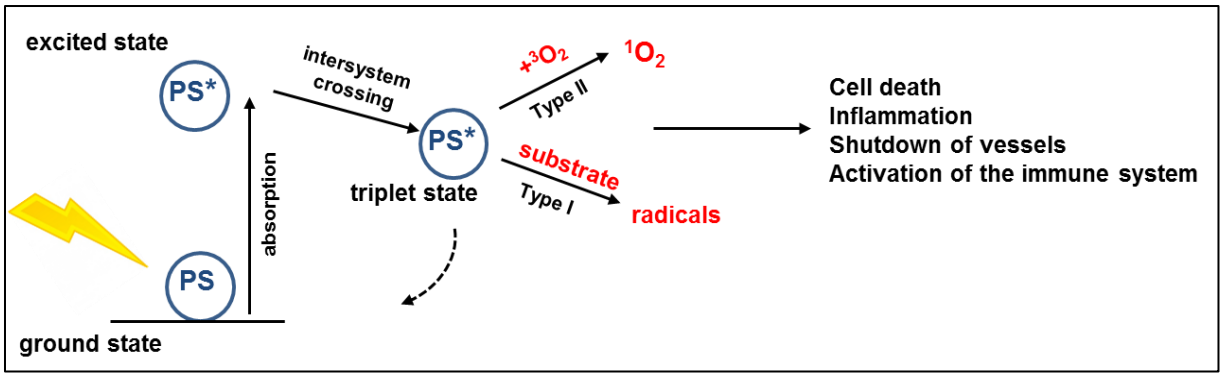

Figure 6: Photodynamic Therapy and its mechanisms of action

4.3.1 Photosensitizer

PS are small non-toxic compounds with a specific pattern of absorption and emission wavelength. Most PS are based on a tetrapyrrole structure (**Figure 7**), such as porphyrin derivates, chlorins, phtalocyonine and porphycenes. Their close structural resemblance to tetrapyrrole in the body such as hemoglobin is probably a reason of the low toxicity of the PS. A perfect PS should have the following features: pure chemical properties, negligible dark-toxicity, high chemical and physical stability, higher uptake in tumor than in normal tissue, rapid clearance from the body, appropriate photophysical attributes, strong absorption in the near infrared region (650-850nm) and suitable solubility for its administration (Josefsen and Boyle 2008; Agostinis, Berg et al. 2011).

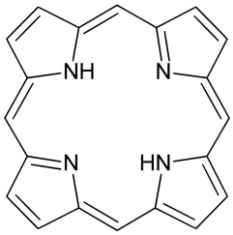

Figure 7: Tetrapyrole structure

4.3.2 The Optical Window of PS and Laser Light Applications

Although PS are taken up by most cells of the body, the limiting factors of PDT are tissue absorbance and limited tissue penetration of the applied light. Light is both scattered and absorbed by different chromophores in the tissue, such as hemoglobin, melanin, cytochromes, water and lipids, giving rise to a so-called optical window of PDT between 650-

1200 nm, where the absorption of the light by those chromophores is the lowest (Plaetzer, Krammer et al. 2009). Tissue penetrance is dependent on the absorption/excitation spectrum of the PS, with the highest tissue penetration in the red and near infrared spectrum (**Figure 8**). Despite an increase in tissue penetration with increasing wavelength, an optimal therapeutic window for PDT is limited due to absorption of water and lipids and due insufficient energy to produce singlet oxygen (Castano, Demidova et al. 2004).

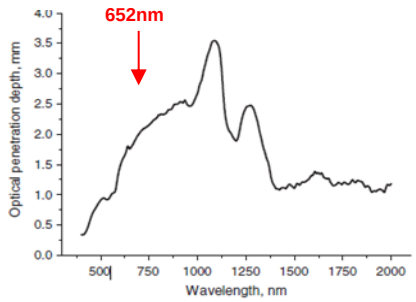

Figure 8: Penetration depth of light of 400 - 2000 nm wavelength into the skin *(adapted from (Bashkatov AN, J. Phys. D: Appl. Phys. 38 (2005) 2543–2555, 2005).*

Because tissue penetration is limited in PDT, optimal light application is fundamental. The development of lasers or light emitting diodes (LED) and the appropriate devices for the light delivery was crucial for effective application of PDT. Although PDT is mostly applied for superficial tumors (e.g. head and neck area, skin, bladder), its application expanded also on tumors not so easily accessible, such as brain tumors, using fiber optic devices (Quirk, Brandal et al. 2015).

4.3.3 Generations of Photosensitizers

One of the first PS is Photofrin. It is a chemical derivate of hematoporphyrin, composed of a mixture of compounds with an absorption peak at 630nm, limiting the penetration depth to only 3-5mm in different tissues (Wang, Zhu et al. 2005). Photofrin is nowadays used for esophageal and endobronchial cancers, high grade dysplasia in Barrett's esophagus, a variety of cutaneous lesions, breast and bladder cancer (O'Connor, Gallagher et al. 2009). First generation PSs are associated with several disadvantages; high dosage (Photofrin 1.5 – 2 mg/kg, approx. 100-200 J/cm2) and long-lasting photosensitivity in the skin (around 30 – 90 days). Approved worldwide, Photofrin is the most frequently used PS in PDT, although it is far from being a perfect PS. Due to the drawbacks of the first generation, second generation PSs were developed such as Foscan, Levulan, Visudyne, Tookad and

Lutrex. All of these second generation PS have a faster biodistribution, an absorption peak at higher wavelengths and a higher quantum yield of singlet oxygen formation.

Foscan (5,10,15,20-tetrakis(meta-hydroxyphenyl)chlorine (mTHPC), Temoporfin) is a chlorin PS approved in Europe since 2001 and is used for a variety of skin lesions, head and neck, pulmonary and esophageal cancers (Allison, Downie et al. 2004). Photophysical properties were investigated demonstrating a high quantum yield of singlet oxygen formation, longer lifetime of singlet state and lower dosage compared to first generation PS (0.1 mg/kg, approx. 5-10 J/cm^2). Foscan with its near-infrared absorbance peak at 652nm allows deeper penetration of the laser light than that achieved with Photofrin at 630 nm. In a preclinical PDT study in mice, tumor necrosis was observed at a depth of approximately 10 mm, making Foscan an attractive PS for PDT treatment of not so easy accessible tumors (Bown, Rogowska et al. 2002).

Another clinically approved second generation PS is Levulan (δ-aminolevulinic acid (ALA)), a biosynthetic porphyrin precursor with an absorption spectrum of 635nm. Levulan can be applied topically and is currently used worldwide for skin, bladder brain and esophagus cancer types. Another clinically approved PS is Visudyne (Verteporfin), a benzoporphyrin with an absorption peak at 690 nm. Verteporfin is approved in the U.S. for ophthalmic, pancreatic and skin cancer (Allison, Downie et al. 2004; Josefsen and Boyle 2008).

While second generation PS improved PDT applications remarkably, the development of third generation PS is in progress to improve the solubility (important for the route of administration) and to achieve higher tumor/healthy tissue ratios than those observed for second generation PS.

A number of different carriers have been developed for PS, such as oil-water emulsions, liposomes or nanoparticles. Liposomes became during the last years valuable carriers for PS, because they allow the delivery of a high payload of PS. In addition, liposomes can carry PS with different chemical properties, such as hydrophobic PS (e.g mTHPC), which normally form aggregates in aqueous solution, reducing the photo-activity (Derycke and de Witte 2004). A number of studies demonstrated a significantly higher accumulation of liposomal formulations in tumor tissue than of standard PS formulations (Johansson, Svensson et al. 2007).

One promising liposomal PS formulation of mTHPC is Foslip (Foscan, Bioltec AG, Jena, Germany). It has a unilamellar liposomal structure of dipalmitoylphosophatidylcholine (DPPC), dipalmitoylphosphatidylglycerol (DPPG), glucose and water. *In vivo* studies in

different preclinical models revealed a faster plasma distribution, a faster tumor accumulation and a lower accumulation in the skin compared to Foscan (Buchholz, Kaser-Hotz et al. 2005; Lassalle, Dumas et al. 2009). Foslip shows high PDT efficacy, shown in a study with feline cutaneous squamous cell carcinoma with a complete response rate of 75% after 1-year follow-up (Buchholz, Wergin et al. 2007). Another study in a subcutaneous colon adenocarcinoma mouse model, revealed a significant longer survival upon treatment with Foslip (44.4 days instead of 22.7 days in the control group treated with Foscan).

Furthermore other PS carriers such as lipid nanoparticles, based on a water/oil nanoemulsion, are additional promising carriers for PS (Navarro, Creusat et al. 2014).

4.3.3.1 Targeted Photosensitizers

A next step in PDT is the targeted PS delivery to the tumor. Different strategies can be used to couple PS to targeting moieties, such as covalent conjugates that bind via PEG-ylated liposomes or also non-covalent binding mediated by avidin or streptavidin and biotin.

The effective targeting is of course dependent on the coupling properties but also on an attractive target. Many tumors, such as OS, lack a common target, making targeted PDT challenging. Possible candidates may include EGFR or CXCR4, which have been reported to be expressed by multiple OS cell lines (Laverdiere, Hoang et al. 2005; Pahl, Ruslan et al. 2012).

4.3.4 PS Tumor Localization

After administration of the PS into the blood stream, it has to bind to the vessel wall for extravasation and to reach the tumor parenchyma. Tetrapyroles are unlikely to be metabolized in other organs other than the liver. The tumor to healthy tissue ratio is important for PDT: the higher the ratio, the lower the toxic effect on surrounding healthy tissue. Upon injection into the blood, PS bind to serum proteins such as albumin, HDL, or LDL, influencing their cellular uptake. PS preferentially localize in the tumor, the exact mechanisms of uptake are not yet clear. A possible explanation is the anatomical difference between solid tumors and normal tissue, including differences in angiogenesis, vascular density, and lymphatic system. Solid tumors have a higher vascular density because of constant neovascularization due to the rapid growth of the tumor. Due to accelerated angiogenesis, the blood vessels are not fully matured, giving rise to an abnormal architecture with fenestrations between the endothelial cells, irregular alignment and a wider lumen compared to normal blood vessels, leading to enhanced leakiness of the vessels for

macromolecules. In addition, the lymphatic clearance is impaired in the tumor, due to the lack of a proper lymphatic system, causing a slower clearance of molecules in the tumor tissue. These anatomical changes in the tumor are causing a so-called enhanced permeability and retention effect (EPR effect). Due to a slower lymphatic drainage, molecules stay longer in the tumor tissue, causing also retention of the PS in the tumor tissue. Therefore, encapsulation of PS into particles such as liposomes like Foslip increases the molecular size and prolongs the half-life in the circulation and enhances the EPR effect.

4.3.5 PDT-Mechanisms of Action

PDT has multiple effects; it does not only induce direct cytotoxic effects, but it also affects the tumor vasculature, induces inflammatory processes and activates the immune system.

4.3.5.1 Cytotoxicity

The uptake of the PS by cells is crucial for PDT efficacy. As the produced singlet oxygen species have a very short half-life and a low diffusion range, cytotoxicity occurs only in the immediate environment of activated PS. PS can localize in different cellular organelles, but they do not accumulate in the nucleus. Porphyrins are for example more associated with lipid membranes, whereas mTHPC is reported to target mitochondria, the plasma membrane, the Golgi apparatus and the endoplasmatic reticulum (Agostinis, Berg et al. 2011). Cytotoxicity is observed already shortly after light exposure, manifested by swelling of the cell, membrane polarization, reduced activity of enzymes in the membrane, shedding of vesicles containing cytosolic and lysosomal enzymes and a rise in intracellular Ca^{2+}. The produced ROS severely damage cellular membranes by oxidation of unsaturated fatty acids and cholesterol. Many pathways are involved in the direct PDT induced cytotoxicity; including MAPK signaling, or cellular adhesion protein receptor signaling. In addition, *in vitro* studies also showed an increase in intracellular Ca2+ levels in cancer cells, causing the release of arachidonic acid, which activates phospholipase A2 that generates superoxide radicals, which induce cell death (Luksiene 2003; Robertson, Evans et al. 2009).

PDT induces all major cell death pathways, necrosis, apoptosis and autophagy. Apoptosis is thought to be the predominant cell death pathway activated by cells in response to PDT. Indicators of apoptosis are cell shrinkage and cell fragmentation into membrane enclosed vesicles, called apoptotic bodies, which are phagocytosed (Castano, Demidova et al. 2004). Apoptosis is a programmed process, involving gene regulation, activation of

endonucleases and caspases. Due to an increase in permeability of the mitochondrial membrane, cytochrome c is released, forming a complex with Apaf-1 and ATP that binds to the initiator caspase 9, forming the apoptosome complex. Caspases are intracellular proteases grouped into initiator and effector caspases. Initiator caspases (e.g. caspase 9) cleave the inactive precursors of effector caspases (e.g. Caspase 3, 7), activating them for proteolytic cleavage of cellular components. Caspase 3/7 cleave poly (ADP-ribose) polymerase (PARP), which maintains cell viability by inducing DNA repair, into an 89 kDa fragment. The process eventually leads to nuclear disintegration (Elmore 2007).

Necrosis, also provoked by PDT, is a violent destruction of cells, caused by cytoplasm swelling, disruption of the plasma membrane and release of cellular contents. Autophagy, also reported as a response to PDT, is characterized by the formation of autophagosomes, membrane-bound structures, which mediate degradation of cellular contents by fusion with lysosomes.

4.3.5.2 Anti-Vascular Effects and Oxygen Consumption

Neo-angiogenesis is an important process in tumor progression, because fast growing tumors are dependent on a sufficient oxygen supply (Bergers and Benjamin 2003). A wide range of vascular effects in response to PDT is reported. Endothelial cells as targets of PDT play a major role in the anti-vasculature effects. A study performed by West et al., in bovine aorta endothelial cells and colon adenocarcinoma cells, showed that exponentially growing endothelial cells were sensitive to PDT (Gomer, Rucker et al. 1988; Gomer, Rucker et al. 1988; West, West et al. 1990). PDT is also known to induce platelet formation, microvasculature collapse, vascular leakage and vessel constriction (Star, Marijnissen et al. 1986). A key study performed by Synder *et al.* revealed that PDT increases vessel permeability, which facilitated the accumulation of a liposomal formulation of doxorubicin in the tumor tissue (Snyder, Greco et al. 2003). Pointing out the importance of the vasculature effect, a study by Maugain et al., displayed that PDT efficacy was higher with a short (3h after injection) than with long drug-light intervals, even though tumor mTHPC accumulation was not at its maximum. PS levels in leukocytes at this time point were high, indicating an early vascular PDT response (Maugain, Sasnouski et al. 2004).

The drug-light interval is a crucial factor in PDT. Interestingly, for Foscan, the concentration of PS in the tumor does not always correlate with PDT efficacy. The PDT response was maximal shortly after the injection of Foscan and not when the accumulation of the PS in the tumor was highest (Cramers, Ruevekamp et al. 2003). Despite these findings,

current standard protocols for Foscan recommend irradiation of the tumor 96 h after PS administration.

Tumor oxygenation is crucial for PDT efficacy. Chen *et al*., demonstrated that the manipulation of tumor oxygenation (treatment under different atmospheric pressure) can alter PDT efficacy. Hyper-oxygenation of the tumor tissue lead a better treatment outcome (Chen, Huang et al. 2002). Lowering light irradiation especially the fluence rate causes slower oxygen consumption and therefore improves the tumor response. Different fluence rates (14 and 112 mW/cm2) were applied in a subcutaneous Colo 26 murine tumor model, low fluence rates caused in 70- 80% of the mice tumor cures compared to 10-15 % tumor cures in the high fluence dose treated animals (Henderson, Gollnick et al. 2004). Therefore, optimal energy settings should be taken into consideration for optimal PDT.

4.3.5.3 Inflammation and the Immune System

PDT evokes a strong inflammatory response, recognized as a local swelling and formation of an edema. An acute inflammatory response is launched immediately after illumination. PDT rapidly induces the so called damage-associated molecular patterns (DAMPs). DAMPs are a variety of molecules normally located within the cells (tumor cells and vasculature), but, upon cell destruction, they are released in the surrounding area. DAMPs are recognized by the innate immune system, but they also stimulate the adaptive immune system. The cells that first arrive at the treated area are neutrophils. Photofrin- and mTHPC-based PDT induced systemic neutrophilia mediated by the acute-phase response and the complement system, both key factors in the innate immune system. Neutrophils release a number of cytokines attracting monocytes/macrophages and mast cells and thereby initiate the removal of residual tumor cells and vasculature (Cecic, Parkins et al. 2001; Cecic, Stott et al. 2006; Garg, Nowis et al. 2010).

The acute phase response (APR) is a stress response that is activated to control the induced damage. APR is activated by the release of various cytokines (such as IL-6, IL-1, TNF) by cells of the innate immune system (neutrophils, macrophages, monocytes) APR induces a wide range of pathophysiological responses like hormone alterations via the adrenal/pituitary axes, changes in plasma protein levels, leukocytosis and neutrophilia (Jain, Gautam et al. 2011). The importance of neutrophils was demonstrated upon their depletion in host mice, which reduced long-term tumor cure (Korbelik and Cecic 1999). In addition, neutrophils are able to induce maturation of dendritic cell (DC) and lymphocytes, establishing

a link between the innate and the adaptive immune response (Yang, de la Rosa et al. 2009; Jaillon, Galdiero et al. 2013).

Numerous studies have shown that PDT induces also the adaptive immune system, potentiating PDT efficacy. Subsequent studies in murine mouse model also showed that local PDT does not only induce anti-tumor immunity, it also suppressed a tumor re-challenge (Castano, Mroz et al. 2006). Phagocytosis of destroyed tumor cells by the innate immune system plays a vital role in presenting tumor associated antigens to cells of the adaptive immune system that results e.g. in the attraction of dendritic cells to the site of treatment and their maturation (Korbelik 2006). An adaptive immunity effect of PDT is supported by pioneer studies performed by Korbelik *et al*.. Mammary sarcoma cells (EMT6) were subcutaneously injected into nude, SCID and Balb/c mice. Nude mice lack T lymphocytes but have normal levels of natural killer (NK) and B lymphocytes, whereas SCID mice have no matured B and T lymphocytes, with normal NK cell and myeloid cell number. Photofrin-mediated PDT revealed a long term cure in BALB/c mice, and a delayed PDT effect in SCID and nude mice with tumor regrowth and no long time cure. Adoptive T cell transfer from BALB/c to SCID mice delayed tumor regrowth and a transfer of bone marrow from BALB/c to SCID lead to an almost 100% long term tumor cure in SCID mice, whereas BALB/c mice with transplanted SCID bone marrow lost long term PDT cure (Korbelik, Krosl et al. 1996). These studies demonstrate the induction of the adaptive immune response with a subsequent immune memory. Although PDT is a local therapy, different studies report not only a local anti-tumor effect, but also a systemic immune effect against the tumor. This was supported by the detection of tumor-sensitized immune cells in tumor distant lymph nodes (Korbelik and Dougherty 1999). Furthermore, a clinical study in angiosarcoma patients, showed spontaneous remission of distant untreated tumor sites after PDT and high T-lymphocytic infiltration was observed in biopsies (Thong, Ong et al. 2007).

Furthermore, it is important to note that PDT can also have direct cytotoxic effects in cells of the tumor microenvironment, such as tumor-supporting cells like various immune cells (e.g. macrophages, lymphocytes, DC).

4.3.6 PDT Applications

PDT has been used for cancer therapy since 1970s by Thomas Dougherty, who successfully treated skin cancer patients using a hematoporphyrin derivative (HPD) and red light. He observed a complete or partial response in 111 of 113 cutaneous or subcutaneous malignant lesions (Dougherty, Kaufman et al. 1978). At the same time J.F. Kelly

demonstrated anti-cancer efficacy of HPD in bladder cancer patients (Kelly and Snell 1976). Since these pioneer studies, a multitude of clinical studies has been performed and a number of PS tested and some of them were clinically approved; these include Foscan (mTHPC), Photofrin (HpD), Metvix (ALA), and Visudyne (Verteporfin). Most PS have been approved for different kinds of premalignant and malignant non-melanoma skin lesions and have been extensively studied with porfimer sodium and ALA. PDT using Photofrin has been shown to induce a complete response in 92% of patients with basal cell carcinoma (BCC) together with a reduced 4 year recurrence rate of only 10% (Zeitouni, Shieh et al. 2001). In potentially metastatic squamous cell carcinoma, on the other hand, the initial response rate ranged from 54% to 100% and a recurrence rate of up to 69% was observed (Braathen, Szeimies et al. 2007).

In an mTHPC-mediated PDT study with 121 oral squamous cell carcinoma 85%, functional and cosmetic benefits were higher compared to patients treated with surgery or radiation (Hopper, Kubler et al. 2004). Furthermore in an mTHPC-based PDT study with 128 patients for which conventional therapy had failed, 38% of the patients showed an overall tumor response and 16% a complete tumor response. Important to mention is also the improvement in quality of life in this study (D'Cruz, Robinson et al. 2004). Tumor suppressive effects were also shown for tumors of the digestive system and for intraperitoneal malignancies, prostate and bladder cancer, and are now subject to clinical investigations (Agostinis, Berg et al. 2011) (Table 1).

Sensitizer	Trade name	Potential indications	Activation wavelength
HPD (partially purified), porfimer sodium	Photofrin	Cervical*, endobronchial*, oesophageal*, bladder* and gastric cancers*, and brain tumours	630 nm
BPD-MA	Verteporfin	Basal-cell carcinoma	689 nm
m-THPC	Foscan	Head and neck tumours*, prostate and pancreatic tumours	652 nm
5-ALA	Levulan	Basal-cell carcinoma, head and neck, and gynaecological tumours Diagnosis of brain, head and neck, and bladder tumours	635 nm 375–400 nm
5-ALA-methylesther	Metvix	Basal-cell carcinoma*	635 nm
5-ALA benzylesther	Benzvix	Gastrointestinal cancer	635 nm
5-ALA hexylesther	Hexvix	Diagnosis of bladder tumours	375–400 nm
SnET2	Purlytin	Cutaneous metastatic breast cancer, basal-cell carcinoma, Kaposi's sarcoma, prostate cancer	664 nm
Boronated protoporphyrin	BOPP	Brain tumours	630 nm
HPPH	Photochlor	Basal-cell carcinoma	665 nm
Lutetium texaphyrin	Lutex	Cervical, prostate and brain tumours	732 nm
Phthalocyanine-4	Pc 4	Cutaneous/subcutaneous lesions from diverse solid tumour origins	670 nm
Taporfin sodium	Talaporfin	Solid tumours from diverse origins	664 nm

Table 2. PDT application. * indicating clinically approved PS *(adapted from Dolmans E.J.G.J. et al., Nat Rev Cancer, 2003)*

Although PDT has been mostly applied for superficial tumors, several studies also investigated the feasibility and efficacy of PDT in a more inaccessible location as an intraoperative approach. Already in 1988, Nambisan et al. applied PDT to recurrent retroperitoneal sarcomas and achieved a complete tumor resection in 8 of 10 patients. In patients with mesothelioma, Foscan-based PDT was also shown to be a safe intraoperative treatment (Friedberg, Mick et al. 2003). Importantly, PDT application as an intraoperative approach or with fiber optics in combination with fluorescence guided tumor resection, making use of the fluorescence of PS and their higher accumulation in tumors than in healthy tissue, revealed promising results in different studies investigating brain tumors (Quirk, Brandal et al. 2015).

Although PDT has a low systemic toxicity, frequent mild side effects of the therapy include local pain after illumination and cutaneous photosensitivity.

4.3.7 PDT in Osteosarcoma

Standard therapy for OS includes surgery and chemotherapy. Unfortunately chemotherapy is often associated with severe side effects and resistance, and certain tumors are located at delicate or hardly accessible locations (Chou and Gorlick 2006). PDT is a promising strategy for the treatment of metastasizing OS. Due to its local application and the per se non-toxic compounds, PDT induces low system toxicity. Compared to other therapies, e.g. chemotherapy or radiation, PDT can elicit an anti-tumor immunity, and therefore inhibit distant metastases through the activation of an immune response. Furthermore, an intraoperative combination of PDT with surgery could improve complete tumor eradication, and a combination with standard chemotherapy could potentially lower toxic doses of chemotherapeutics, thereby reducing recurrences, immediate and long-term side effects and consequently improve patient survival. Unfortunately, only a few studies have been published on these combinations. However, PDT has already been successfully applied in combination with chemotherapy and radiation (Agostinis, Berg et al. 2011). Interestingly, PDT, in combination with cisplatin, potentiated treatment efficacy in different OS mouse models (Nahabedian, Cohen et al. 1988; Canti, Nicolin et al. 1998). PDT was also shown to sensitize cancers cells to radiotherapy (Pogue, O'Hara et al. 2003), with an increase in anti-cancer effects (Luksiene 2003).

Unfortunately only a few preclinical studies have been published until now using PDT for the treatment of OS. Kusuzaki *et al.* tested acridine orange- based PDT on multi-drug resistant OS cell lines and observed a strong cytotoxic effect, which is in line with other *in*

vitro data, which demonstrated ALA-based PDT toxicity in HOSM-1 and HOSM-2 cell lines (Kusuzaki, Minami et al. 2000; Yanase, Nomura et al. 2009). In preclinical studies in mice, Nomura *et al*. showed that subcutaneous OS tumors injected with HpD and treated with light exhibited reduced tumor growth (Nomura, Yanase et al. 2004) Unfortunately, this subcutaneous model has only minimal clinical relevance. A very recent study performed by Sun *et al*., using Hiporfin mediated PDT, showed tumor suppression in subcutaneous and tibial OS mouse models (Sun, Zhou et al. 2015), but their models lacked a proper immune system, which might explain the only slight reduction in tumor growth in response to PDT.

A preclinical study in seven dogs with spontaneous OS used the PS Visudyne (Vetoporfin) intravenously. Upon injection the tumors were locally irradiated with light provided by a 0.94 mm fiber optic cable. Tissue staining and MRI after PDT showed remarkable tumor necrosis. Unfortunately the affected legs were amputated 48 h after the treatment and a systemic impact on potential metastases or long-term treatment effects were therefore not reported (Burch, London et al. 2009).

OS mortality is mostly caused by metastatic spread; therefore, PDT may represent a promising treatment option due to a potential systemic effect on the immune system and the options for combined and repetitive treatment. In addition, PDT on metastatic lesions such as lung metastases might also be a novel treatment possibility, because in patients with lung cancer, PDT was shown to be an effective, preserving lung function (Usuda, Kato et al. 2006). Altogether, PDT is an interesting and promising novel option in OS therapy with minimal side effects and, if necessary, applicable in a repetitive manner.

5 Aims of the Thesis

5.1 Aim 1

Activin A is a member of the TGFβ superfamily and has been implicated in the `vicious cycle` between bone tumors and their microenvironment. It not only influences bone remodeling, including osteoclastogenesis and osteoblastogenesis, but was also shown to have a tumor promoting role in a variety of bone homing tumors, e.g. MM, breast, prostate and lung cancers. Similar to these bone homing tumors, a `vicious cycle` of pathological bone remodeling driving tumor progression is also assumed to be crucial in OS, therefore, the inhibition of activin A signaling, is a promising strategy for the treatment of OS.

The aim of this study was to investigate the role of activin and its inhibition on OS growth. To achieve this, we used two engineered fusion-proteins inhibiting activin A; a soluble fusion protein acting as a decoy receptor for activin A, consisting of the extracellular domain of the ActRIIA receptor fused to the murine immunoglobulin G (IgG) Fc domain (ActRIIA-mFc); and an engineered analogue of follistatin (FST_{315}), a natural occurring inhibitor of activin A with a heparin-binding site deletion (ΔHBS), fused to an Fc of an human IgG (FST_{315}ΔHBS-hFc). (**Figure 9 A, B**). Additionally, we analyzed the effects of both activin A inhibition in combination with the bisphosphonate ZOL, a gold standard for the inhibition of cancer-associated bone remodeling with anti-tumor efficacy, on OS progression.

As a first sub-aim, activin A inhibitors, as single compounds or in combination with ZOL, were studied *in vitro* on osteosarcoma cells and cells of the bone microenvironment, and levels of activin A in serum samples collected from osteosarcoma patients were assessed.

As a second sub-aim, we studied the efficacies of the activin A inhibitors, with or without combination of ZOL, to disrupt tumor growth, tumor associated bone remodeling, as well as metastasis formation in an intratibial xenograft osteosarcoma model.

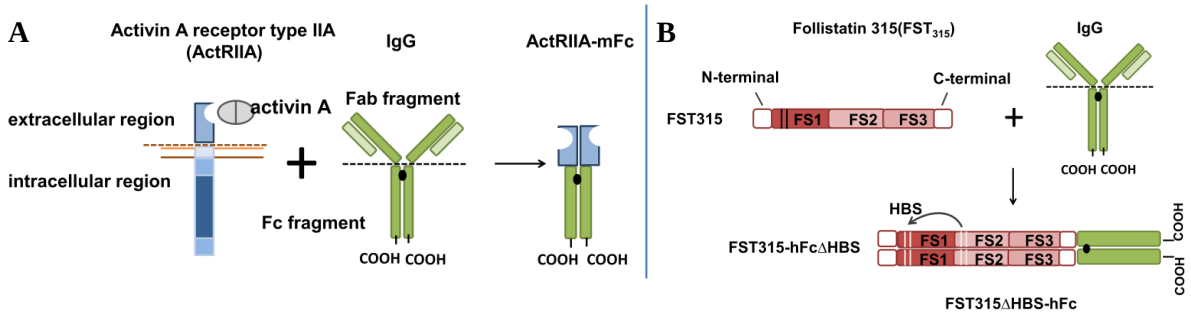

Figure 9: **Engineered fusion proteins for the inhibition of activin A.** (A) A soluble decoy receptor ActRIIA-mFc (B) and a FST315 analogue FST_{315}ΔHBS-hFc.

5.2 Aim 2

Current osteosarcoma therapies cause severe treatment-related side effects and chemoresistance, and have low success rates. Thus, alternative treatment options are needed. PDT is associated with low systemic toxicity, local application, and anti-tumor immunity, and has been effective against a variety of tumors, such as skin and head and neck cancers. In this second part of the thesis, we therefore investigated PDT as a therapeutic approach against OS.

To accomplish this aim, we performed *in vitro* and *in vivo* studies with one of the most powerful PS, mTHPC (Foscan) and two novel liposomal formulations, Foslip (biolitec, Jena, Germany) and lipid-based nanoparticles (LNP).

The purposes of the *in vitro* experiments were to compare the uptake of Foscan, Foslip and LNP and their dark- and phototoxicity in the highly aggressive OS cell lines and to characterize the induced cell death pathways.

The experiments *in vivo* were performed in intratibial human xenograft and syngeneic OS mouse models, both metastasizing to the lung. First, the uptake of Foscan, Foslip and LNP within the tumor tissue was compared. Subsequently, their tumor- and metastasis-suppressive potential in PDT applied in the xenograft and syngeneic intratibial OS mouse models was investigated. In addition, we studied the impact of PDT on the tumor tissue and vasculature in the syngeneic intratibial OS mouse model.

6 Results

6.1 Manuscript 1

Blockage of the Osteosarcoma Microenvironment: Activin A Inhibitors as a Novel Intervention against Osteosarcoma.

Daniela Meier[1], Sander M. Botter[1], Marco Eijken[2], Giovanni Pellegrini[3], Ana Gvozdenovic[1], Olga Neklyudova[1], Walter Born[1], Bruno Fuchs[1]

[1]Laboratory for Orthopedic Research, Department of Orthopedics, Balgrist University Hospital, Zurich, Switzerland

[2]Arcarios B.V., Rotterdam, The Netherlands

[3]Laboratory for Animal Model Pathology, Institute of Veterinary Pathology, University of Zurich, Zurich, Switzerland

*Corresponding author e-mail: bfuchs@research.balgrist.ch (Bruno Fuchs)

Running Title: Activin A Inhibitors as a Novel Intervention against Osteosarcoma

Key words: Osteosarcoma, activin A, bone remodeling, zoledronic acid

Article category: Research Article, Cancer Therapy: Preclinical

Conflict of interest: Marco Eijken as a shareholder of Arcarios

Submission: Clinical Cancer Research, May 2016

Abstract

Purpose: Osteosarcoma is thought to elicit a `vicious cycle` of bone remodeling to provide a fertile soil for tumor growth and progression. Activin A, a member of the TGFβ superfamily, may play a critical role in this cycle. We evaluated the impact of activin A inhibition *in vitro* and *in vivo* in osteosarcoma and its microenvironment.

Experimental Design: The effects of an engineered follistatin analogue (FST_{315}-ΔHBS-hFc) and an engineered activin decoy receptor (ActrIIA-mFc) in combination with zoledronic acid (ZOL) were evaluated *in vitro* in osteosarcoma and bone cells. Using an orthotopic 143B osteosarcoma xenograft mouse model, the efficacy of activin A inhibitors (i.p. 10 mg/kg, biweekly) and ZOL (s.c. 100 µg/kg, biweekly) as single treatment or in combination on tumor growth, bone remodeling and metastases development was determined.

Results: Despite a functional activin A signaling in 143B cells, activin A neutralization had no effect on cell viability or migration *in vitro*, whereas ZOL was cytotoxic. On the other hand, activin A-induced osteoclastogenesis was effectively inhibited using the two activin A inhibitors. Both activin A inhibitors successfully disrupted tumor growth and tumor-associated bone remodeling. When combined with ZOL, tumor growth was further reduced and a decreased metastatic spread was observed in mice treated with ActrIIA-mFc and ZOL.

Conclusions: This study shows that activin inhibitors, as single treatment or in combination with bisphosphonates, successfully disturbed the osteosarcoma microenvironment. Because both classes of compounds interfere with different pathways and were well tolerated, clinical application of this combined treatment may be feasible and promising.

Translational Relevance

Current therapies for osteosarcoma have not been able to overcome the currently plateaued patient survival curve. To overcome chemoresistance and the high diversity of osteosarcoma in phenotype, anatomical location and histology, novel interventions are needed. In recent years, a `vicious cycle` between the tumor and its bone microenvironment was proposed to play an important role in osteosarcoma development. Some bone cancers identified activin A as a novel component involved in this cycle. This study shows that activin inhibitors and zoledronic acid (ZOL), administered as single treatment or in combination, successfully disturb this microenvironment, leading to a significant reduction of osteosarcoma tumor growth, tumor associated bone remodeling and metastatic spread. The effects of ZOL against osteosarcoma are currently under clinical investigation, and our results suggest that a combination of this compound with activin A inhibitors may offer additional clinical benefit. Therefore, Activin A may promise a novel and potentially more potent approach for future osteosarcoma therapy.

Introduction

Osteosarcoma is the most common malignant primary tumor of bone and the second leading cause of cancer-associated death in childhood and adolescence (1, 2). Since the introduction of multi-agent chemotherapy, 5-year survival rates in patients with localized disease increased above 60%, but in case of metastatic or recurrent disease, the survival rate remains poor with 20-30%.

Tumor heterogeneity presents a real challenge in finding a therapeutic target to treat osteosarcoma. Further, osteosarcoma includes a number of different subtypes, which differ in their anatomical location, histology, phenotype and genetic profile (3). Therefore, this study concentrates on a common factor for all osteosarcoma subtypes: the bone and its microenvironment. Bone is a dynamic tissue, and physiological micro-damages within the bone matrix are being constantly absorbed by osteoclasts and rebuilt by osteoblasts. This bone remodeling is strictly regulated and in an equilibrium in healthy individuals (4). In patients with cancers affecting the bone, these processes become unbalanced, leading to excessive bone remodeling. This in turn offers the tumor access to growth factors stored within the bone matrix, which then allows it to grow and spread. Osteosarcoma cells are reported to directly cross-talk with bone cells, and thus play an important role in regulating bone remodeling (5). Consequently, researchers nowadays believe that a `vicious cycle` between the tumor and the bone microenvironment exists in osteosarcoma, as it was previously proposed for other tumors affecting bone, such as breast, prostate cancer, multiple myeloma, Ewing's sarcoma and chondrosarcoma (6-10).

In prostate and breast cancers and multiple myeloma, activin A was identified as a novel component involved in this `vicious cycle` (11-13). Activin A is a homodimeric protein belonging to the TGF-β superfamily, a known regulator of pituitary follicular stimulating hormone (FSH), cell proliferation and differentiation, immune response, wound healing and embryogenesis (14). Additionally, it is abundantly present in the bone microenvironment and acts as a regulator of bone remodeling. Activin A has been shown to be a cofactor for RANKL, a key cytokine for osteoclastogenesis (15). Although its effects on osteoblasts are more controversial, an inhibition in the mineralization capacity of osteoblast has been reported (16). Activin A is also involved in tumor growth and progression in osteosarcoma and tumors metastasizing to the bone (13, 17, 18). Serum levels of activin A were found to be elevated in patients with bone metastasis of breast and prostate cancers and multiple myeloma (13, 19) and in the latter, these serum levels inversely correlated with patient survival (20).

Finally, inhibition of activin A in preclinical in vivo models for multiple myeloma, lung, and breast cancer led to suppression of cancer associated bone remodeling (11, 13, 21) as well as an effective reduction of tumor progression (13, 22, 23). However, in osteosarcoma, the role of activin A, its involvement in the tumor microenvironment and its potential as a therapeutic target is not well studied. Therefore, we investigated whether the inhibition of activin A is able to counteract osteosarcoma tumor growth both locally and systemically. To this end, we used two different types of inhibitors, a soluble engineered activin A receptor type 2A inhibitor fused with the fragment crystallizable region (Fc) of an IgG (ActRIIA-mFc) and an engineered analogue of follistatin (FST_{315}), which has high affinity for activin A and lower affinity for myostatin and bone morphogenetic proteins, fused to an Fc of an IgG (FST_{315}ΔHBS-hFc). The FST protein carries additionally a heparin binding sulfate deletion (ΔHBS) to prolong circulation (24). Moreover, we also combined activin A inhibitors with the bisphosphonate zoledronic acid (ZOL). ZOL has anti-tumor efficacy (25) and is currently being used as a gold standard for the inhibition of cancer-associated bone remodeling by inhibition of osteoclast differentiation and activity (26, 27). In this study, we analyzed the effects of both activin A inhibition and ZOL *in vitro* on osteosarcoma cells as well as cells of the bone microenvironment. We further assessed the levels of activin A in serum samples collected from osteosarcoma patients. In addition, we studied the efficacies of the activin A inhibitors and ZOL to disrupt tumor growth and associated bone remodeling as well as metastasis formation in an intratibial xenograft osteosarcoma model. Our studies revealed activin A as an important regulator of the osteosarcoma microenvironment and demonstrated therapeutic efficacy of ActRIIA-mFc and FST_{315}ΔHBS-hFc, with or without ZOL against osteosarcoma.

Materials and Methods

Cells and culture conditions

Human 143B (CRL-8303), SaOS-2 (HTB-85), murine K7M2 (CRL-2836) and HEK293 (CRL-3216) cells were obtained from the American Type Culture Collection. Cells were cultured in DMEM (4.5 g/l glucose)/HamF12 (1:1) tissue culture medium (Invitrogen, CA, USA), supplemented with 10% heat-inactivated FCS (GIBCO, Basel, Switzerland), at 37°C in a humidified atmosphere (5% CO_2). 143B were transduced with the *LacZ* and mCherry gene as described before (143B/*lacZ*/mCherry) (28).

Cells were authenticated by multiplex PCR (Microsynth, Switzerland) using the PowerPlex®16HS system (Promega, Fitchburg, USA) and verified by comparison with the database at the Collection of Microorganisms and Cell Cultures (DSMZ, Braunschweig, Germany).

Peripheral blood mononuclear cells (PBMC) were obtained from the whole blood of healthy individuals (HI) and sorted for CD14-positive PBMC with a human CD14 Selection Kit (#18058, STEMCELL Technologies, Vancouver, Canada) following manufacturer's instruction using the Manual EasySep® protocol with the Purple EasySep® Magnet (#18000, STEMCELL Technologies). Cells were cultured in MEM Alpha Medium (#22561.021, Gibco) supplemented with 15% heat-inactivated FCS.

Activin A inhibitors and zoledronic acid

FST-$_{315}$ΔHBS-hFc represents human follistatin (FST_{315}), in which FST's heparin binding sulfate is replaced (ΔHBS) as described by Sidis *et al*. (29), and fused to the fragment crystallizable region (Fc) of a human IgG1. ActRⅡA-mFc is a fusion protein of the human activin A receptor type 2A (ActRIIA) with the Fc of a murine IgG2a. FST_{315}, FST_{315}ΔHBS-hFc and ActRⅡA-mFc were kindly provided by Arcarios (Rotterdam, Netherlands). Zoledronic acid (ZOL) was purchased from Novartis (Zometa, Switzerland).

Activin A Elisa in human blood samples and osteosarcoma cell lines

Human blood was collected in serum collection tubes (# 368774, BD, New Jersey, USA) from 19 osteosarcoma patients and 14 healthy individuals (HI). Tubes were centrifuged for 10 minutes at 3700 rpm at room temperature (RT). Blood serum was transferred to a new 15 ml tube, aliquoted and stored at -20°C.

Cells were cultured in 25 cm^2 cell culture flasks under tissue culture conditions until 60% confluency, washed with PBS and starved for 24 hours with 2ml/well DMEM(4.5 g/l glucose)/HamF12 (1:1) without FCS. Supernatant was collected by centrifugation (2 minutes, 1200 rpm), stored at -20°C and normalized to the number of cells.

Activin A ELISA (ab113316, Abcam, Cambridge, UK) was performed following manufacturer's instructions.

Binding assay

Activin A binding was quantified using a luciferase based bioassay. Briefly, HEK293 cells containing a (CAGA) 12-luciferase reporter (as described in 30) were stimulated with 0.2 nM activin A and co-treated with a concentration range of activin A inhibitors. After 24

hours cells were lysed and luciferase signal was measured in a microplate reader (Wallac 1420 victor2, PerkinElmer, MA, USA). The corresponding dose-response curves were analyzed and the half maximal inhibitory concentration (IC50) calculated using GraphPad Prism v5.01 software (GraphPad PRISM, Inc, California Corporation, CA, USA).

Western blot analysis

Serum-starved 143B/*lacZ*/mCherry cells were pre-incubated under tissue culture conditions for 1 hour with or without FST_{315} (10 nM, 100 nM), FST_{315}ΔHBS-hFc (10 nM, 100 nM) or ActRⅡA-mFc (10 nM, 100 nM). Cells were then stimulated with 2 nM activin A (# 338-AC, R&D systems, Minneapolis, MN, USA) for 15 minutes.

CD14-positive PBMC were differentiated into pre-osteoclasts for 7 days in the presence of m-CSF (25 ng/ml, #216-MC, R&D Systems, MD, USA) and RANKL (60 ng/ml, #310-01, Peprotech Inc., Rocky Hill, USA) under tissue culture conditions. On day 7, pre-osteoclasts were starved for 6 hours in tissue culture medium without FCS and then pre-incubated for 1 hour with or without FST_{315} (100 nM), FST_{315}ΔHBS-hFc (100 nM) or ActRIIA-mFc (100 nM) and stimulated for 60 minutes with 2 nM activin A.

The preparation of protein extracts and western blot analysis were performed as previously described (31). Phospho-Smad2 (1:1000, #3108, Cell Signaling, Boston, USA), total Smad2 and Smad3 (1:1000, #8685, Cell Signaling), GAPDH (1:3000, FL-335, Santa Cruz Biotechnologies, Dallas, Texas, USA) and HRP-conjugated secondary antibody (1:1000, sc-2054, Santa Cruz Biotechnologies) were used.

Cell viability assay

143B/*lacZ*/mCherry cells were seeded in 96-well plates (750 cells/well) and allowed to adhere overnight. The cells were then incubated in triplicates with activin A and/or FST_{315}, FST_{315}ΔHBS-hFc, ActRⅡA-mFc, ZOL and their combination FST_{315}ΔHBS-hFc/ZOL or ActRⅡA-mFc/ZOL at indicated concentrations for 48 hours. Cell viability was measured with the WST-1 assay (#05015944001, Roche, Basel, Switzerland) according to the manufacturer's protocol.

Migration assay

Cells were seeded into 6-well plates; when confluency reached 90%, cells were starved for 12 hours with tissue culture medium containing 1% FCS. On the confluent cells, tissue culture medium (containing 1% FCS) with or without activin A (0.5 nM or 2 nM activin

A) was added to the wells. Six wounds per well, in duplicate, were applied and the migration rate assessed as previously described (32).

PBMC differentiation into TRAP-positive large multinucleated cells

CD14-positive cells (60`000 cells/well in a 96 well plate) were differentiated with m-CSF (25 ng/ml, #216-MC, R&D Systems, MD, USA) and soluble RANKL (60 ng/ml, #310-0, Peprotech Inc., Rocky Hill, USA) as described (33). From day 4 onwards, activin A (0.5 nM), FST_{315} (100 nM), FST_{315}ΔHBS-hFc (100 nM), ActRⅡA-mFc (100 nM), ZOL (0.5 µM) and their combination FST_{315}ΔHBS-hFc and ZOL or ActRⅡA-mFc and ZOL were added to the tissue culture medium.

Following fixation, tartrate-resistant acid phosphatase (TRAP) histochemistry was performed by incubating the cells with 0.2 M acetate buffer for 20 minutes at RT. Cells were then incubated with 0.5 mg/ml naphtol AS-MX phosphate (#855, Sigma Aldrich) and 1.1 mg/ml Fast Red TR Salt (# F8764, Sigma Aldrich) in the presence of 50 mM sodium tartrate for 1 hour at 37°C and then washed with PBS and stained with Hoechst (#H3570, Life Technologies, Carlsbad, USA, 1:10`000, 10 minutes, RT). Wells were photographed in quadruplicate and the number of TRAP-positive, huge multinucleated osteoclasts (approx. 100-200 µm) were determined with ImageJ software (http://rsb.info.nih.gov/ij/).

Osteoclast resorption activity

Osteoclast resorption activity was measured using an OsteoLyse™ Assay Kit (#PA-1500, Lonza, Basel, Switzerland). Osteoclast precursors (#2T-110, Lonza) were seeded following the manufacturer's protocol at a density of 10'000 cells/well on an 96-well OsteoLyse™ cell culture plate coated with fluorophore-derivatized human bone matrix in differentiation medium (OCP BulletKit, #PT-8201, #PT-9501) and differentiated, following the manufacturer`s protocol. Precursors without RANKL served as undifferentiated controls. On day 6, the differentiation medium was replaced and activin A (0.5 nM), with or without FST_{315} (100 nM), FST_{315}ΔHBS-hFc (100 nM), ActRⅡA-mFc (100 nM), ZOL (50 nM) or their combination FST_{315}ΔHBS-hFc and ZOL or ActRⅡA-mFc and ZOL was added. On day 10 resorption activity was measured following manufacturer`s instructions. Results were displayed as relative fluorescence unit (RFU).

Intratibial human xenograft osteosarcoma mouse model

All *in vivo* studies were conducted with approval of the Veterinary Office Kanton Zurich, Switzerland (animal application license 42/2013) and in accordance with the

guidelines of the Swiss Federal Veterinary Office. Eleven-week-old female SCID (C.B-17/lcr Prkdc$^{scid/scid}$) mice were obtained from Charles River Laboratories (Sulzfeld, Germany) and kept for a 10 day acclimation period before tumor cell injection (TCI). For orthotopic TCIs, mice were intratibially (i.t) injected with 10^5 143B/*lacZ*/mCherry cells as previously described (34). Mice were randomized according to their weight into the following six experimental groups and injected one week after TCI with vehicle (KPO_4, 100 µl, n=11), FST_{315}ΔHBS-hFc (biweekly, intraperitoneally (i.p.), 10 mg/kg, n=11), ActR‖A-mFc (biweekly, i.p., 10mg/kg, n=10), ZOL and KPO_4 (biweekly, subcutaneously (s.c.), 100 µg/kg, n=11), FST_{315}ΔHBS-hFc (biweekly, i.p., 10 mg/kg) plus ZOL (biweekly, s.c., 100 µg/kg) (n=12) or ActR‖A-mFc (biweekly, i.p., 10 mg/kg) plus ZOL (biweekly, s.c., 100 µg/kg) (n=11).

Tumor growth in all mice was monitored by caliper measurements as described (34). All mice were sacrificed 34 days after TCI, lungs were *in situ* perfused and lung surface metastasis counted as previously described (35). All major organs and the tumor tissue were dissected, snap-frozen in liquid nitrogen or placed into 4% paraformaldehyde/PBS until analysis.

IVIS optical imaging

In vivo fluorescence imaging was performed for the visualization of mCherry-expressing 143B cells within the intratibial primary tumors. Mice were monitored weekly using the IVIS Lumina XR (PerkinElmer) under gas anaesthesia (2-5% isoflurane). Epi-fluorescence (excitation 605 nm, emission 660, 680 and 700 nm,) was analyzed using Living Image v4.4 software (PerkinElmer). Epi-fluorescence is indicated as radiant efficiency (p/sec/cm^2/sr)/(µW/cm^2).

Micro–computed tomography analysis

Animals were anesthetized (2-5% isoflurane/O_2). Hind limbs of mice were scanned in the Bruker/SkyScan-1176 *in vivo* X-ray micro–computed tomography (µCT) in supine position (Bruker, MA, USA). µCT scanning was commenced with a voxel size of 17 µm, source voltage of 50 kV, source current of 500 µA, exposure of 290 ms with a rotation step of 0.8 degrees. Three-dimensional datasets were generated using Cone-Beam reconstruction (NRecon v1.6.9.18.SkyScan/Bruker). A region of interest (ROI) of the tibia was manually selected (CtAnalyser v1.13.11.0, Bruker/Skyscan), starting from the tibial plateau until the point in the distal tibia where the fibula and tibial bones converge. After segmentation of the ROI, the amount of bone volume (BV, in mm^3) was calculated.

Alkaline Phosphatase (ALP) Assay

ALP assay was performed using a fluorometric Alkaline Phosphatase Assay (ALP) Kit (ab83371, Abcam) following manufacturer's instructions. Fluorescence (Ex/Em = 360/440 nm) was measured in a Spectramax Gemini XS plate reader (Molecular Devices, Sunnyvale, CA). ALP activity was calculated using the following formula: ALP activity = A/T (mU/min), with A = amount of 4-methylumbelliferone (4-MU) generated, T = reaction time in minutes and normalized to the total protein concentration in the tissue lysates.

Assessment of tumor necrosis

Upon sacrifice, the tumor in the hind limb was cut in half along the longitudinal axis, fixed in 4% buffered paraformaldehyde for 2 days and decalcified for 2 weeks using Osteosoft (# 101728, Merck Millipore, Germany). After routine paraffin wax embedding, sections (3-5 µm thick) were stained with hematoxylin and eosin (HE) for histological examination. The amount of tumor necrosis was scored in the HE-stained, blindly labeled slides by a veterinary pathologist, as follows: Grade 0: no necrosis; Grade 1: necrosis below 20% of the total tumor surface; Grade 2: necrosis greater than 20% but less than 40%; Grade 3: necrosis greater than 40% but less than 60%; Grade 4: necrosis greater than 60% but less than 80%; and Grade 5: necrosis greater than 80%.

Quantitative real-time PCR

mRNA isolation from 143B cell line derived primary tumor tissue was performed with an RNeasy Plus Universal Mini Kit (#73404, Qiagen, Valencia, CA, USA, catalogue # 73404) following manufacturer`s guidelines. Purified mRNA was reverse-transcribed into cDNA using the high-capacity cDNA reverse transcription kit (# 4368814, Applied Biosystems, Foster City, CA, USA). Quantitative real-time PCR (qRT-PCR) was quantified as previously described (36). Primers used were; murine *Cathepsin K* forward: 5'-GCACCCTTAGTCTTCCGCTC-3', reverse: 5'-ACCCACATCCTGCTGTTGAG-3'; murine *Gapdh* forward: 5'-TTGTGCAGTGCCAGCCTCGT-3', reverse: 5'-TGCAAATGGCAGCCCTGGTGA-3'.

Statistical analysis

In vitro experiments show results of three independent experiments. Results are presented as mean ± standard error of the mean (SEM). All results were analyzed using GraphPad Prism v5.01 software (GraphPad PRISM, Inc, California Corporation). One-way ANOVA analysis was used when comparing a variable in three and more groups with

indicated post hoc analysis. Two-way repeated measures analysis was performed when comparing two categorical independent, repeatedly measured variables, with Bonferroni post hoc analysis. $P < 0.05$ was considered statistically significant.

Results

Activin A serum levels

In order to investigate the clinical significance of circulating activin A levels in osteosarcoma patients (OS), we compared their activing A serum levels to the levels of healthy individuals (HI). The overall comparison between HI and OS revealed a tendency for increased serum activin A levels (Fig. 1A). The clinical data of patients and healthy individuals are presented in Fig. 2B.

Activin A and its inhibitors in osteosarcoma cells

Activin A is secreted by cells within the osteosarcoma microenvironment, such as osteoblasts, osteoclasts and bone marrow stromal cells (13). Here, we demonstrated that osteosarcoma cell lines 143B, SaOS-2 and K7M2 also secrete significant amounts of activin A into their culture supernatant (Fig. 2A).

To block activin A, the FST_{315}, a FST_{315}-based fusion protein $FST_{315}\Delta HBS$-hFc and a soluble decoy receptor ActR‖A-mFc were used and their binding capacities shown using a luciferase reporter assay. The IC_{50} concentrations are displayed for all activin A inhibitors and show similar binding abilities within the pM range for activin A, without significant differences (Fig. 2B).

Activin A induced intracellular Smad2 phosphorylation within 15 minutes in 143B osteosarcoma cells and upon pre-incubating for 1 hour with FST_{315}, $FST_{315}\Delta HBS$-hFc or ActR‖A-mFc, Smad2 phosphorylation was evidently inhibited (Fig. 2C). Nonetheless, 48 hour long treatment with activin A inhibitors had no effect on cell viability in 143B cells, whereas the incubation with ZOL resulted in a dose-related inhibition of cell viability (Fig. 2D). Similar data was obtained for K7M2 and SaOS-2 osteosarcoma cell lines (Supplementary Fig. S1A, B). Also, the cell migration of 143B was not affected by activin A stimulation (Fig. 2E).

Collectively, functional binding efficacy for both activin A inhibitors was shown, with no direct effects on cell viability or migratory behavior of osteosarcoma cells. Therefore, the subsequent *in vitro* experiments consequently focused on the tumor microenvironment.

FST_{315}ΔHBS-hFc and ActRⅡA-mFc inhibit osteoclast differentiation *in vitro*

Because activin A has been reported to induce osteoclastogenesis (15), we investigated differentiation of human CD14-positive PBMC towards multinucleated TRAP-positive osteoclasts, in the presence or absence of activin A, and FST_{315}, FST_{315}ΔHBS-hFc, ActRⅡA-mFc or ZOL. Activin A significantly ($P < 0.001$) increased the number of multinucleated TRAP-positive osteoclasts, whereas FST_{315}, FST_{315}ΔHBS-hFc, ActRⅡA-mFc reversed activin A induced osteoclastogenesis. Furthermore, the combination of ZOL with FST_{315}ΔHBS-hFc or ActRⅡA-mFc additionally inhibited osteoclastogenesis, compared to the control condition (i.e., only RANKL and m-CSF) and not only in relation to the activin A-enhanced osteoclastogenesis (Fig. 3A, B). We next investigated the involvement of intracellular Smad signaling proteins in activin A induced osteoclastogenesis. Activin A induced Smad2 phosphorylation in a time-dependent manner in pre-osteoclasts (Supplementary Fig. S2) and activin A inhibitors impeded the activin A induced Smad phosphorylated within pre-osteoclasts (Fig. 3C).

Resorption activity of osteoclasts, on the other side, measured on human collagen coated plates, remained unchanged upon activin A stimulation (Fig. 3D) and consequently, FST_{315}, FST_{315}ΔHBS-hFc, ActRⅡA-mFc had no effect on the resorption activity of the osteoclasts. Osteoclasts treated with ZOL showed a clear reduction in their collagen resorbing activity.

In conclusion, activin A induced intracellular Smad2 phosphorylation in pre-osteoclasts and promoted osteoclastogenesis without affecting osteoclast activity. The activin inhibitors with or without ZOL successfully inhibited osteoclastogenesis, but did not affect the resorptive activity of osteoclasts.

Activin A inhibition and ZOL treatment reduces osteosarcoma tumor growth in an orthotopic osteosarcoma mouse model

The impact of FST_{315}ΔHBS-hFc, ActRⅡA-mFc, and ZOL treatment on the tumor and its microenvironment was investigated in a metastatic, orthotopic xenograft osteosarcoma mouse model. The highly metastatic human 143B/*lacZ*/mCherry cells were injected into the left tibia of SCID mice (Fig. 4A, left panel). IVIS imaging exposed that all mice developed a viable tumor one week after tumor cell injection (TCI) (Fig. 4A, right panel), therefore, treatment was started and mice were injected with either FST_{315}ΔHBS-hFc, ActRⅡA-mFc, ZOL or their combination FST_{315}ΔHBS-hFc/ZOL, ActRⅡA-mFc/ZOL according to the previously described treatment schedule. To verify stable serum levels over the treatment

period, FST_{315}ΔHBS-hFc and ActRⅡA-mFc levels measured at day 5, 12 and 19 of the treatment revealed stable serum levels throughout the study (Supplementary Fig. S3A, B).

After three weeks of treatment with activin A inhibitors and ZOL, significantly smaller tumors were observed both in the ZOL (-59.8%) treated and the combination treated groups FST_{315}ΔHBS-hFc/ZOL (-62%), ActRⅡA-mFc/ZOL (-83.6%) compared to the control group (KPO_4) set as 100%. Continuation of treatment considerably inhibited tumor growth in all treated groups ($P < 0.001$). At the end of the treatment, single compound treated mice showed significantly smaller tumor volumes compared to that of the KPO_4 treated mice (FST_{315}ΔHBS-hFc -46%, ActRⅡA-mFc -36.5%, ZOL -48%, $P < 0.001$). The single arm treatment efficiency was confirmed in a second *in vivo* study (data not shown). Mice injected with the combination of activin A inhibitor and ZOL displayed the smallest tumor volume compared to the control group (FST_{315}ΔHBS-hFc/ZOL -66.1%, ActRⅡA-mFc/ZOL -77.5%). Furthermore, the ActRIIA-mFc/ZOL treated mice developed also a significantly smaller tumor volume compared to the single compound ActRIIA-mFC- and ZOL- treated mice (-64%, resp. -56.8%, $P < 0.01$) (Fig. 4B).

Taken together, activin A inhibitors alone had a significant impact on osteosarcoma tumor development, and the combination with ZOL further reduced tumor growth.

The effect of activin A inhibition and ZOL treatment on pulmonary metastases

Mice treated with FST_{315}ΔHBS-hFc and ActRIIA-mFc (with and without ZOL co-treatment) showed a tendency for reduced pulmonary metastatic spread. However, a statistically significantly (Plower number of metastases was observed in the ZOL (56 ± 17, $P < 0.05$) and in the ActRIIA-mFC/ZOL (16.14 ± 4.9, $P < 0.01$) treated groups when compared to the KPO_4 treated control group (269 ± 100.8) (Fig. 4C, D).

The combination of activin A inhibition and ZOL treatment leads to tumor necrosis

Microscopically, the primary tumor tissue consisted of large areas of bone and soft tissue effacement associated with infiltrating neoplastic osteosarcoma cells exhibiting numerous mitotic figures, prominent anisocytosis, cellular atypia and a variable amount of necrosis. This was represented either by multifocal scattered small groups of necrotic neoplastic cells or more discrete, confluent areas of necrosis, infiltrated by neutrophils.

Histological responses to the combination (FST_{315}ΔHBS-hFc/ZOL and ActRⅡA-mFc/ZOL) and single ZOL treatments were characterized by higher amounts of necrosis within the primary tumors as compared to those observed in osteosarcomas exposed to the

activin inhibitors or the vehicle-controls (Fig. 5A, B), indicating a direct cytotoxic effect of ZOL.

Activin A inhibition and ZOL impedes tumor-associated bone remodeling in an orthotopic osteosarcoma mouse model

An intramedullary injection of 143B osteosarcoma cells results mainly in an osteolytic phenotype, however, both osteolytic and osteoblastic lesions are present. Representative µCT images of the tumor bearing hind limbs show the presence of these osteolytic lesions (Fig. 6A).

Following four weeks of treatment, all treated groups demonstrated a significantly higher bone volume compared to the vehicle treated KPO_4 group (Fig. 6B). Extensive pathological bone remodeling in the vehicle treated groups was observed, with a 28% reduction of bone volume compared to the initiation of the treatment. The activin A inhibitors, ZOL or combination treated groups showed a diminished loss of bone volume (FST_{315}ΔHBS-hFc -21%, ActR⅄A-mFc -6%) or even an increase in the ZOL (+21%), FST_{315}ΔHBS-hFc/ZOL (+18%) and ActR⅄A-mFc/ZOL (+21%) treated mice compared to the beginning of their treatment (Fig. 6B).

Histological analysis revealed that in all groups the originally intramedullary tumor cells had infiltrated and effaced the cortical bone, expanding into the adjacent soft tissues. Localized or multifocal formation of new bone was evident at the periosteal, and, to a lesser extent, at the endosteal surface in all compound-treated groups (Fig. 6C), confirming the mixed bone phenotype of this model.

To further confirm the increase of anabolic activity in the tumor-bone microenvironment, alkaline phosphatase (ALP) activity, an important indicator for bone mineralization (37), was determined in tissue extracts of tumor-bearing hind limbs. ALP levels had a propensity for higher activity in the single-compound treated groups (FST_{315}ΔHBS-hFc, ActR⅄A-mFc and ZOL) with a significant increase in activity in the combination treated groups FST_{315}ΔHBS-hFc/ZOL and ActR⅄A-mFc/ZOL ($P < 0.01$) (Fig. 6D). Furthermore, comparative gene expression analysis of the primary tumor tissue showed a downregulation of the key enzyme for osteoclast function, cathepsin K, in all treated groups compared to the KPO_4 treated group (Fig. 6E).

Thus, in line with µCT bone volume analysis and histological observations, we found evidence for increased osteoblast activity and decreased osteoclast activity upon activin A inhibition or/and ZOL treatment.

Treatment induced side effects

After four weeks of treatment, FST_{315}ΔHBS-hFc and FST_{315}ΔHBS-hFc/ZOL injected mice experienced a significant increase in body weight compared to all other treated mice ($P < 0.001$) (Supplementary Fig. S4A). Furthermore, to investigate whether the activin A-inhibiting compounds or their combination with ZOL induced additional side effects, overall histological analysis of several major organs (heart, liver, spleen, lungs, and kidneys) was performed. Additionally, we observed an increase in extramedullary hematopoiesis (EMH) in the spleen in ActRⅡA-mFc and ActRⅡA-mFc/ZOL treated mice (Supplementary Fig. S4B, C).

These observations point towards a safe application of both activin A inhibitors and ZOL or their combination.

Discussion

Osteosarcoma is a highly aggressive cancer, associated with destruction of the bone, so called tumor-associated bone remodeling (5, 6). Illuminating the function of activin A in the interaction between the tumor, the bone and its `vicious cycle`, may give new insights in the cancerogenesis of osteosarcoma, as current understanding is still limited.

In this study, we showed a tumor promoting role of activin A in osteosarcoma, through altering the `vicious cycle` between bone remodeling and osteosarcoma tumor growth. The effects of the activin A inhibitors FST_{315}ΔHBS-hFc, ActRⅡA-mFc and the bisphosphonate ZOL were compared *in vitro* on osteosarcoma cells and osteoclasts, and *in vivo* as a potential novel therapeutic approach against osteosarcoma tumor growth in a clinically relevant model. Our data supports the importance of activin A in the osteosarcoma microenvironment, as its inhibition altered the osteolytic phenotype in our intratibial xenograft osteosarcoma mouse model and caused a significant reduction of tumor growth *in vivo*. Finally, we showed another benefit of a combination therapy of activin A inhibitors and ZOL, which exhibited the highest treatment efficacy.

In contrast to the findings of elevated activin A serum levels in breast and prostate cancer patients with bone metastases, compared to patients without metastases (19), we could not detect statistical differences in activin A serum levels between osteosarcoma patients and healthy individuals. Due the rarity of this disease, with an incidence of three to five per million per year in the general population (1), the number of patients analyzed was low; nevertheless, a higher number of patients may turn the tendency into significance.

Both, the engineered FST analogue and a soluble decoy activin type 2 receptor were shown to effectively bind activin A and block intracellular phosphorylation of Smad2 in osteosarcoma cells *in vitro*. Nevertheless, the neutralization of activin A did not inhibit cell viability or migration in 143B cells, as opposed to a previous study, in which MG63 osteosarcoma cells were depleted of activin A, leading to decreased cell proliferation and migration (18). However, our data confirmed results reporting direct cytotoxicity of ZOL (38). Furthermore, activin A has been reported to not only have tumor promoting characteristics (12, 13, 19), but also a tumor protective function in different cancers, such as liver and pancreatic cancers (39). Likewise, the effects of ZOL on tumor growth are still widely debated (26). Nonetheless, the here presented data demonstrate a tumor suppressive effect for both, activin A inhibition and ZOL treatment in osteosarcoma.

Investigation of the microenvironment revealed imbalanced bone remodeling in our osteosarcoma mouse model. Osteosarcoma usually has a mixed osteolytic and osteoblastic phenotype (3, 6), with osteoclasts and osteoblasts activity playing a substantial part. Activin A is a known inducer of osteoclastogenesis, whereas ZOL induces osteoclast apoptosis by inhibiting farnesyl pyrophosphate synthase, a key enzyme in the mevalonate pathway important for osteoclast polarization (15, 27). Our results are in line with these data; activin A induced intracellular Smad phosphorylation and osteoclastogenesis, and the inhibition of activin A demonstrated inhibition of osteoclast differentiation with both engineered activin A inhibitors. These observations were confirmed by our *in vivo* study showing an inhibition of tumor-associated osteolysis, via inhibition of osteoclastogenesis. Although osteoclast resorptive activity was not observed *in vitro*, downregulation of cathepsin K gene expression, a key enzyme in osteoclast activity, was observed *in vivo* in the tumor microenvironment. These findings are concurrent with the described association of osteoclasts and increased tumor tissue cathepsin K levels, and osteosarcoma aggressiveness (40).

The effects of activin A and ZOL on osteoblasts are more controversial, both osteoblast inhibition (41, 42) and activation (43, 44) were reported. We observed an increase in bone volume in the compound treated groups compared to the vehicle treated mice with evidence of local periosteal new bone formation. These observations are in agreement with the demonstrated increased activity of the ALP enzyme, important for osteoblast activity (37) and support reports of an inhibiting role of activin A and an activating role of ZOL on osteoblasts (41, 44). Although our model displays an osteolytic phenotype, both osteoblast and osteoclast are involved in the tumor associated bone remodeling. We therefore speculate that both activin A inhibitors and ZOL treatment would also exhibit anti-tumor effects in

predominantly osteoblastic osteosarcoma, which may be supported by a study of Labrinidis *et al.*, who demonstrated that ZOL is effective in inhibiting both osteoclastic and osteoblastic lesions in osteosarcoma (45).

Both activin A inhibition and ZOL acid treatments are reported to be well tolerated and safe (46). Nevertheless, treatment with the FST analogue led to an increase in bodyweight, possibly due to the affinity of FST to other members of the TGFβ superfamily, such as BMP and myostatin. Myostatin is known as a major negative regulator of skeletal muscle mass (47), therefore inhibition of myostatin by FST_{315}ΔHBS-hFc likely led to an increase in muscle mass, hence, to an increase in body weight (24). Also an increase in EMH was shown in soluble ActRIIA treated mice, which has been previously reported to induce erythropoiesis and red blood cell formation and to have beneficial outcome for anemic patients (48). The observed side effects are not undesirable, as osteosarcoma is associated with anemia and cancer cachexia, those patients might therefore additionally benefit from an activin A inhibition treatment (49, 50).

In conclusion, this study supports the important role of the `vicious cycle` between osteosarcoma and its bone microenvironment, with activin A as one of its main components. Inhibition of activin A and ZOL treatment led to a disturbed microenvironment for the tumor to grow and spread. Therefore, their combination might be a particularly effective treatment approach, assumed to work via independent pathways, by inducing a disruption of tumor-associated bone remodeling and by having direct and systemic anti-cancer effects. The exact molecular mechanisms of activin A action in osteosarcoma tumor progression still remain unknown and need to be further elucidated.

Acknowledgements

The authors thank Matthias JE Arlt for his help with intratibial injections of tumor cells. This study was supported by the University of Zurich, the Schweizerischer Verein Balgrist (Zurich, Switzerland), the Walter L. & Johanna Wolf Foundation (Zurich, Switzerland), the Highly Specialized Medicine for Musculoskeletal Oncology program of the Canton of Zurich, the Zurcher Krebsliga (Zurich, Switzerland), the “Kind und Krebs” fund (Zollikerberg, Switzerland), and the Swiss National Science Foundation SNF Nr.310030_149649.

Authors' Contributions

Conception and design: DM, SMB, WB, BF; Development of methodology: DM, SMB, AG; Acquisition of data: DM, GP, SMB, ME, ON; Analysis and interpretation of data (e.g. statistical analysis, biostatistics, computational analysis): DM, GP, SMB; Writing, review, and/or revision of the manuscript: DM, SMB, GP, AG, ME, BF, ON; Study supervision: SMB, BF.

References

1. Mirabello L, Troisi RJ, Savage SA. Osteosarcoma incidence and survival rates from 1973 to 2004: data from the Surveillance, Epidemiology, and End Results Program. Cancer. 2009;115:1531-43.
2. Trends in childhood cancer mortality--United States, 1990-2004. MMWR Morb Mortal Wkly Rep. 2007;56:1257-61.
3. Klein MJ, Siegal GP. Osteosarcoma: anatomic and histologic variants. Am J Clin Pathol. 2006;125:555-81.
4. Crockett JC, Rogers MJ, Coxon FP, Hocking LJ, Helfrich MH. Bone remodelling at a glance. Journal of cell science. 2011;124:991-8.
5. Garimella R, Washington L, Isaacson J, Vallejo J, Spence M, Tawfik O, et al. Extracellular Membrane Vesicles Derived from 143B Osteosarcoma Cells Contain Pro-Osteoclastogenic Cargo: A Novel Communication Mechanism in Osteosarcoma Bone Microenvironment. Transl Oncol. 2014;7:331-40.
6. Akiyama T, Dass CR, Choong PF. Novel therapeutic strategy for osteosarcoma targeting osteoclast differentiation, bone-resorbing activity, and apoptosis pathway. Mol Cancer Ther. 2008;7:3461-9.
7. Mundy GR. Metastasis to bone: causes, consequences and therapeutic opportunities. Nature reviews Cancer. 2002;2:584-93.
8. Abe M, Hiura K, Wilde J, Shioyasono A, Moriyama K, Hashimoto T, et al. Osteoclasts enhance myeloma cell growth and survival via cell-cell contact: a vicious cycle between bone destruction and myeloma expansion. Blood. 2004;104:2484-91.
9. Redini F, Heymann D. Bone Tumor Environment as a Potential Therapeutic Target in Ewing Sarcoma. Front Oncol. 2015;5:279.
10. David E, Blanchard F, Heymann MF, De Pinieux G, Gouin F, Redini F, et al. The Bone Niche of Chondrosarcoma: A Sanctuary for Drug Resistance, Tumour Growth and also a Source of New Therapeutic Targets. Sarcoma. 2011;2011:932451.
11. Chantry AD, Heath D, Mulivor AW, Pearsall S, Baud'huin M, Coulton L, et al. Inhibiting activin-A signaling stimulates bone formation and prevents cancer-induced bone destruction in vivo. J Bone Miner Res. 2010;25:2633-46.
12. Leto G. Activin A and bone metastasis. J Cell Physiol. 2010;225:302-9.
13. Vallet S, Mukherjee S, Vaghela N, Hideshima T, Fulciniti M, Pozzi S, et al. Activin A promotes multiple myeloma-induced osteolysis and is a promising target for myeloma bone disease. Proc Natl Acad Sci U S A. 2010;107:5124-9.
14. Xia Y, Schneyer AL. The biology of activin: recent advances in structure, regulation and function. J Endocrinol. 2009;202:1-12.
15. Fuller K, Bayley KE, Chambers TJ. Activin A is an essential cofactor for osteoclast induction. Biochem Biophys Res Commun. 2000;268:2-7.
16. Alves RD, Eijken M, Bezstarosti K, Demmers JA, van Leeuwen JP. Activin A suppresses osteoblast mineralization capacity by altering extracellular matrix (ECM) composition and impairing matrix vesicle (MV) production. Mol Cell Proteomics. 2013;12:2890-900.
17. Kang HY, Huang HY, Hsieh CY, Li CF, Shyr CR, Tsai MY, et al. Activin A enhances prostate cancer cell migration through activation of androgen receptor and is overexpressed in metastatic prostate cancer. Journal of bone and mineral research : the official journal of the American Society for Bone and Mineral Research. 2009;24:1180-93.
18. Zhu J, Liu F, Wu Q, Liu X. Activin A regulates proliferation, invasion and migration in osteosarcoma cells. Mol Med Rep. 2015;11:4501-7.

19. Leto G, Incorvaia L, Badalamenti G, Tumminello FM, Gebbia N, Flandina C, et al. Activin A circulating levels in patients with bone metastasis from breast or prostate cancer. Clin Exp Metastasis. 2006;23:117-22.
20. Terpos E, Kastritis E, Christoulas D, Gkotzamanidou M, Eleutherakis-Papaiakovou E, Kanellias N, et al. Circulating activin-A is elevated in patients with advanced multiple myeloma and correlates with extensive bone involvement and inferior survival; no alterations post-lenalidomide and dexamethasone therapy. Ann Oncol. 2012.
21. Pearsall RS, Canalis E, Cornwall-Brady M, Underwood KW, Haigis B, Ucran J, et al. A soluble activin type IIA receptor induces bone formation and improves skeletal integrity. Proc Natl Acad Sci U S A. 2008;105:7082-7.
22. Lonardo E, Hermann PC, Mueller MT, Huber S, Balic A, Miranda-Lorenzo I, et al. Nodal/Activin signaling drives self-renewal and tumorigenicity of pancreatic cancer stem cells and provides a target for combined drug therapy. Cell Stem Cell. 2011;9:433-46.
23. Ogino H, Yano S, Kakiuchi S, Muguruma H, Ikuta K, Hanibuchi M, et al. Follistatin suppresses the production of experimental multiple-organ metastasis by small cell lung cancer cells in natural killer cell-depleted SCID mice. Clin Cancer Res. 2008;14:660-7.
24. Datta-Mannan A, Yaden B, Krishnan V, Jones BE, Croy JE. An engineered human follistatin variant: insights into the pharmacokinetic and pharmocodynamic relationships of a novel molecule with broad therapeutic potential. J Pharmacol Exp Ther. 2013;344:616-23.
25. Ory B, Heymann MF, Kamijo A, Gouin F, Heymann D, Redini F. Zoledronic acid suppresses lung metastases and prolongs overall survival of osteosarcoma-bearing mice. Cancer. 2005;104:2522-9.
26. Coleman R. The use of bisphosphonates in cancer treatment. Ann N Y Acad Sci. 2011;1218:3-14.
27. Dunford JE, Thompson K, Coxon FP, Luckman SP, Hahn FM, Poulter CD, et al. Structure-activity relationships for inhibition of farnesyl diphosphate synthase in vitro and inhibition of bone resorption in vivo by nitrogen-containing bisphosphonates. J Pharmacol Exp Ther. 2001;296:235-42.
28. Kumar RM, Arlt MJ, Kuzmanov A, Born W, Fuchs B. Sunitinib malate (SU-11248) reduces tumour burden and lung metastasis in an intratibial human xenograft osteosarcoma mouse model. Am J Cancer Res. 2015;5:2156-68.
29. Sidis Y, Schneyer AL, Keutmann HT. Heparin and activin-binding determinants in follistatin and FSTL3. Endocrinology. 2005;146:130-6.
30. Dennler S, Itoh S, Vivien D, ten Dijke P, Huet S, Gauthier JM. Direct binding of Smad3 and Smad4 to critical TGF beta-inducible elements in the promoter of human plasminogen activator inhibitor-type 1 gene. EMBO J. 1998;17:3091-100.
31. Gvozdenovic A, Arlt MJ, Campanile C, Brennecke P, Husmann K, Li Y, et al. CD44 enhances tumor formation and lung metastasis in experimental osteosarcoma and is an additional predictor for poor patient outcome. Journal of bone and mineral research : the official journal of the American Society for Bone and Mineral Research. 2013;28:838-47.
32. Steinmann P, Walters DK, Arlt MJ, Banke IJ, Ziegler U, Langsam B, et al. Antimetastatic activity of honokiol in osteosarcoma. Cancer. 2012;118:2117-27.
33. Susa M, Luong-Nguyen NH, Cappellen D, Zamurovic N, Gamse R. Human primary osteoclasts: in vitro generation and applications as pharmacological and clinical assay. Journal of translational medicine. 2004;2:6.

34. Sabile AA, Arlt MJ, Muff R, Bode B, Langsam B, Bertz J, et al. Cyr61 expression in Osteosarcoma indicates poor prognosis and promotes intratibial growth and lung metastasis in mice. J Bone Miner Res. 2011.
35. Arlt MJ, Born W, Fuchs B. Improved Visualization of Lung Metastases at Single Cell Resolution in Mice by Combined In-situ Perfusion of Lung Tissue and X-Gal Staining of lacZ-Tagged Tumor Cells. J Vis Exp. 2012.
36. Ram Kumar RM, Betz MM, Robl B, Born W, Fuchs B. DeltaNp63alpha enhances the oncogenic phenotype of osteosarcoma cells by inducing the expression of GLI2. BMC Cancer. 2014;14:559.
37. Hessle L, Johnson KA, Anderson HC, Narisawa S, Sali A, Goding JW, et al. Tissue-nonspecific alkaline phosphatase and plasma cell membrane glycoprotein-1 are central antagonistic regulators of bone mineralization. Proceedings of the National Academy of Sciences of the United States of America. 2002;99:9445-9.
38. Kubista B, Trieb K, Sevelda F, Toma C, Arrich F, Heffeter P, et al. Anticancer effects of zoledronic acid against human osteosarcoma cells. J Orthop Res. 2006;24:1145-52.
39. Risbridger GP, Schmitt JF, Robertson DM. Activins and inhibins in endocrine and other tumors. Endocr Rev. 2001;22:836-58.
40. Avnet S, Longhi A, Salerno M, Halleen JM, Perut F, Granchi D, et al. Increased osteoclast activity is associated with aggressiveness of osteosarcoma. International journal of oncology. 2008;33:1231-8.
41. Eijken M, Swagemakers S, Koedam M, Steenbergen C, Derkx P, Uitterlinden AG, et al. The activin A-follistatin system: potent regulator of human extracellular matrix mineralization. FASEB J. 2007;21:2949-60.
42. Basso FG, Silveira Turrioni AP, Hebling J, de Souza Costa CA. Zoledronic acid inhibits human osteoblast activities. Gerontology. 2013;59:534-41.
43. Gaddy-Kurten D, Coker JK, Abe E, Jilka RL, Manolagas SC. Inhibin suppresses and activin stimulates osteoblastogenesis and osteoclastogenesis in murine bone marrow cultures. Endocrinology. 2002;143:74-83.
44. Koch FP, Merkel C, Al-Nawas B, Smeets R, Ziebart T, Walter C, et al. Zoledronate, ibandronate and clodronate enhance osteoblast differentiation in a dose dependent manner--a quantitative in vitro gene expression analysis of Dlx5, Runx2, OCN, MSX1 and MSX2. J Craniomaxillofac Surg. 2011;39:562-9.
45. Labrinidis A, Hay S, Liapis V, Ponomarev V, Findlay DM, Evdokiou A. Zoledronic acid inhibits both the osteolytic and osteoblastic components of osteosarcoma lesions in a mouse model. Clin Cancer Res. 2009;15:3451-61.
46. Rosen LS, Gordon D, Tchekmedyian NS, Yanagihara R, Hirsh V, Krzakowski M, et al. Long-term efficacy and safety of zoledronic acid in the treatment of skeletal metastases in patients with nonsmall cell lung carcinoma and other solid tumors: a randomized, Phase III, double-blind, placebo-controlled trial. Cancer. 2004;100:2613-21.
47. Lee SJ, McPherron AC. Regulation of myostatin activity and muscle growth. Proc Natl Acad Sci U S A. 2001;98:9306-11.
48. Carrancio S, Markovics J, Wong P, Leisten J, Castiglioni P, Groza MC, et al. An activin receptor IIA ligand trap promotes erythropoiesis resulting in a rapid induction of red blood cells and haemoglobin. Br J Haematol. 2014;165:870-82.
49. Tisdale MJ. Cachexia in cancer patients. Nature reviews Cancer. 2002;2:862-71.
50. Hockenberry MJ, Hinds PS, Barrera P, Billups C, Rodriguez-Galindo C, Tan M, et al. Incidence of anemia in children with solid tumors or Hodgkin disease. J Pediatr Hematol Oncol. 2002;24:35-7.

Figure Legends

Figure 1. Analysis of activing A circulating levels in osteosarcoma patients and healthy individuals. (A) Serum levels of activin A (pg/ml) in osteosarcoma (OS) patients and healthy individuals (HI) assessed by ELISA. Results are presented as scatter dot plot. (B) Clinical characteristics of osteosarcoma patients and healthy individuals.

Figure 2. The activin A system and its inhibition. (A) Activin A secretion by different OS cell lines determined in the supernatant by ELISA (results are presented as mean ± SEM). (B) Binding assay in HEK/CAGA/luc cells with activin A (0.2 nM) and FST_{315}, FST_{315}ΔHBS-hFc and ActRIIA-mFc. Luciferase activity was measured and IC_{50}s of the three activin A inhibitory compounds indicated in pM. (C) Blockage of the activin induced Smad2 phosphorylation in 143B osteosarcoma cells using FST315 (100 nM), FST315ΔHBS-hFc (100 nM) or ActRIIA-mFc (100 nM). Protein expression of phosphorylated Smad2 and total Smad2 (upper black arrow) and 3 (lower black arrow) and GAPDH was assessed by Western blot. (D) Cell viability of 143B/*lacZ*/mCherry cells treated with either activin A, FST_{315}, FST_{315}ΔHBS-hFC, ActRIIA-mFC, or ZOL at indicated concentrations (results are presented as mean ± SEM). (E) Effects of activin A on 143B/*lacZ*/mCherry cell migration at indicated concentrations (results are presented as mean ± SEM).

Figure 3. Activin inhibitors impede osteoclast differentiation and induce intracellular Smad phosphorylation. (A) CD14-positive PBMC were differentiated into TRAP-positive huge (approx. 100-200 µm) multinucleated osteoclasts in the presence of m-CSF (25 ng/ml), RANKL (30-60 ng/ml), activin A (0.5 nM) and with either FST_{315}, FST_{315}ΔHBS-hFc (100 nM), ActRIIA-mFc (100 nM) or ZOL (0.5 µM) or their combination FST_{315}ΔHBS-hFc and ZOL, ActRIIA-mFc and ZOL. Numbers of TRAP-positive huge multinucleated osteoclasts were counted after 14 days of culture. Results represent mean ± SEM, *** $P < 0.01$ all groups vs. activin A treated group, ++ $P < 0.01$, + $P < 0.05$ combination groups vs. control group (1-way ANOVA, Dunnett post test). (B) Representative images of TRAP-positive huge multinucleated osteoclasts with indicated treatment, scale bar 100 µm. (C) Blockage of the activin induced Smad2 phosphorylation in pre-osteoclasts using FST_{315} (100 nM), FST_{315}ΔHBS-hFc (100 nM) or ActRIIA-mFc (100 nM). Protein expression of phosphorylated Smad2 and total Smad2 (upper black arrow) and 3 (lower black arrow) and GAPDH was assessed by Western blot. (D) Osteoclast resorption activity. Differentiated osteoclasts

cultured on a europium-conjugated collagen matrix were incubated with activin A (0.5 nM), FST_{315} (100 nM), FST_{315}-hFcΔHBS (100 nM), ActRIIA-mFc (100 nM) or ZOL (50 nM) or their combinations. Resorption activity was measured based on the released europium-conjugated collagen in the supernatant. RFU: relative fluorescence unit. Results are presented as mean ± SEM, *** $P < 0.01$, ** $P < 0.01$, * $P < 0.05$ vs. activin A treated group (1-way ANOVA, Bonferroni post test).

Figure 4. Activin inhibition and ZOL treatment reduces tumor growth in the orthotopic 143B osteosarcoma mouse model. (A) X-Ray image of the intratibial injection of metastatic 143/*lacZ*/mCherry cells into SCID mice (left panel) and a representative picture of a viable tumor by IVIS imaging of the mCherry fluorescence (right panel). (B) Intratibial tumor growth over time measured with caliper. Mice were treated with vehicle (KPO_4), FST_{315}ΔHBS-hFc, ActRIIA-mFc, ZOL or the combinations FST_{315}ΔHBS-hFc and ZOL, or ActRIIA-mFc and ZOL. Results represent the mean ± SEM, *** $P < 0.001$ treated group vs. KPO4 group, ^{oo} $P < 0.01$ FST_{315}ΔHBS-hFc/ZOL, ActRIIA-mFc/ZOL, ZOL vs. KPO4, ++ $P < 0.01$ ActRIIA-mFc /ZOL vs. single compounds ActRIIA-mFc or ZOL (2-way ANOVA, Bonferroni post-test). (C) *Ex vivo* quantification of X-Gal stained 143B/*lacZ*/mCherry derived metastatic nodules on the lung surface. Scatter dot blot with mean ± SEM, ** $P < 0.01$, * $P < 0.05$ treated group vs. KPO4 group. (D) Representative images of whole mounts of lungs of SCID mice in indicated treatment groups. Arrows indicate metastases. Scale bar, 200 µm.

Figure 5. ZOL treatment alone or in combination with activin A inhibition induces higher amounts of tumor necrosis in the orthotopic 143B osteosarcoma mouse model. (A) Representative images of 143B cell line-derived tumors sections stained for H&E. Proportions of tumor necrosis are indicated with arrowheads in the designated treatment groups. Scale bar 250 µm. (B) Summary incidence table indicating the average severity (scores 0 to 5) of necrosis in the different groups.

Figure 6. Activin A inhibition and ZOL treatment interrupted tumor associated bone remodeling in the intratibial 143B osteosarcoma mouse model. (A) Representative µCT images of tumor bearing hind limbs of SCID mice treated with KPO_4 (1), FST_{315}ΔHBS-hFc (2), ActRIIA-mFc (3), ZOL (4) or their combination FST_{315}ΔHBS-hFc and ZOL (5), ActRIIA-mFc and ZOL (6) after four weeks of treatment. Arrows indicate areas of tumor associated osteolysis of the bone. White circle indicates ROI for µCT analysis. (B) Bone volume before and after treatment with activin A inhibitors with or without addition of ZOL.

Results represent the mean ± SEM, ***P < 0.001, *P < 0.05 treated group vs. KPO4 group; 2-way ANOVA, Bonferroni post-test. (C) H&E-stained sections indicating periosteal (black arrowhead) and endosteal (white arrowhead) new bone formation in all groups, except in the vehicle-controls. BM: bone marrow cavity, scale bar 500 μm. (D) Alkaline phosphatase activity shown as 4-MU generation per mg of protein in tumor tissue extracts. Results are presented as mean ± SEM. **P < 0.01 treated group vs. KPO4 group. (E) Molecular investigation of relative gene expression of cathepsin K in tumor tissue extracts. Results presented as mean ± SEM, ***P < 0.001, **P < 0.01, *P < 0.05 treated group vs. KPO4 group (1-way ANOVA, Dunnett post-test).

A

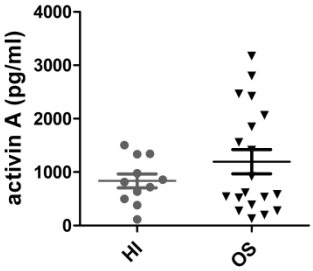

B

Clinical characteristics of osteosarcoma patients		
Gender	n= 19	%
male	11	58
female	8	42
Age	n= 19	
<10	2	10.5
10-19	10	53
20-29	4	21
30-39	2	10.5
50-59	1	5
Tumor type	n= 19	
conventional	17	89
telangiectatic	1	5.5
parosteal	1	5.5
Anatomical site	n= 19	
extremities	18	95
torso	1	5
Metastasis	n= 19	
yes	3	16
no	16	84

Clinical characteristics of healthy individuals		
Gender	n= 14	%
male	7	50
female	7	50
Age	n= 14	
20-29	7	50
30-39	5	36
40-49	1	7
50-59	1	7

Figure 1.

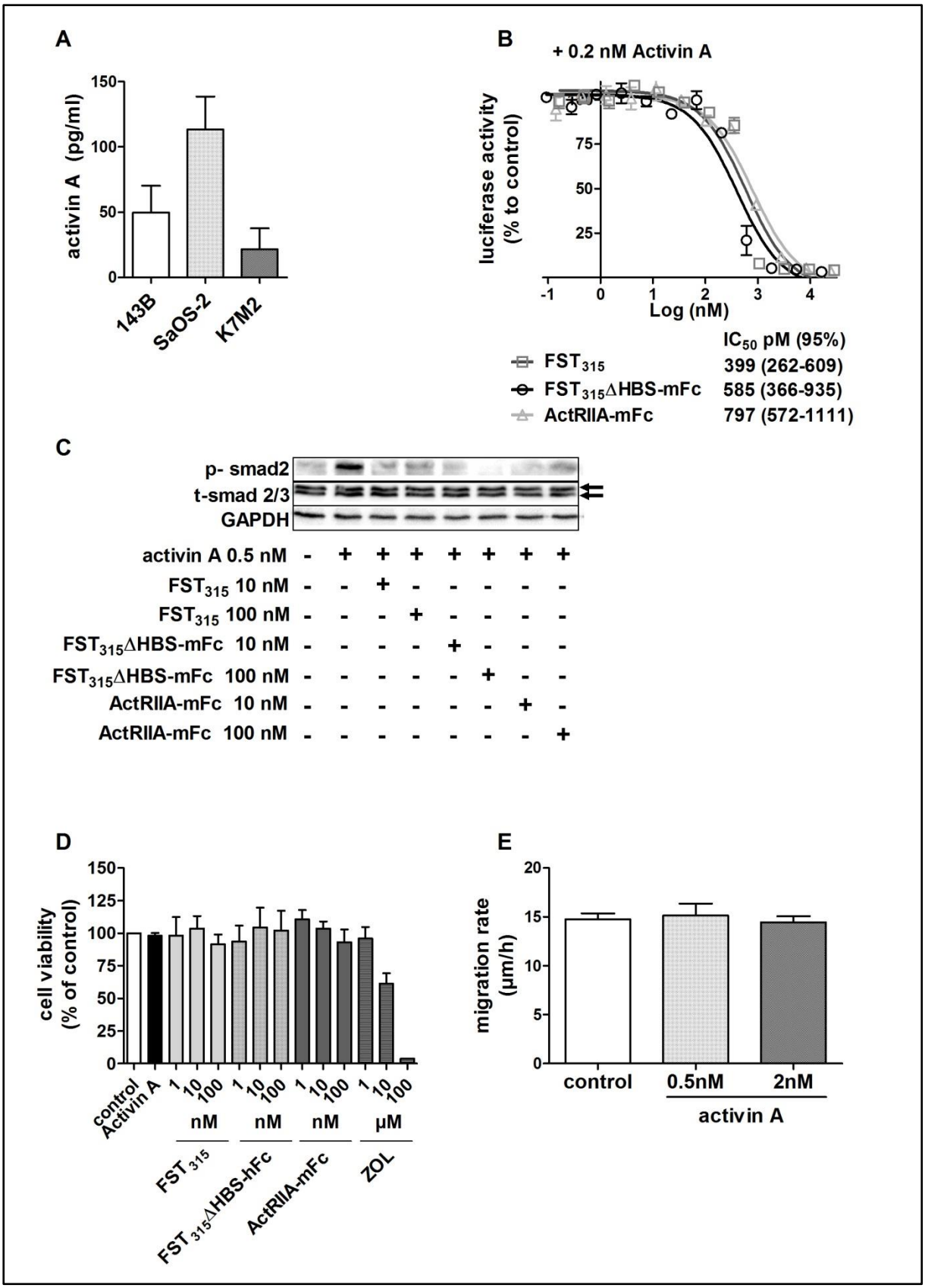
A
activin A (pg/ml)
150
100
50
0
143B
SaOS-2
K7M2
B
+ 0.2 nM Activin A
luciferase activity (% to control)
75
50
25
-1
0
1
2
3
4
Log (nM)
IC50 pM (95%)
FST315 399 (262-609)
FST315ΔHBS-mFc 585 (366-935)
ActRIIA-mFc 797 (572-1111)
C
p- smad2
t-smad 2/3
GAPDH
activin A 0.5 nM - + + + + + + +
FST315 10 nM - - + - - - - -
FST315 100 nM - - - + - - - -
FST315ΔHBS-mFc 10 nM - - - - + - - -
FST315ΔHBS-mFc 100 nM - - - - - + - -
ActRIIA-mFc 10 nM - - - - - - + -
ActRIIA-mFc 100 nM - - - - - - - +
D
cell viability (% of control)
150
125
100
75
50
25
0
control
Activin A
1
10
100
nM
nM
nM
µM
FST315
FST315ΔHBS-hFc
ActRIIA-mFc
ZOL
E
migration rate (µm/h)
20
15
10
5
0
control
0.5nM
2nM
activin A

Figure 2.

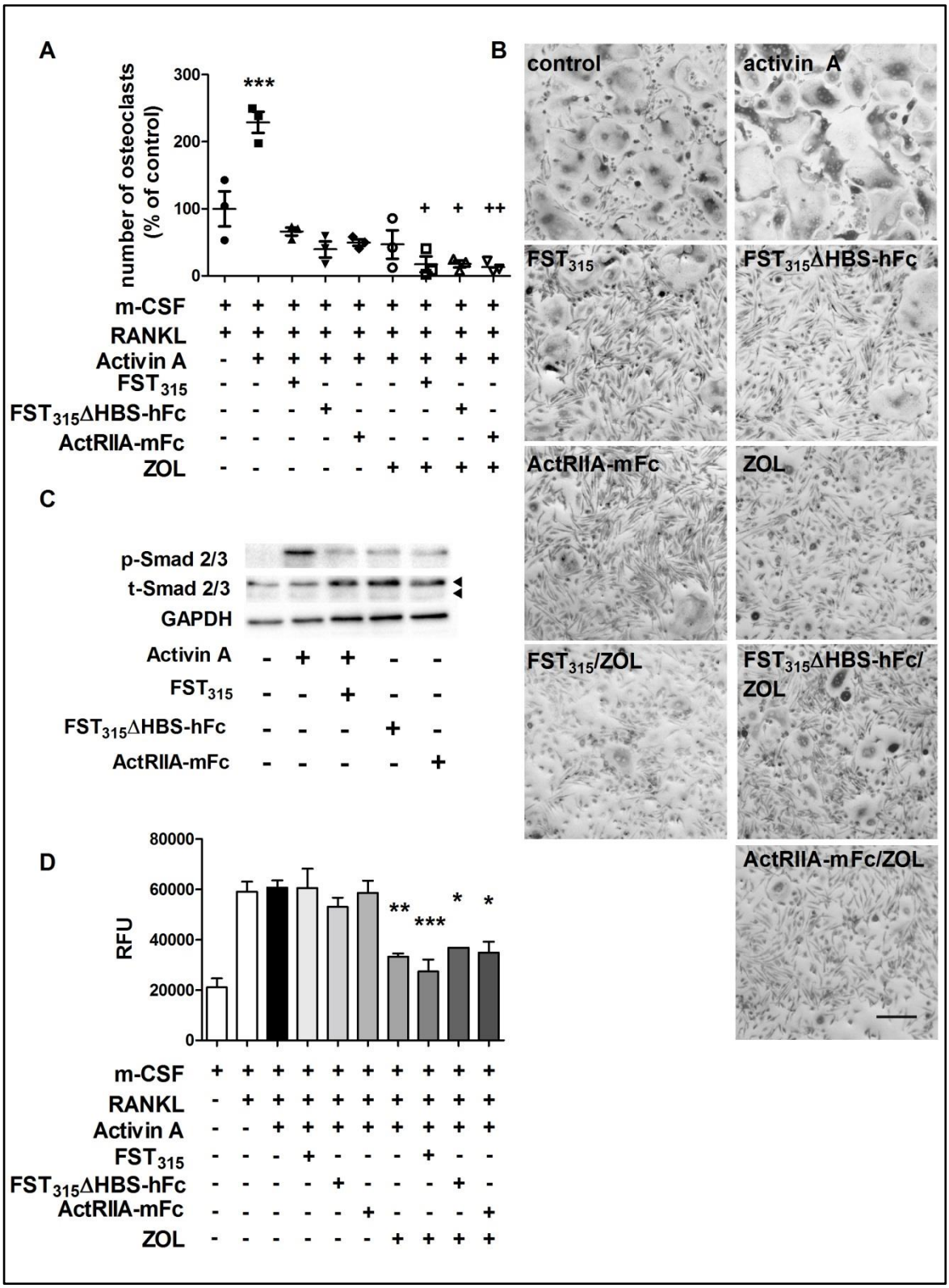
A
number of osteoclasts (% of control)
300
200
100
0
***
+
+
++
m-CSF + + + + + + + + +
RANKL + + + + + + + + +
Activin A - + + + + + + + +
FST315 - - + - - - + - -
FST315ΔHBS-hFc - - - + - - - + -
ActRIIA-mFc - - - - + - - - +
ZOL - - - - - + + + +
B
control
activin A
FST315
FST315ΔHBS-hFc
ActRIIA-mFc
ZOL
FST315/ZOL
FST315ΔHBS-hFc/ ZOL
ActRIIA-mFc/ZOL
C
p-Smad 2/3
t-Smad 2/3
GAPDH
Activin A - + + - -
FST315 - - + - -
FST315ΔHBS-hFc - - - + -
ActRIIA-mFc - - - - +
D
RFU
80000
60000
40000
20000
0
**
***
*
*
m-CSF + + + + + + + + + +
RANKL - + + + + + + + + +
Activin A - - + + + + + + + +
FST315 - - - + - - - + - -
FST315ΔHBS-hFc - - - - + - - - + -
ActRIIA-mFc - - - - - + - - - +
ZOL - - - - - - + + + +

Figure 3.

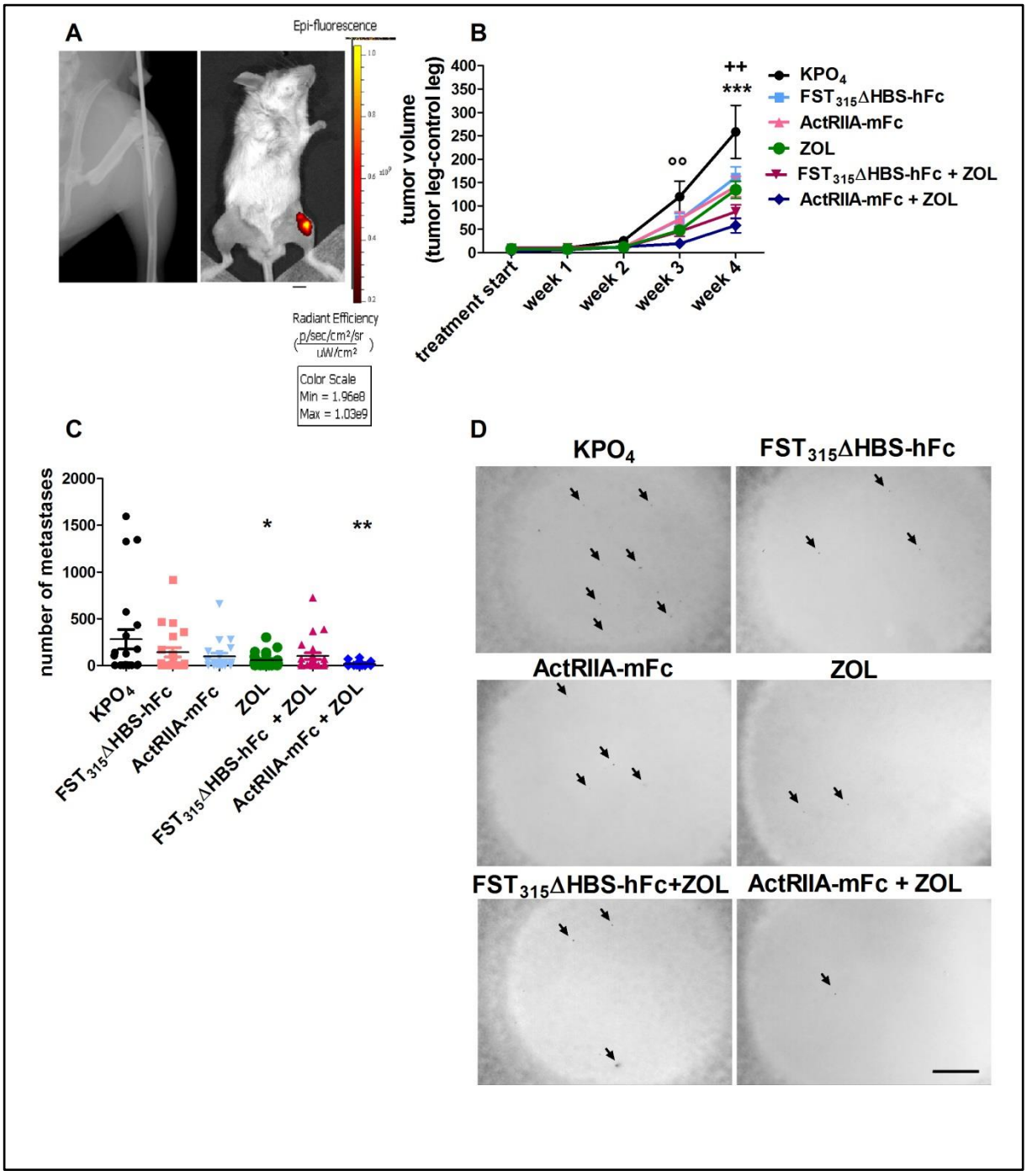
A
Epi-fluorescence
Radiant Efficiency
Color Scale
Min = 1.96e8
Max = 1.03e9
B
tumor volume
(tumor leg-control leg)
treatment start
week 1
week 2
week 3
week 4
KPO4
FST315ΔHBS-hFc
ActRIIA-mFc
ZOL
FST315ΔHBS-hFc + ZOL
ActRIIA-mFc + ZOL
C
number of metastases
D
KPO4
FST315ΔHBS-hFc
ActRIIA-mFc
ZOL
FST315ΔHBS-hFc+ZOL
ActRIIA-mFc + ZOL

Figure 4.

A

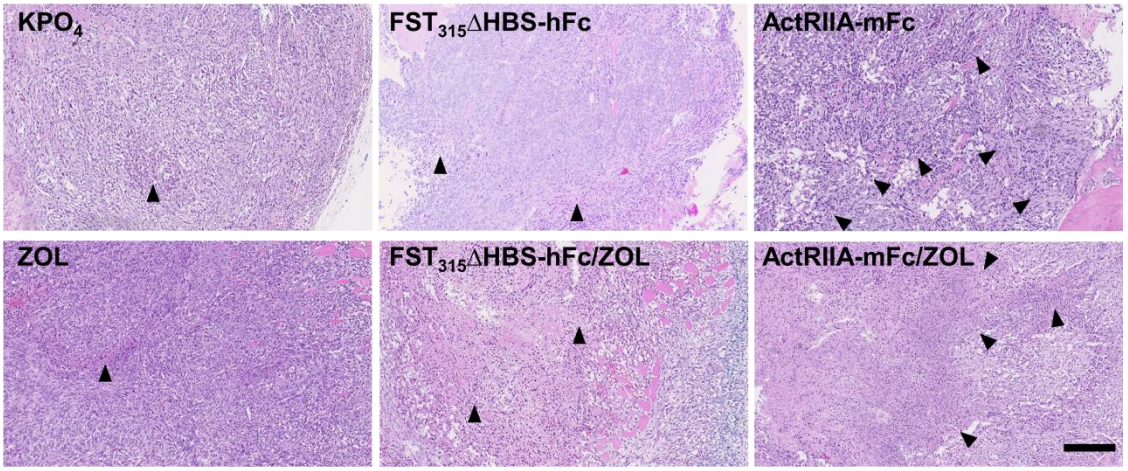

B

treatment	tumor necrosis (score)
KPO_4	1.3
FST_{315}ΔHBS-hFc	1.8
ActRIIA-mFc	1.3
ZOL	2.5
FST_{315}ΔHBS-hFc + ZOL	2.4
ActRIIA-mFc + ZOL	2.7

Figure 5.

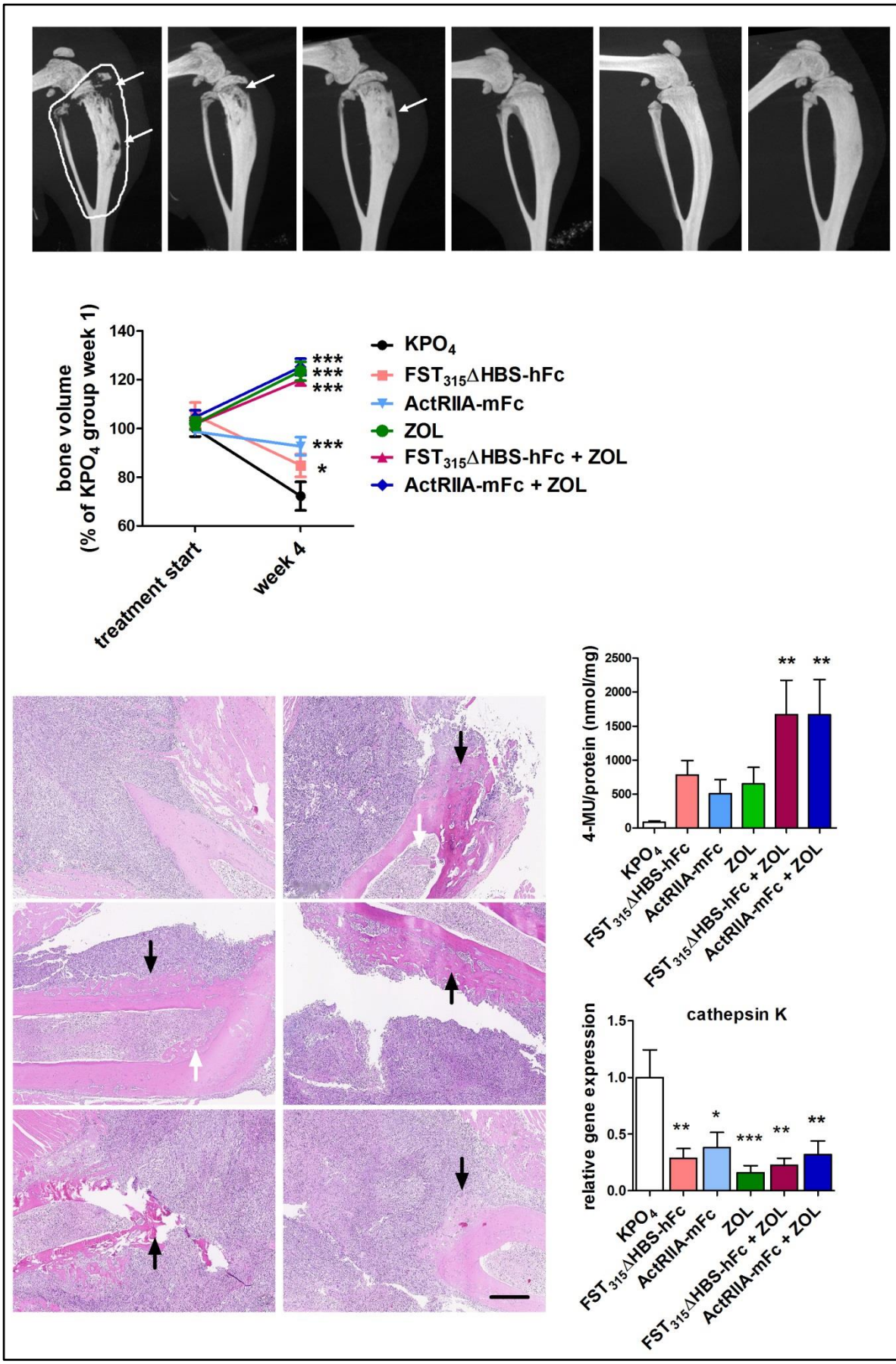
bone volume
(% of KPO4 group week 1)
140
120
100
80
60
treatment start
week 4
***
***
***
***
*
KPO4
FST315ΔHBS-hFc
ActRIIA-mFc
ZOL
FST315ΔHBS-hFc + ZOL
ActRIIA-mFc + ZOL
4-MU/protein (nmol/mg)
2500
2000
1500
1000
500
0
**
**
KPO4
FST315ΔHBS-hFc
ActRIIA-mFc
ZOL
FST315ΔHBS-hFc + ZOL
ActRIIA-mFc + ZOL
cathepsin K
relative gene expression
1.5
1.0
0.5
0.0
**
*
***
**
**
KPO4
FST315ΔHBS-hFc
ActRIIA-mFc
ZOL
FST315ΔHBS-hFc + ZOL
ActRIIA-mFc + ZOL

Figure. 6.

Supplementary Materials & Methods

Activin induced Smad phosphorylation in pre-osteoclasts

CD14-positive PBMC were differentiated with m-CSF (25 ng/ml) and RANKL (60 ng/ml RANKL) for 7 days. On day 7 the emerged pre-osteoclasts were serum starved for 6 hours and stimulated with or without activin A (2 nM) in a time-dependent manner. Protein expression of phosphorylated Smad 2 and total Smad2 (upper black arrow) and 3 (lower black arrow) and GAPDH was assessed by Western Blot.

Quantification of serum levels of FST_{315}ΔHBS-hFc and ActRIIA-mFc

Mice i.p. were injected with FST_{315}ΔHBS-hFc or ActRIIA-mFc (10 mg/kg) and serum was collected from the tail vein 24 hours later. FST_{315}ΔHBS-hFc serum levels were quantified using a Human Follistatin ELISA Development Kit (Peprotech, 900-K299) according to the manufacturer's protocol. As an adaptation we used corresponding standard curves using purified FST_{315}ΔHBS-hFc. ActRIIA-mFc was quantified by ELISA using anti-human activin receptor type 2A antibody as a capture antibody (1:150; #NB120-10595, Novus Biologicals, cat) and biotinylated anti-human activin receptor type 2A antibody as a detection antibody (1:150; # R1265, Leinco Technologies) in combination with HRP-conjugated streptavidin (DAKO, P0397).

Splenic extramedullary hematopoiesis EMH

EMH was evaluated histologically and scored as follows: 0, absent; 1, minimal (only scattered hematopoietic cells, mainly megakaryocytic precursors, observed in the red pulp); 2, mild (numerous erythroid and megakaryocytic precursors observed in the red pulp, occasionally forming small groups); 3, moderate (numerous erythropoietic cells forming small to large clusters in the red pulp); 4, marked (the red pulp is filled with hematopoietic precursors, with moderate enlargement of the organ); 5, severe (the red pulp is expanded by hematopoietic cells, with distortion of the white pulp and marked enlargement of the organ).

Supplementary Figure Legends

Supplementary Figure S1: Cell viability of human SaOS-2 (A) and murine K7M2L2 (B) osteosarcoma cells treated with either activin A, FST_{315}, FST_{315}ΔHBS-hFC, ActRIIA-mFC, or ZOL at indicated concentrations for 48 hours. Cell viability was determined by WST-1 assay as described in the Materials and Methods (results as ± SEM).

Supplementary Figure S2: Activin A induces time-dependent phosphorylation of Smad2 in pre-osteoclasts, which were stimulated with m-CSF (25 ng/ml) and RANKL (60 ng/ml RANKL) for 7 days. Upon time dependent stimulation with or without activin A (2 nM) protein expression of phosphorylated Smad2, total Smad2 (upper black arrow) and Smad3 (lower black arrow) and GAPDH was assessed by Western Blot.

Supplementary Figure S3. FST_{315}ΔHBS-hFc and ActRⅡA-mFc serum levels in an orthotopic 143B/SCID osteosarcoma mouse model 24 hours after i.p. injections of either FST_{315}ΔHBS-hFc or ActRIIA-mFc at indicated treatment days.

Supplementary Figure S4. Activin A treatment increased body weight and extramedullary haematopoiesis (EMH) in an orthotopic 143B osteosarcoma mouse model. (A) Statistical differences in body weight of all treated groups compared to the KPO_4 group (*** $P < 0.001$, ** $P < 0.01$, * $P < 0.05$ vs. FST_{315}ΔHBS-hFc, $^{+++}$ $P < 0.001$ vs. FST_{315}ΔHBS-hFc/ZOL) (1-way ANOVA, Bonferroni post-tests). (B) Splenic EMH was determined on histological paraffin sections (H&E stained) and scored for their amount of EMH (score 1 - 5, with 5 having the highest grade of EMH) (*** $P < 0.001$, 1way ANOVA, Bonferroni post-test). (C) Images of spleen sections stained for H&E from representative SCID mice treated with KPO4, ActRIIA-mFc or ActRIIA-mFc/ZOL treated groups. Arrows indicate EMH, represented by megakaryocytes and expanded red pulp, scale bar 500 μm.

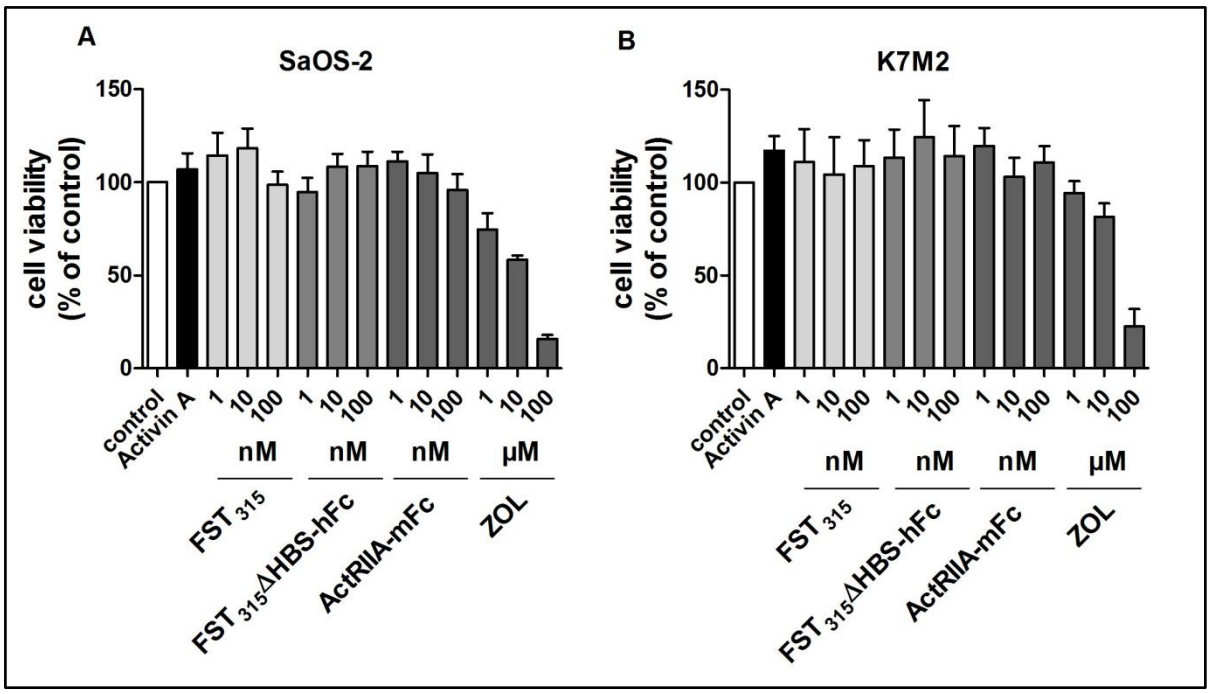

Supplementary Figure S1.

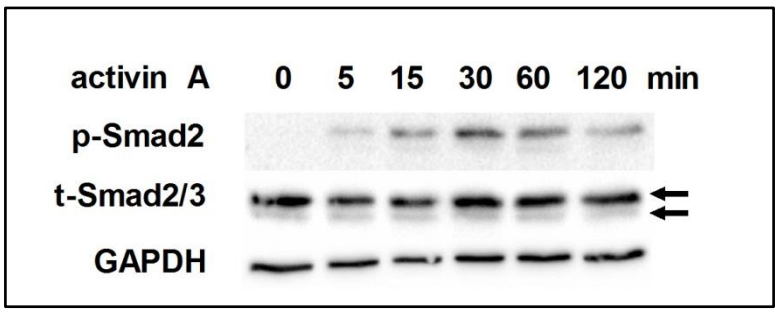

Supplementary Figure S2.

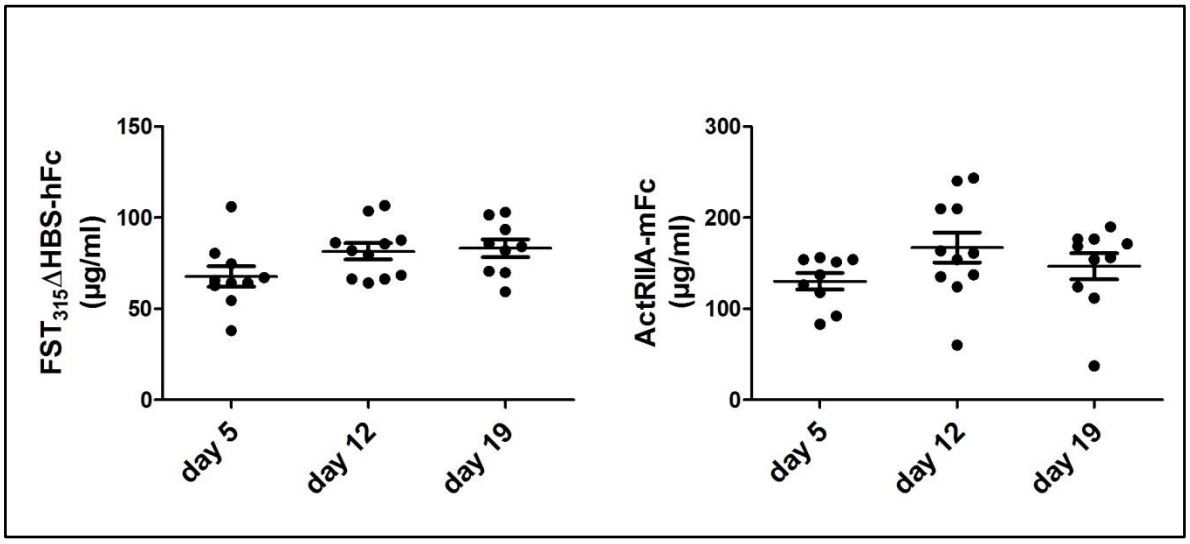

Supplementary Figure S3.

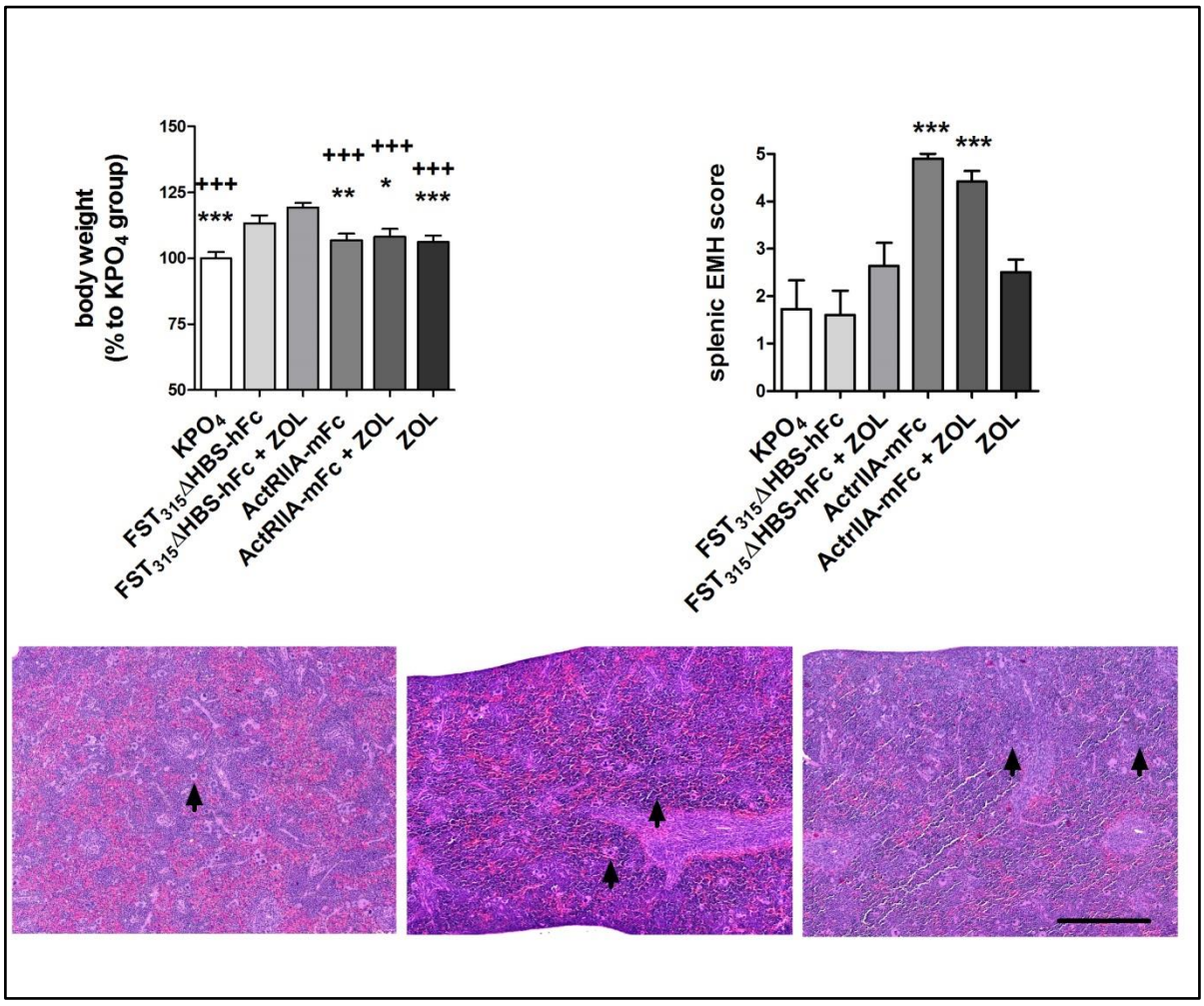

Supplementary Figure S4.

6.2 Manuscript 2

Cytotoxic Efficacy of Photodynamic Therapy in Osteosarcoma Cells *In Vitro*

Daniela Meier*[1], Carmen Campanile*[1], Sander M. Botter[1], Walter Born[1], Bruno Fuchs[1]

[1]Laboratory for Orthopedic Research, Balgrist University Hospital, Zurich, Switzerland

*These authors contributed equally

URL: http://www.jove.com/video/51213

DOI: doi:10.3791/51213

Keywords: Photodynamic Therapy (PDT), 5, 10, 15, 20-tetrakis(meta-hydroxyphenyl)chlorin (mTHPC), phototoxicity, dark-toxicity, osteosarcoma (OS), photosensitizer

Date Published: 3/18/2014 in the Journal of Visualized Experiments

Vis. Exp. (85), e51213, doi:10.3791/51213 (2014).

The video component of this article can be found at http://www.jove.com/video/51213/

Disclosures: The authors declare that they have no competing financial interests or conflict of interest

Abstract

In recent years, there has been the difficulty in finding more effective therapies against cancer with less systemic side effects. Therefore Photodynamic Therapy is a novel approach for a more tumor selective treatment.

Photodynamic Therapy (PDT) that makes use of a non-toxic photosensitizer (PS), which, upon activation with light of a specific wavelength in the presence of oxygen, generates oxygen radicals that elicit a cytotoxic response[1]. Despite its approval almost twenty years ago by the FDA, PDT is nowadays only used to treat a limited number of cancer types (skin, bladder) and non-oncological diseases (psoriasis, actinic keratosis)[2] .

The major advantage of the use of PDT is the ability to perform a local treatment, which prevents systemic side effects. Moreover, it allows the treatment of tumors at delicate sites (*e.g.* around nerves or blood vessels). Here, an intraoperative application of PDT is considered in osteosarcoma (OS), a tumor of the bone, to target primary tumor satellites left behind in tumor surrounding tissue after surgical tumor resection. The treatment aims at decreasing the number of recurrences and at reducing the risk for (postoperative) metastasis.

In the present study, we present *in vitro* PDT procedures to establish the optimal PDT settings for effective treatment of widely-used OS cell lines that are used to reproduce the human disease in well-established intratibial OS mouse models. The uptake of the PS mTHPC was examined with a spectrophotometer and phototoxicity was provoked with laser-light excitation of mTHPC at 652 nm to induce cell death assessed with a WST-1 assay and by the counting of surviving cells. The established techniques enable us to define the optimal PDT settings for future studies in animal models. They are an easy and quick tool for the evaluation of the efficacy of PDT *in vitro* before an application *in vivo*.

Introduction

Today's state of the art treatment of osteosarcoma (OS), a primary bone tumor, encompasses a combination of neo-adjuvant chemotherapy and surgery. This treatment regimen revealed an increase in the survival rate of patients with localized disease from approximately 20% before the use of chemotherapy, to currently between 60-70%[3,4]. However, in the last two decades, the overall survival of OS patients with local disease has plateaued[4,5]. Moreover, 30-40% of these patients relapse within 3 years after diagnosis and

patients with metastatic disease continue to have a poor survival of 20-30%[4,6,7]. To improve the outcome of these patients, new therapeutic strategies need to be developed.

Photodynamic Therapy (PDT), a rather novel anticancer therapy, uses light of a specific wavelength for excitation of a photosensitizer (PS), which accumulates in the tumor cells after its injection into the bloodstream. Laser-light excitation of the PS generates oxygen radicals in the presence of oxygen, which induce cytotoxic reaction in tumor cells and cell death. Besides this primary mechanism, two additional PDT-evoked biological processes contribute to reduced tumor growth: PDT causes vasoconstriction and thrombus formation of the tumor microvasculature and, consequently local hypoxia and anoxia inside the tumor, leading to tumor infarction. Finally, PDT-injured and dying tumor cells trigger a local immune response, a rather unique feature of PDT. This involves the complement system and the activation of antigen-presenting dendritic cells[8]. Thus, conditions are created for the presentation of tumor antigens with subsequent activation of lymphoid cells, leading to tumor-specific immunity.

So far, PDT has been used to treat several types of soft tissue tumors and hyperplasia's, such as actinic keratosis, Barrett's esophagus, endobronchial tumors, bladder cancer, basal cell carcinomas and palliative treatment of head and neck cancer[2]. The treatment is known to induce local, large-scale necrosis with only little side effects, and thus has the potential to selectively eradicate tumor tissue. Despite these advantages, the application of PDT remains technically more demanding than the administration of chemotherapeutic drugs. In order to achieve maximal efficacy, the PS concentration, light exposure time and total light energy transfer need to be optimized. This can be done in *in vivo* experiments, but, because of the relative large number of parameters that need to be optimized, it is more efficient to initially determine optimal conditions *in vitro*.

In the experiments described below, we tested the *in vitro* efficacy of PDT using the PS 5,10,15,20-tetrakis(meta-hydroxyphenyl)chlorin, abbreviated mTHPC (Figure 1A). mTHPC is the active substance in the medicinal product Foscan, which is currently used in the clinic for palliative treatment of head and neck cancer. It is one of the most potent PS, inducing massive cell damage already at low concentrations, and it was demonstrated to be superior to other PS in terms of tissue penetration[9,10]. Its light absorption spectrum (Figure 1B) shows two prominent peaks, one at 417 nm and a second at 652 nm, which are used for tissue localization of accumulating PS and for PDT induction, respectively.

Currently, a liposomal formulation for mTHPC is under development. Here, we describe the procedures to quantify the uptake of this liposomal formulation, and to perform PDT in two human OS cell lines; the low-metastatic HOS and the high-metastatic 143B cells. Some of the data presented here have been reported earlier[11]. The approach described here enables us to study the effect of a metastatic phenotype on PDT efficacy. 143B cells, orthotopically injected into the hind limbs of immune-deficient SCID mice cause intratibial metastasizing primary tumors, a model closely mimicking the human metastasizing disease. Thus, the proposed *in vitro* experiments are perfectly suitable to assess the optimal PDT settings to be later used in *in vivo* experiments.

Protocol

1. Comparison of the Uptake of mTHPC in the Respective Low and Highly Metastatic HOS and 143B OS Cell Lines

1. Prepare cell culture medium containing DMEM, Ham F12, and heat inactivated fetal calf serum in a ratio 4.5:4.5:1.

   Note: The liposomal formulation of the PS mTHPC was dissolved in water at a final concentration of 1.5 mg/ml mTHPC.
2. Plate 0.2 x 106 HOS and 143B cells/well in 6-well plates (triplicates for each condition) and let the cells adhere overnight.

   Note: the number has to be adjusted to individual cell lines. A confluency of 80-90% is most suitable at the time of the experiment.
3. On the following day, incubate the cells with a fixed concentration of mTHPC for different time periods (time dependent uptake), or with increasing concentrations of mTHPC during a fixed time period (dose dependent uptake).
4. Incubate the cells with mTHPC for specific time points or concentrations of mTHPC.

   Note: In this study, both the HOS and 143B cell lines were incubated with 0.6 µg/ml mTHPC for 0, 2.5, 5, or 10 hr, or with 0, 0.6, 2.5, and 10 µg/ml mTHPC for 5 hr. The applied time periods and dosages may vary depending on the cell line that is used.
5. Remember to always work in the dark or in dimmed light conditions to prevent direct light exposure of the cells.
6. After incubation of the cells at the indicated conditions, aspirate the medium and wash the cells three times with PBS. Next, detach the cells with 0.5 ml trypsin/EDTA and count the cells.

7. After detachment, centrifuge the cells at 400 x g for 5 min, aspirate the medium and resuspend the cells in PBS to a final density of 200,000 cells/ml.
8. Pipette 100 µl of the obtained cell suspension (i.e. 20,000 cells) in a 96-well plate and measure the fluorescence of these cells in a fluorescence spectrophotometer. The settings for mTHPC fluorescence measurements are: 417 nm for the excitation and 652 nm for the emission.
9. In order to calculate the amount of internalized mTHPC per cell, normalize the relative fluorescence unit (RFU) for the cell number and cell volume as follows:
10. Prepare a standard curve using different concentrations of mTHPC in PBS from 0-4 µg/ml (use triplicate measurements). Pipette 100 µl of each dilution in a 96-well plate and measure the fluorescence of the wells using the settings described under step 1.6.
11. Divide the RFU (obtained for 20,000 cells) by the slope of the linear standard curve of mTHPC, which gives the concentration of mTHPC (in µg/ml) in the well.
12. Divide this mTHPC concentration by 10 to get the total amount of mTHPC in one well (in µg, representing 100 µl of cell suspension) and divide this value by the volume of 20,000 cells.
13. Calculate the volume with the formula for a sphere: (4/3 x π) x r3. Obtain the radius r by measuring the diameter of 20 trypsinized cells under a microscope, and dividing this value by 2.
14. Finally, normalize all the values to those obtained for HOS cells after 10 hr of incubation (dose dependent uptake) or treated with 10 µg/ml mTHPC (time dependent uptake), which were set to 100%.

2. Measurement of Phototoxicity of PS *In Vitro*

1. Seed 3,000 cells/well in a 96-well plate (triplicates for each concentration of mTHPC used) and let them adhere overnight. Similarly prepare an additional 96-well plate and treat the cells as described below, but then put them aside for phase contrast imaging.

   Note: the number has to be adjusted for each individual cell line. A confluency of 50-60% at the time of the experiment is ideal.

1. Keep in mind to add the corresponding dark toxicity control of cells for each of the mTHPC concentrations. These are cells that will be incubated in the absence or presence of selected concentrations of mTHPC, but will not be illuminated.

2. On the following day, incubate the cells with different concentrations of mTHPC (0, 0.0001, 0.001, 0.01, 0.03, 0.075, 0.15, 0.3, 0.6, 1.25, 2.5, 5, and 10 μg/ml) depending on the cell lines and keep them in the dark for 5 hr.

   1. Refer to Section 1.3.2

   Note: The incubation time before illumination depends on the cell line and on the PS used, therefore it is advisable to test different concentrations and different time points in separate experiments.

3. Following incubation for the indicated time period, wash the cells twice with PBS and add new fresh medium without mTHPC.
4. Illuminate the cells with a 652 nm diode laser, specific for the mTHPC absorption spectrum (see **Figure 1**).

   1. Set the laser to 21.88 mW/cm2 power at a height of 13.5 cm distance from the cells, in order to get an energy dose of 5 J/cm2. Illuminate the cells for 230 sec. Do not illuminate the dark toxicity control cells (with and without mTHPC).

   Note: Always wear glasses to protect the eyes from the laser light used for excitation of the PS.

5. After illumination, keep the cells in the dark at 37 ºC for 24 hr. Subsequently, add water soluble tetrazolium (WST-1) reagent (10 μl/100 μl of medium).
6. Three hours after the addition of the WST-1 reagent, measure the absorbance of individual wells of the 96-well plate at 415 nm.
7. In order to calculate the percentage of surviving cells, set the mean of the values obtained for the non mTHPC treated cells for each condition to 100% (i.e. illuminated, without mTHPC and nonilluminated, without mTHPC).

3. Estimation of Cell Number by Cell Counting

1. Seed 20,000 cells/well in a 24-well plate and let them adhere overnight.
2. Incubate the cells for 5 hr with mTHPC (0.001, 0.003, 0.15, 0.6, and 1.25 μg/ml) and illuminate them as described above.
3. Collect the medium, wash the cells once with PBS, trypsinize them and collect them by centrifugation at 400 x g for 5 min.
4. After centrifugation, aspirate the medium and resuspend the cells in 200 μl of fresh medium.
5. Count the cells in a Neubauer chamber.

Representative Results

With the here reported techniques, we investigated mTHPC-based PDT in human OS cells. First, the time- and dose-dependent uptake of mTHPC was investigated in the low metastatic HOS and in the highly metastatic 143B OS cell lines. mTHPC uptake can be assessed by measuring the fluorescence of mTHPC with a fluorescence spectrophotometer (**Figure 2**, reproduced with permission from Reidy *et al.*[11]). **Figure 2 A** illustrates the uptake of mTHPC in a time-dependent manner. The fluorescence intensity of the cell suspension represents the intracellular levels of mTHPC. **Figure 2 B** illustrates the dose-dependent mTHPC uptake in HOS and 143B cells after 5 hr incubation. The uptake in the high-metastatic cell line 143B tended to be higher than in the low- metastatic parental HOS cell line.

Dark- and photo-toxicity of mTHPC in 143B cells was assessed by determining the cell metabolic activity (with a WST-1 assay) and by counting the number of residual cells after 5 hr of incubation with mTHPC, subsequent incubation in the dark or treatment with laser light for 230 sec and further incubation for 24 hr in the dark.

Dose-dependent dark-toxicity is shown in **Figure 3** (reproduced with permission from Reidy *et al.*[11]). In **Figure 3A**, 143B cells were treated with different mTHPC dosages and compared to untreated cells. A dose-dependent decrease of cell number and metabolic activity was observed. Decreased cell viability was recognized at an mTHPC concentration equal and higher than 2.5 µg/ml. Dose-dependent phototoxicity of mTHPC is illustrated in **Figure 3B**. Cells were treated with different mTHPC doses and with subsequent illumination (5 J/cm^2). A consequential decrease in cell metabolic activity (measured with the WST assay), as well as a decrease in cell number was observed. The resulting decrease in cell number after applying PDT is visualized in **Figure 4**.

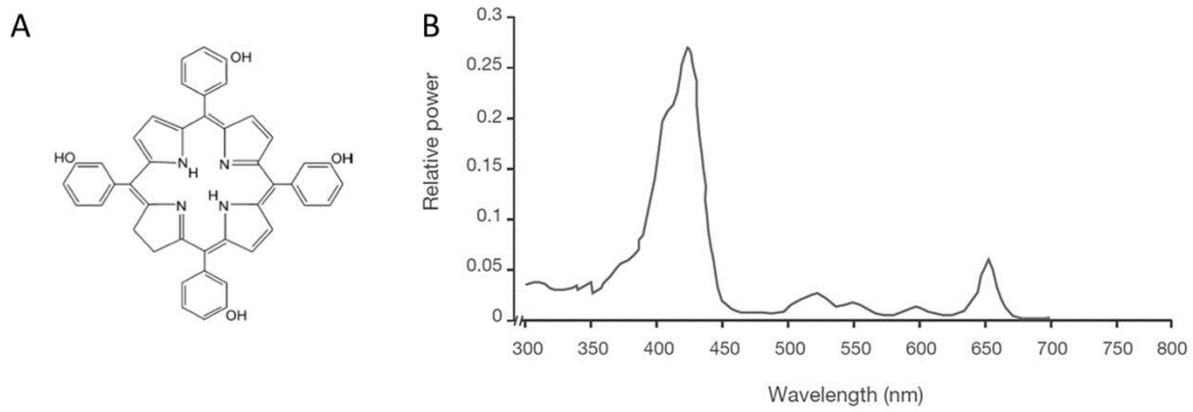

Figure 1: Chemical structure of mTHPC (A) and light absorption spectrum (B). Figures were provided by biolitec research GmbH.

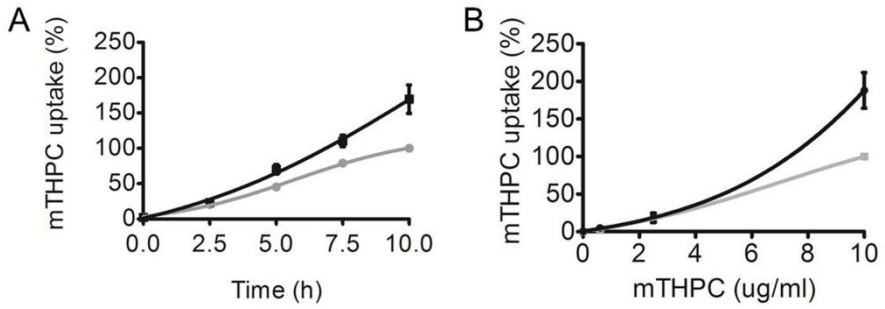

Figure 2: Time- and dose-dependent uptake of mTHPC by the human OS cell lines HOS and 143B. A. HOS (in grey) and 143B (in black) were seeded in 6-well plates (0.2 x 20^6 cells per well). After overnight culturing, the cells were incubated with 0.6 µg/ml mTHPC for 0, 2.5, 5, 7.5 and 10 hr (**A**), or for 5 hr with 0, 0.6, 2.5 and 10 µg/ml mTHPC (**B**). Fluorescence intensity was determined by measuring the fluorescence of 20.000 cells at 652 nm upon excitation at 417 nm. Values were normalized to the calculated cell volume and the mTHPC uptake of HOS cells at 10 hr (**A**) or after incubation with 10 µg/ml (**B**) was set to 100%. Values are the mean ± SEM of three independent experiments. Adapted from Reidy, K., *et al*. (Reidy, Campanile et al. 2012).

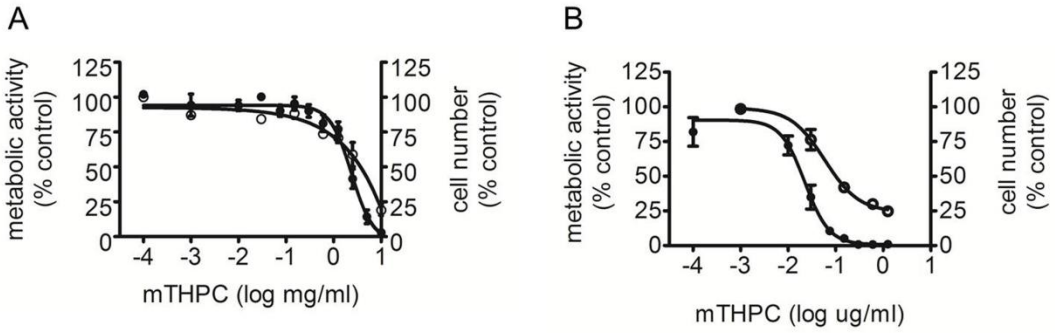

Figure 3: Dark and phototoxicity of mTHPC in 143B cells. Cells were seeded and grown overnight before treatment. To determine mTHPC dose-dependent dark toxicity, 143B cells were incubated for 5 hr in the dark in

the absence or presence of indicated mTHPC concentrations (**A**). To determine mTHPC dose-dependent photo-toxicity, 143B cells were incubated with or without mTHPC for 5 hr at indicated concentrations and then illuminated with 5 J/cm^2 with a power of 21.88 mW/cm^2 for 230 sec (**B**). For measurements of the metabolic activity (●) with the WST-1 assay, 143B cells were seeded in 96-well plates at a density of 3.000 cells per well. Cell numbers (○) were counted from cells seeded at 20.000 cells per well in 24-well plates. Values are the mean ± SEM of three independent experiments. Adapted from Reidy, K., *et al*. (Reidy, Campanile et al. 2012).

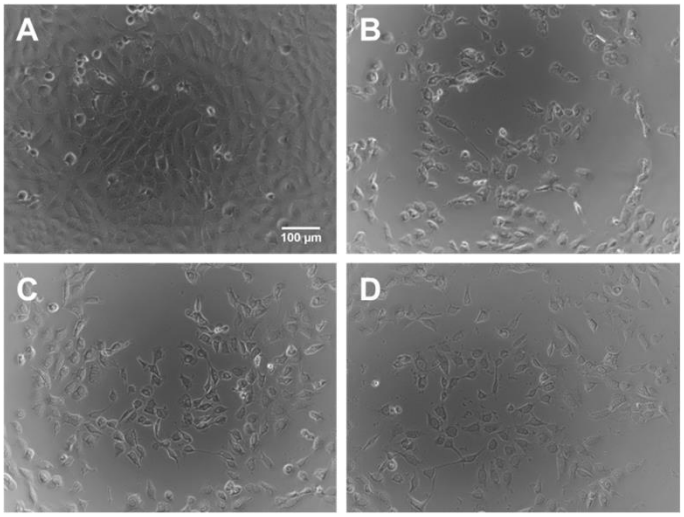

Figure 4: Phase- contrast images of 143B cells before and after PDT. Cells were seeded and left to adhere overnight as described in the protocol. To visualize dose-dependent, mTHPC mediated light toxicity, 143B cells were incubated for 5 hr in the dark with 0, 0.6, 2.5 and 10 µg/ml mTHPC (panels **A-D**, respectively). The cells were then illuminated with 5 J/cm^2 light of 652 nm wavelength for 230 seconds, and photographed after 24 hr. Scale bar: 100 µm.

Discussion

To achieve optimal cytotoxicity in response to PDT, it is crucial to choose the right laser light settings and incubation times. The here described procedures are consistent and efficient to determine PS uptake and to quantify PDT-induced cytotoxicity *in vitro*. Using the specific absorption wavelengths of the PS mTHPC, the cellular PS uptake can be determined in a direct manner, and the PS can be activated to generate cytotoxic reactive oxygen species.

Using this *in vitro* setup, all parameters such as PS concentration, drug-light interval and laser light intensity can be easily adjusted to the characteristics of the PS and the cell lines used. Cell count gives a direct read out of surviving attached cells, which together with the WST-1 assay (monitoring metabolic activity) gives a good estimate for cell survival. However, the presented method can only model the "first hit", i.e. the cell toxicity of reactive oxygen species immediately after activation of the PS. The *in vivo* observed subsequent

vasoconstriction and the activation of the immune system, necessary for full tumor eradication, can only be investigated in animals.

Figure 2 demonstrated a time- and dose-dependent uptake of mTHPC to a higher level in the highly metastatic 143B than in its parental low metastatic HOS cell line. Dark-toxicity of mTHPC in 143B OS cells was observed after incubation for 5 hr only at high concentrations (Figure 3). 143B cells show a high sensitivity to PDT, shown by the mTHPC and light-dose dependent phototoxic effect. A phototoxic effect was observed already at an mTHPC concentration as low as 0.075 µg/ml, and a half-maximal lethal concentration of 0.022 ± 0.006 µg/ml was observed (**Figure 3**).

Although PDT is minimally invasive and efficient against many tumor types, minor side effects can occur when applying the technique in patients (e.g. swelling, erythema). This indicates that the PS is not only taken up by tumor cells, as shown here, but also by non-tumor cells, causing toxicity after PDT also in these cells. Triesscheijn *et al.* was able to show an increased photosensitivity of tumor cells compared to human fibroblasts. In contrast, human microvascular endothelial cells showed a higher uptake of mTHPC than the other tested cell lines, which led to a high photosensitivity[12]. These findings also correlate with PDT associated anti-vascular effects, which are frequently observed[2].

The described methods can also be applied for other PS. Incubation time and laser light intensity need to be adapted to the characteristics of the PS. Additionally, PDT can also be induced in other than OS cells, since only the settings are cell line dependent but not the method itself. As additional read-outs, cell death mechanisms can be analyzed, *e.g*. by Western Blot analysis of proteins involved in apoptosis, necrosis or autophagy. Also the subcellular localization of PS can be visualized *e.g.* by confocal laser scanning microscopy.

The different steps that have been described for PDT *in vitro*, *i.e.* incubation of the cells with the PS and induction of PDT with laser light, closely resemble the clinical situation. Patients receive (i.v. or s.c. applied) the PS, and after a distinct drug light interval, the area of interest (*e.g*. tumor tissue) is illuminated with laser light[12]. Although not yet applied in OS, its potential advantages are obvious; PDT is considered to be particularly attractive for the intraoperative treatment of tumor satellites, which frequently grow as primary tumor cell clusters close to the main rim of the primary tumor and may initiate a recurrence when missed during surgical resection of the primary tumor. Even large osseous tumors may be treated with this technique. This has been shown by a promising study in dogs[14]. In addition, eradication of tumor cells that cannot be resected by surgery (*e.g.* multiple metastases mostly

occurring in the lungs), may also represent a possible future application of PDT in patients with OS metastatic disease.

It is important to note that, while performing the experiments, care should be taken that all working steps are performed under minimal light exposure after adding the PS to the cells, as normal daylight also contains the wavelength necessary to activate mTHPC. Likewise, for *in vivo* application in preclinical models, care needs to be taken to shield the animals from direct light after injecting mTHPC. It also needs to be noted that the WST-1 assay only assesses the metabolic activity of tumor cells, which is an indirect indicator of cell death. Therefore, a combination with a total cell count, as presented here, is recommended.

In conclusion, the combination of the described methods (PS-uptake and PDT-induced cell toxicity) provides a fast and cost effective procedure to characterize toxicity properties of a PS *in vitro*. With these *in vitro* results, the range of the optimal light intensity and the drug light interval can be estimated, which gives a good indication of how PDT can be applied *in vivo*.

Acknowledgments

The authors would like to thank biolitec research GmbH (Jena, Germany) for kindly providing us with the liposomal mTHPC formulation, with special thanks to Susanna Gräfe and Arno Wiehe for their help and technical expertise. We also would like to thank Kerstin Reidy, who generated a large part of the results and was co-responsible for its publication (Reidy, Campanile et al. 2012).

This work was supported by grants from the Schweizerischer Verein Balgrist, the University of Zurich, the Krebsliga Zurich as well as by a grant from the Walter L. and Johanna Wolf Foundation, Zurich, Switzerland and a grant from EuroNanoMed ERA-NET /SNF Swiss National Science Foundation 31NM30-131004 / 1. This work was also supported by the HSM (Highly Specialized Medicine) program for Musculoskeletal Oncology of the Kanton Zurich.

Authors' Contributions

Conception and design: DM, CC, SMB, WB; Development of methodology: DM, SMB, CC; Acquisition of data: DM, CC; Analysis and interpretation of data (e.g. statistical analysis, biostatistics, computational analysis): DM, SMB, CC; Writing, review, and/or revision of the manuscript: DM, CC, SMB, WB, BF; Study supervision: SB, BF

References

1 Juarranz, A., Jaen, P., Sanz-Rodriguez, F., Cuevas, J. & Gonzalez, S. Photodynamic therapy of cancer. Basic principles and applications. Clin Transl Oncol 10, 148-154 (2008).

2 Agostinis, P. et al. Photodynamic therapy of cancer: an update. CA Cancer J Clin 61, 250-281 (2011).

3 D'Adamo, D. R. Appraising the current role of chemotherapy for the treatment of sarcoma. Semin Oncol 38 Suppl 3, S19-29 (2011).

4 Allison, D. C. et al. A meta-analysis of osteosarcoma outcomes in the modern medical era. Sarcoma 2012, 704872 (2012).

5 Anninga, J. K. et al. Chemotherapeutic adjuvant treatment for osteosarcoma: where do we stand? Eur J Cancer 47, 2431-2445 (2011).

6 Bacci, G. et al. Pattern of relapse in patients with osteosarcoma of the extremities treated with neoadjuvant chemotherapy. Eur J Cancer 37, 32-38 (2001).

7 Briccoli, A. et al. Resection of recurrent pulmonary metastases in patients with osteosarcoma. Cancer 104, 1721-1725 (2005).

8 Milla Sanabria, L. et al. Direct and indirect photodynamic therapy effects on the cellular and molecular components of the tumor microenvironment. Biochim Biophys Acta 1835, 36-45 (2013).

9 Mitra, S. & Foster, T. H. Photophysical parameters, photosensitizer retention and tissue optical properties completely account for the higher photodynamic efficacy of meso-tetra-hydroxyphenyl-chlorin vs Photofrin. Photochem Photobiol 81, 849-859 (2005).

10 Ma, L., Moan, J. & Berg, K. Evaluation of a new photosensitizer, meso-tetra-hydroxyphenyl-chlorin, for use in photodynamic therapy: a comparison of its photobiological properties with those of two other photosensitizers. Int J Cancer 57, 883-888 (1994).

11 Reidy, K., Campanile, C., Muff, R., Born, W. & Fuchs, B. mTHPC-mediated photodynamic therapy is effective in the metastatic human 143B osteosarcoma cells. Photochem Photobiol 88, 721-727 (2012).

12 Triesscheijn, M., Ruevekamp, M., Aalders, M., Baas, P. & Stewart, F. A. Comparative sensitivity of microvascular endothelial cells, fibroblasts and tumor cells after in vitro photodynamic therapy with meso-tetra-hydroxyphenyl-chlorin. Photochem Photobiol 80, 236-241 (2004).

13 Triesscheijn, M., Baas, P., Schellens, J. H. & Stewart, F. A. Photodynamic therapy in oncology. Oncologist 11, 1034-1044 (2006).

14 Burch, S. et al. Treatment of canine osseous tumors with photodynamic therapy: a pilot study. Clin Orthop Relat Res 467, 1028-1034 (2009).

6.3 Manuscript 3

Foscan and Foslip based photodynamic therapy in osteosarcoma *in vitro* and in intratibial mouse models

Daniela Meier[1], Sander M. Botter[1], Carmen Campanile[1], Bernhard Robl[1], Susanna Gräfe[3], Giovanni Pellegrini[2], Walter Born[1], Bruno Fuchs[1].

[1] Laboratory for Orthopedic Research, Department of Orthopedics, Balgrist University Hospital, Zurich, Switzerland

[2] Laboratory for Animal Model Pathology, Institute of Veterinary Pathology, University of Zurich, Zurich, Switzerland

[3] Biolitec Research GmbH, Otto-Schott-Straße 15, Jena, Germany

*Corresponding author e-mail: bfuchs@research.balgrist.ch (Bruno Fuchs)

Short title: Foscan and Foslip based photodynamic therapy in osteosarcoma.

Novelty and impact: Osteosarcoma is a devastating disease associated with impaired survival rates and treatment induced side effects, which is explained by high tumor heterogeneity, chemoresistance and drug toxicity, respectively. Here the authors suggest photodynamic therapy using Foscan and its liposomal formulation Foslip as a novel approach for the treatment of metastasizing osteosarcoma. The present study demonstrates the inhibition of tumor growth and immune system-dependent suppression of metastatic spread by PDT with Foscan and Foslip in two different clinical relevant osteosarcoma mouse models.

Key words: osteosarcoma, photodynamic therapy, Foslip, Foscan, metastasis

Abbreviations: 5-ysr: five-year survival rate; ANOVA: analysis of variance; CC: cleaved caspase; CD31: cluster of differentiation 31; HE: hematoxylin & eosin; IC50: half-maximal inhibitory concentration; i.p.: intraperitoneally; i.v.: intravenous; mTHPC: 5,10,15,20-tetrakis(meta-hydroxyphenyl)chlorine; PDT: photodynamic therapy; PS: photosensitizer; RFU: relative fluorescence unit; ROI: region of interest; WST-1: water-soluble tetrazolium; X-Gal: 5-bromo-4-chloro-3-indolyl-beta-D-galacto-pyranoside

Article category: Research Article, Cancer Therapy and Prevention

Conflict of interest: The Authors declare that there is no conflict of interest

Submission: International Journal of Cancer, May 2016

Abstract

Current osteosarcoma therapies cause severe treatment-related side effects and chemoresistance, and have low success rates. Consequently, alternative treatment options are urgently needed. Photodynamic therapy (PDT) is a minimally invasive, local therapy with proven clinical efficacy for a variety of tumor types. PDT is cytotoxic, provokes anti-vascular effects and stimulates tumor cell targeting mechanisms of the immune system and, consequently, has potential as a novel therapy for osteosarcoma patients. This study investigated first the uptake and the dark- and phototoxicity and cytotoxic mechanisms of the photosensitizer (PS) 5,10,15,20-tetrakis(meta-hydroxyphenyl) chlorine (mTHPC, Foscan) and a liposomal mTHPC formulation (Foslip) in the human 143B and a mouse K7M2-derived cell line (K7M2L2) *in vitro*. Secondly the tumor- and metastasis-suppressive efficacies of mTHPC formulations based PDT and associated mechanisms in intratibial, metastasizing osteosarcoma mouse models (143B/SCID and syngeneic K7M2L2/BALB/c) derived from the two cell lines were studied. The uptake of Foscan and Foslip *in vitro* was time- and dose-dependent and resulted in mTHPC and light dose-dependent phototoxicity associated with apoptosis. *In vivo*, the uptake of both i.v. administered mTHPC formulations was higher in tumor than in healthy control tissue. PDT caused significant (Foscan $P < 0.05$, Foslip $P < 0.001$) tumor growth inhibition in both models, and significant (Foscan $P < 0.001$, Foslip $P < 0.001$) immunsystem-dependent suppression of lung metastasis in the K7M2L2/BALB/c model.

In conclusion, mTHPC-based PDT is effective in clinically relevant experimental osteosarcoma and suppresses lung metastasis in immunocompetent mice with beneficial effects of the liposomal mTHPC formulation Foslip.

Introduction

Osteosarcoma is the most common primary high-grade bone neoplasm and one of the deadliest cancer types in children and adolescents[1, 2]. Since the introduction of new treatment protocols in the 70ies, including neoadjuvant and adjuvant chemotherapy, the 5-year survival rate (5-ysr) of patients with localized disease increased significantly to approximately 60% but plateaued ever since[3,4]. However, patients with metastatic disease, with lesions most frequently developing in the lungs and other bones, continue to have a poor 5-ysr of approximately 30%5.

Current therapy combines primary tumor surgery with chemotherapy using high-dose methotrexate, cisplatin, and doxorubicin. Unfortunately this multi-drug therapy is associated with a variety of severe side effects ranging from gastrointestinal problems, neutropenia, cardiac toxicity, neurological dysfunction, second malignant neoplasms to even death6, 7. Although multi-agent chemotherapy increased the survival of patients, it plateaued over the last three decades, most probably owing to the high tumor heterogeneity of osteosarcoma and to chemoresistance[8,9]. The lack of novel, more effective therapeutic strategies for metastasizing osteosarcoma has become an increasing problem.

During the last four decades, photodynamic therapy (PDT) evolved into a novel attractive treatment option for a variety of cancer types[10]. PDT is a multi-step process making use of three components; photosensitizer (PS), light and oxygen[11]. In a first step of the therapy, PS are injected into the blood stream and are taken up by tumor and also by healthy cells. Next, tumor-selective PDT is achieved by local illumination of the tumor site with light, which activates the light-sensitive PS to a higher energy state and results in the direct or indirect transfer of excess energy to neighboring oxygen molecules or tissue molecules, producing cell-toxic reactive oxygen. Finally, in addition to eliciting direct cytotoxicity, PDT provokes a variety of additional beneficial anti-tumor effects such as an acute inflammatory response, anti-vascular effects and an activation of the immune system[11]. PDT has commonly been employed for the treatment of solid tumors at superficial anatomical locations, however, its application in other tumors at more inaccessible sites has become an aim of clinical investigations[12, 13]. Additionally to the advantage of PDT as a local application, also a systemic immune response against tumors have been reported[14-16], therefore PDT is potentially not only effective against local tumor growth but also against distant metastases.

PDT has proven clinical value, due to good functional and aesthetic outcomes and clinical studies reported it as a good treatment option for patients unsuitable for other treatments in head and neck cancers[17, 18], but studies investigating potential therapeutic applications in osteosarcoma are scarce. *In vitro* investigations demonstrated strong cytotoxic effects of PDT in different osteosarcoma cells lines[19-22]. Preclinical studies in osteosarcoma mouse models showed an inhibition of local tumor growth[23, 24], but these studies were either performed in subcutaneous osteosarcoma mouse models, which do not reproduce the clinical situation, or in immune suppressed mice, where the impact on distant metastases cannot be

evaluated. Nevertheless, a preclinical study by Burch *et al*., who applied PDT in dogs that spontaneously developed osteosarcoma, demonstrated substantial tumor necrosis, indicating the potential of PDT for effective treatment of osteosarcoma, long-term effects or treatment impact on metastases were not reported[25].

One of the most powerful and commonly used PS is 5,10,15,20-tetrakis(meta-hydroxyphenyl)chlorine (mTHPC), traded under the name Foscan®. In Europe, Foscan has been licensed for clinical use in 2001 for the treatment of head and neck cancer and of prostate and pancreatic tumors[26]. In addition to being one of the most potent PS on the market, mTHPC has advantageous physical properties compared to other PS, which made it attractive for this study. The right shift of the excitation wavelength (652 nm) compared to other clinically approved PS such as Photofrin (635 nm) results in deeper tissue penetration of the applied laser light than light of shorter wavelength. Although mTHPC is a potent PS, its high hydrophobicity restricts the routes of administration. Encapsulation of mTHPC into liposomal structures, however, achieved with the formulation Foslip used in the present study, makes it water soluble, which potentially increases PDT efficacy[27-29].

In this study, we investigated the uptake and the dark- and phototoxicity of Foscan and Foslip in the human 143B and in a derivative (K7M2L2) of the mouse K7M2 osteosarcoma cell line. In addition, we studied the efficacies of Foscan- and Foslip-based PDT in a 143B cell line-dependent intratibial xenograft osteosarcoma model in SCID mice and in an intratibial K7M2L2 cell line-derived model in syngeneic, immune competent BALB/c mice. Tumors in both models metastasize to the lung. Thus, these models allowed us to compare the tumor- and metastasis-suppressive potential of Foscan-and Foslip-based PDT in the absence and in the presence of a functional immune system. The results demonstrated promising tumor and immune system-dependent metastasis suppressive effects and anti-vascular activity of the here applied PDT in a clinically relevant experimental osteosarcoma model.

Materials and Methods

Photosensitizer and OS cell lines

Foscan and Foslip were kindly provided by Biolitec research GmbH (Jena, Germany). Foscan was reconstituted and diluted in ethanol (40% w/w) and propylene glycol (60% w/w). Foslip, a liposomal formulation of mTHPC, is a 9:1 mixture of dipalmitoylphosphatidylcholine (DPPC) and dipalmitoylphosphatidylglycerol (DPPG; >99% purity). Foslip (freeze-dried product) was reconstituted with water to 1.5 mg mTHPC/ml and further diluted in 5% glucose.

Cells were cultured in DMEM (4.5 g/l glucose)/HamF12 (1:1) medium (Invitrogen, Carlsbad, CA), supplemented with 10% heat-inactivated FCS (GIBCO, Basel, Switzerland), at 37°C in a humidified atmosphere of 5% CO2 air.

Human 143B osteosarcoma cells were purchased from ECACC (Salisbury, UK) and murine K7M2 osteosarcoma cells (CRL-2836) were kindly provided by Dr. Chand Khanna (Center for Cancer Research National Institute, Bethesda, MD, USA). Both cell lines were transduced with a *lacZ* reporter gene[30]. 10 µl PBS/0.05% EDTA containing 3 x 10^5 of K7M2/*lacZ* cells were intratibially (i.t.) injected into female, 8 week old BALB/c mice as described before[31]. The K7M2L2/*lacZ* cell line was obtained after two rounds of *in vivo* selection according to Fidler's method[32]. Briefly, approximately three weeks after i.t. injection of K7M2/*lacZ* cells, mice developed large primary tumors and were sacrificed. The lungs of these mice were collected and metastatic lacZ-expressing cells (K7M2L1/*lacZ*) were isolated by digestion of the lung tissues in a collagenase B solution (Roche, Switzerland) and subsequent selection in cell culture medium containing 800 µg/ml G418 (Invitrogen, Life Technologies, Carlsbad, CA, USA). Selected K7M2L1/*lacZ* cells were then reinjected i.t. into BALB/c mice in order to obtain K7M2L2/*lacZ* cells in the same manner.

Uptake of mTHPC *in vitro*

143B/*lacZ* and K7M2L2/*lacZ* (referred to as 143B and K7M2L2) cells were seeded in six well plates (2000 cells/well for dose dependent uptake and 800 cells/well for time-dependent uptake) and allowed to adhere overnight. In time-course experiments, cells were incubated under tissue culture conditions with Foscan or Foslip equivalent to 0.6 µg/ml mTHPC for 0 - 48 h. For dose-dependent uptake, the cells were incubated for 5 h in the dark in tissue culture medium containing PS formulations equivalent to 0 - 10µg/ml mTHPC. Subsequently, the cells were washed two times with 100 µl PBS before the fluorescence of the cells in 100 µl PBS was measured at 652 nm with excitation at 417 nm in a Spectramax

Gemini XS plate reader (Molecular Devices, Sunnyvale, CA). Results were obtained as relative fluorescence unit (RFU).

Subcellular localization of mTHPC (Foscan and Foslip) was visualized by confocal laser scanning microscopy as previously described[19]. Cells were stained with Hoechst (Life Technologies, Carlsbad, USA).

Cytotoxicity assay

143B and K7M2L2 cells (2500 cells / well) were incubated under tissue culture conditions for 5 h at different concentrations of Foslip or Foscan (0 - 200 µg/ml mTHPC) and left untreated in the dark or illuminated with 652 nm laser light at an energy dose of 1 J/cm^2 or 5 J/cm^2 (21.88 mW/cm^2) as described previously[19]. 24 hours later, the cell viability was measured with the water-soluble tetrazolium (WST-1) assay (Roche, Basel, Switzerland) according to the manufacturer's protocol.

Western Blot analysis of apoptosis

10^6 143B or K7M2L2 cells were seeded in 6 cm cell culture dishes. After overnight adherence, cells were incubated under tissue culture conditions for 5 h with Foscan or Foslip (0.6 µg/ml mTHPC) and pre-incubated for 1 h with or without the pan-caspase inhibitor Z-VAD-FMK (100 µM) or its solvent control (1% DMSO) (BD Pharmingen AG, Allschwil, Switzerland). Cells were illuminated with 5 J/cm^2 (21.88 mW/cm2) 652 nm laser light or kept in the dark, and cell lysates were collected 90 min after illumination as previously described19. Protein extracts were analyzed for PARP and cleaved PARP (1:1000, Cell Signaling Technology) and GAPDH (1:3000, Santa Cruz Biotechnologies, Texas, USA) as a protein loading control as previously described[19].

Intratibial human xenograft and syngeneic osteosarcoma mouse models

All studies were conducted with the approval of the Veterinary Office Kanton Zurich, Switzerland (animal application license 167/2012) and in accordance with the guidelines of the Swiss Federal Veterinary Office. Eight-week-old female SCID and BALB/c mice were obtained from Charles River Laboratories and kept in the mouse facility for one week of adaptation before tumor cell injection. 10^5 143B/l*acZ* cells in 10 µl PBS/0.05% EDTA were injected i.t. into SCID mice (143B/SCID) (human xenograft mouse model) and 10^5

K7M2L2/*lacZ* cells in 10 µl PBS/0.05% EDTA i.t. into BALB/c mice (K7M2L2/BALB/c) (syngeneic mouse model) as previously described[31].

In vivo uptake of Foscan and Foslip by intratibial tumors

Upon formation of a tumor (>50 mm^3), Foscan or Foslip at doses equivalent to 1.5 mg/kg mTHPC were administered to the mice (143B/SCID n=10, K7M2L2/BALB/c n=14) with a slow (4-6 min) intravenous (i.v.) injection in the tail vein. The mice were then kept in a darkened environment for the rest of the experiment. The area of the leg where the tumor was localized was shaved and the mTHPC uptake by the tumor was measured with a PDT fluorometer (JETI Technische Instrumente GmbH, Jena, Germany) in three different locations on the surface of the skin covering the tumor (excitation 405 nm, emission 550-800 nm). Background fluorescence of intratibial tumor tissue was measured (integration time 7500 ms) in a mouse without PS injection and was subtracted from each measurement resulting in RFU. The mean RFU of the tumor in individual PS-injected mice was calculated from all three emission peak values detected at 652 nm. Upon sacrifice, tumors were cut longitudinally into halves and mTHPC fluorescence was measured inside the tumor tissue in three different locations as described above.

PDT protocol

In both, the xenograft and the syngeneic osteosarcoma model, the mice were randomly assigned to three groups; a control group receiving PS but no illumination (143B/SCID n=10, K7M2L2/BALB/c n=15), a group receiving Foscan-based PDT (143B/SCID n=7, K7M2L2/BALB/c n=8) and a group that was subjected to Foslip-based PDT (143B/SCID n=7, K7M2L2/BALB/c n=9). Foscan or Foslip control mice revealed no difference in any experimental analyses and were therefore merged and presented as one control group (data not shown). A control group of mice that were only illuminated without PS injection was not included in the study to reduce the number of animals. Results of preliminary studies conducted at our facility showed that laser light treatment of tumors in the absence of mTHPC did not affect tumor development (data not shown). Treatment was started after the formation of a tumor (>50 mm^3). Both legs were shaved and the mice were injected with Temgesic (i.p., 0.1 mg/kg). Foscan or Foslip (mTHPC 0.15 mg/kg) were administered by i.v. injection (4-6 min). The mice were kept in a darkened environment for the rest of the experiment. 24 h after

mTHPC injection, the mice were anaesthetized (1-5% isoflurane/O_2) and covered with aluminum foil and black paper such that only the primary tumor within the left hind leg was exposed. The tumors in the PDT groups were illuminated at an energy dose of 10 J/cm^2 (26.817 mW/cm^2, 720 sec) with a 652 nm diode laser (Applied Optronics Corp., South Plainfield, NJ), equipped with a fiber-based frontal light distributor (Medlight SA, Ecublens, Switzerland). Primary tumor growth over time after PDT was monitored by caliper ruler measurements at indicated time points and the data are presented as tumor volume fold-change, comparing the tumor volume in individual mice with the respective volume on the day of PDT.

In the xenograft model (143B/SCID), the mice were sacrificed 14 days after PDT. In the syngeneic model (K7M2L2/BALB/c), three mice per group were sacrificed 2 days after illumination for histological analyses of tumor tissue; all other mice were sacrificed 10 days after PDT.

Pulmonary metastases

After sacrifice of the mice in situ, lung perfusion was performed. The lungs were dissected and stained with X-gal for lacZ-transduced tumor cells as previously described[33].

Histological analyses

mTHPC fluorescence in primary tumor tissue: Pieces of primary tumor tissue were embedded in mounting medium (Dako, Denmark) and snap frozen in liquid nitrogen. mTHPC in 10 µm sections of primary tumor tissue was visualized with an AxioCam MRm camera connected to a Zeiss Observer.Z1 inverted microscope (Carl Zeiss MicroImaging GmbH) set to 4x magnification and equipped with a fluorescent filter for excitation at 488 nm and detection of emission at 600-700 nm.

Histological stainings: Tumor tissue dissected from the hind-limb at sacrifice was fixed in 4% paraformaldehyde and subsequently decalcified in Osteosoft (Merck Millipore, Germany). The tumors were trimmed, dehydrated in graded alcohol and embedded in paraffin according to standard protocols. Sections of 3-5 µm were mounted on glass slides, deparaffinized in xylene, rehydrated in graded alcohol and stained with hematoxylin and eosin (HE).

Tumor necrosis was assessed in the HE-stained sections as follows: Grade 0: no necrosis; Grade 1: necrosis below 20%; Grade 2: necrosis higher than 20% but lower than 40%; Grade 3: necrosis higher than 40% but lower than 60%; Grade 4: necrosis higher than 60% but lower than 80%; and Grade 5: necrosis higher than 80%. Apoptosis was assessed by immunostaining with an antibody to cleaved caspase 3 (Cell Signaling) and tumor vascularization by staining with an antibody to CD31 (Santa Cruz Biotechnologies), a cell surface marker of endothelial cells34. The number of apoptotic cells present in tumor sections was normalized to the total number of cells (apoptotic index35). The apoptotic index was determined by counting at least 2500 cells in randomly selected areas of tumor tissue sections free of necrotic regions using Visiomorph software (Visiopharm, Denmark).

Assessment of hind limb blood vessel perfusion

Mice were anesthetized (1-5% isoflurane) and placed in supine position under the laser Doppler perfusion imager (LDI-2, Moor instruments Ltd., UK). A window (5.5 x 2.3 cm), comprising both hind limbs, was set and tissue perfusion was measured before PDT and 2, 7 and 10 days after illumination at a speed of 4 ms/pixel using moorLDI Measurement v6.0 software (Moor instruments Ltd., UK). The results were analyzed by drawing a region of interest (ROI) around areas of tumor growth and the corresponding contralateral region in the control limb (normal tissue) using moorLDI Review v6.0. The branching of the epigastric vein from the femoral vein and the branching of the caudal femoral vein were used as anatomical landmarks to define the ROI. The percent difference in perfusion of tumor compared to normal tissue was calculated using the following formula: (1- (fluxnormal / fluxtumor)) x 100.

Statistical analysis

In vitro experiments show results of three independent experiments. The results are presented as the mean ± standard error of the mean (SEM) if not described otherwise. Statistical significance of differences between groups was determined using one-way ANOVA with Bonferroni post hoc test. Two-way repeated measures ANOVA with Bonferroni's post-test analysis was used to compare mTHPC uptake *in vitro* and *in vivo* and treatment efficacy (tumor volume, blood vessel perfusion). Statistical analyses were performed using GraphPad Prism Version 5.01 software (GraphPad Software, Inc.). A *P* value below 0.05 was considered to be statistically significant.

Results

Cellular uptake of Foscan and Foslip in osteosarcoma cell lines

In both human 143B and murine K7M2L2 osteosarcoma cells, Foscan and Foslip were taken up in a dose- and time-dependent manner (**Figs. 1a, b**). No differences in cellular uptake of Foscan and Foslip were observed at mTHPC concentrations up to 10 µg/ml (**Fig 1a**). In time course experiments, both the 143B and K7M2L2 cell lines exhibited a slightly delayed uptake of Foslip compared to Foscan, but the difference was no longer significant after 48 h of incubation (**Fig. 1b**). Confocal laser scanning microscopy of 143B and K7M2L2 cells incubated with Foscan and Foslip showed a cytoplasmic localization of mTHPC, but no mTHPC in the nucleus (**Fig. 1c**).

Cytotoxicity of Foscan and Foslip

To investigate differences in photo- and dark-toxicity of Foscan and Foslip in 143B and K7M2L2 osteosarcoma cells, the cells were incubated with the mTHPC formulations at indicated mTHPC concentrations. Foscan exhibited a dose-dependent dark-toxicity in 143B and K7M2L2 cells with half-maximal inhibitory doses (IC_{50}) equivalent to 11.74 µg/ml and 10.4 µg/ml mTHPC, respectively (**Fig. 2a**). In contrast, Foslip showed no detectable dark-toxicity in both cell lines. Both, Foscan and Foslip showed mTHPC and a laser light dose-dependent phototoxicity (**Fig 2b**). IC_{50} of Foscan and Foslip in 143B and K7M2L2 cells illuminated with 1 J/cm^2 or 5 J/cm^2 laser light are summarized in **Supporting Information Table 1**. The data shows that the sensitivity of 143B and K7M2L2 cells to Foscan- and Foslip-based PDT was laser light energy dose-dependent and overall comparable, but, interestingly, K7M2L2 cells were slightly more sensitive to Foscan than to Foslip when illuminated with the higher energy dose.

Both Foscan and Foslip-based treatment induced apoptotic cell death, shown by the presence of cleaved PARP in extracts of cells subjected to PDT in both 143B (**Fig. 2c**) and K7M2L2 cells (**Fig. 2d**). In both cell lines, PARP cleavage was suppressed by pretreatment of the cells with the pan-caspase inhibitor Z-VAD-FMK prior to PDT, indicating a caspase dependent apoptosis pathway, confirmed by the detection of cleaved of caspase 3, 7 and 9 in the cell extracts (**Supporting Information Figures 1a, b**).

In vivo uptake of Foslip and Foscan by primary tumors in the xenograft and syngeneic osteosarcoma mouse models

In order to compare the uptake of the mTHPC formulations Foscan and Foslip by intratibial primary tumors in the xenograft 143B/SCID and the syngeneic K7M2L2/BALB/c osteosarcoma mouse models, the PS formulations were i.v. injected into respective tumor-bearing mice. The uptake by tumor tissue was monitored *in vivo* during 48 h and subsequently analyzed *ex vivo*. In both models, the two mTHPC formulations were taken up by the tumor tissue in a time dependent manner (**Figs. 3a, b**). In 143B cell line derived tumors, Foslip was taken up significantly more efficiently than Foscan (**Fig. 3a**), whereas in the K7M2L2 cell line derived tumors, the uptake of Foslip compared to Foscan was only significantly higher at 6 h after PS administration (**Fig. 3b**). *Ex vivo* measurements of mTHPC fluorescence in dissected tumor and healthy control leg tissue revealed a significant 2.4- and 2.7-times higher uptake of Foscan and Foslip, respectively, in 143B cell line-derived tumors than in the control tissue (**Fig. 3c**). Similarly, in the K7M2L2/BALB/c model, the uptake of Foscan and Foslip by tumor tissue was 3.4-and 4-times higher, respectively, than by control tissue (**Fig. 3d**). Based on these *ex vivo* measurements, the uptake of the two mTHPC formulations by tumor tissue was indistinguishable in both osteosarcoma mouse models.

Fluorescence microscopy of tumor tissue cryosections showed a rather uniform distribution of mTHPC fluorescence of Foscan and Foslip in both osteosarcoma mouse models. The fluorescence in adjacent muscle tissue was considerably lower than in tumor tissue in both tumor models indicating again more efficient uptake of both mTHPC formulations by tumor than by healthy tissue (**Fig. 3e**).

Anti-tumor efficacy of Foscan or Foslip–based PDT in the xenograft and syngeneic osteosarcoma mouse models

We next assessed the tumor suppressive potential of Foscan- and Foslip-based PDT in the two osteosarcoma mouse models. The growth of i.t. tumors derived from 143B cells in SCID mice, lacking functional T and B lymphocytes, was significantly inhibited by Foscan and Foslip-based PDT and Foslip was slightly more effective than Foscan (**Figs. 4a, c**). Treatment-induced swelling of the tumor leg 3 days after PDT explained the observed transient increase in tumor volume. One week after PDT, the tumor volume of Foslip-treated mice was only 1.2-times and that of Foscan-treated animals only 1.8-times larger compared to

the non-treated control mice, which had a 2.2-times larger tumors compared to before PDT. Two weeks after PDT, the tumor volume of the control mice was 4-times larger than before treatment start, whereas mice subjected to Foscan and Foslip-based treatment had only a 2.6-time and 1.8-times, respectively, larger tumors compared to before PDT. The difference in tumor volume in both groups of PDT treated mice was not statistically significant.

In BALB/c mice with an intact immune system, the inhibition of tumor growth by Foscan- and Foslip-mediated PDT was even more pronounced than in SCID mice (**Figs. 4b, d**). One week after PDT, the tumors in Foscan- or Foslip-based PDT treated mice was indistinguishable and only 2.4 times larger than before treatment compared to the non-treated control mice, which had a 7.8 times larger tumors compared to before PDT. At sacrifice of the mice, K7M2L2 cell line-derived tumors in non-treated mice were 14.3-times larger than at the beginning of the experiment. The tumors of Foscan/PDT treated animals were still only 2.7 times larger and those of Foslip/PDT treated mice only 4.7 times larger than before treatment. In contrast, two days after laser light illumination of the tumor, a swelling and edema formation in the leg where the tumor was localized was observed in all mice subjected to PDT.

In the PDT study performed in the KM2L2/BALB/c osteosarcoma model, three mice per group were sacrificed 48 h after PDT to assess the extent of necrosis and apoptosis in the tumor tissue of treated and non-treated animals (**Fig. 4e**). Overall, the level of necrosis and apoptosis was remarkably higher in the PDT-treated than in control tumors, which only showed negligible areas of necrosis and cleaved-caspase 3 staining (average necrosis histological score: 0.3; average apoptotic index: 0.02%). Despite substantial variability among the PDT-treated tumors, Foscan/PDT treated tumors exhibited on average higher necrosis (average necrosis histological score: 4.5) and apoptosis (average apoptotic index: 7.5%) scores than those subjected to Foslip- based PDT (average necrosis histological score: 2.7; average apoptotic index: 2.6%).

The effect of Foscan and Foslip - based PDT on pulmonary metastases

To study the impact of the immune system on a putative systemic anti-tumor effect of PDT in experimental osteosarcoma, lungs were dissected at sacrifice from 143B/SCID and from K7M2L2/BALB/c mice 14 and 10 days after Foscan- or Foslip- based PDT. The number of micro- and macrometastases was assessed on the surface of lung whole mounts (**Fig. 5**). PDT with either Foscan or Foslip had no effect on pulmonary metastasis in SCID mice with

intratibial 143B cell line derived tumors (**Figs. 5a, b**). In contrast, in immunocompetent BALB/c mice with intratibial tumors derived from the syngeneic K7M2L2 cell line, Foscan- and Foslip-based PDT significantly inhibited the formation of lung micro- and macro-metastases to a comparable extent (**Figs. 5c, d**). Thus, in experimental osteosarcoma investigated here, PDT requires an intact immune system to provoke a systemic anti-tumor effect.

PDT inhibits tumor perfusion in the syngeneic K7M2L2/BALB/c osteosarcoma mouse model

Blood perfusion of the tumor-bearing and the healthy control hind limb was measured prior to and after Foscan- and Foslip-based PDT. The perfusion of the tumor-bearing hind limb area before PDT was on average 45.5% higher than in the corresponding hind limb area of the control leg in all experimental groups of mice (**Fig. 6a**). Two days after PDT, a striking reduction of tumor perfusion was observed in the Foscan- and Foslip-based PDT treated mice ($P < 0.001$). Remarkably, on experimental day 7, the perfusion in the tumors in both treatment groups recovered to levels prior to PDT (**Figs. 6.a, b**).

The effects of PDT on tumor vascularization were also investigated by histology and immunohistochemistry (**Fig. 6c**). CD31-immunostained endothelial cells were virtually absent in predominantly necrotic PDT-treated tumor areas, indicating disruption of vessels. In non-necrotic areas of PDT-treated tumors CD31 immunostaining remained detectable, but at overall less density than that observed in tumor tissue not subjected to PDT, which showed moderate to high numbers of CD31-stained blood vessels.

Discussion

This study investigated the potential use of PDT in two clinically relevant models of experimental osteosarcoma as a novel approach for effective treatment of metastasizing osteosarcoma. The study compared the uptake and dark- and phototoxicity *in vitro* and the efficacy of PDT *in vivo* with mTHPC in the free formulation Foscan and the liposomal formulation Foslip. It took advantage of the orthotopic human 143B and the mouse K7M2L2 cell line, which form primary intratibial tumors and lung metastases within two weeks after

inoculation in immune-defective SCID and in syngeneic immune-competent BALB/c mice, respectively.

The results of the experiments carried out *in vitro*, demonstrating comparable time- and dose-dependent uptake of both Foscan and Foslip in the two osteosarcoma cell lines, are in line with the results of previous studies performed in human biliary cancer cell lines[36]. Despite a slightly less efficient uptake of Foslip compared to Foscan by the two osteosarcoma cell lines over time, both compounds showed a comparable phototoxicity triggering apoptosis, but importantly, Foslip, unlike Foscan, showed hardly any dark-toxicity at the concentrations used in the present study. This later finding was again in good agreement with those of the study with the human biliary cancer cell lines[36] due to the considerable toxicity of ethanol/propandiol (data not shown), which is used as a solvent for Foscan in place of water for Foslip.

Crucial for the success of PDT in cancer therapy is a predominant uptake of PS by tumor compared to healthy tissue. This was indeed observed *in vivo* and *ex vivo* for i.v. administered Foscan and Foslip in both osteosarcoma mouse models investigated in the present study. These results confirmed a previously reported higher content of both formulations in tumor than in adjacent muscle tissue[28, 37]. Two mechanisms have been proposed to account for these findings. Both Foscan and Foslip bind to serum proteins such as albumin and high and low density lipoproteins (HDL/LDL) that facilitate their cellular uptake, which is apparently accelerated in fast proliferating cancer cells that are dependent on a high transport rate of lipoproteins[38, 39]. Increased PS uptake in tumor compared to healthy tissue is also caused by anatomical changes within the tumor, characterized by an enhanced leakiness of tumor blood vessels, and a slower lymphatic drainage, causing an accumulation of the PS in the tumor tissue, called the enhanced permeability and retention (EPR) effect[40, 41].

The results of the here reported experiments, analyzing the time-dependent uptake of mTHPC by tumor tissue, showed a significantly higher uptake of Foslip than of Foscan at all time points investigated in the 143B/SCID model and at 6 hours after mTHPC administration in the K7M2L2/BALB/c model. These observations are consistent with the findings of De Visscher *et al.*, who reported a significantly higher increase of Foslip than of Foscan fluorescence intensities upon i.v. PS administration in a subcutaneous adenocarcinoma mouse model[42]. Thus, Foslip appears to enhance the bioavailability of mTHPC in tumor tissue. Along

these lines, it is assumed that liposomal carriers enhance the EPR effect due to the formation of larger macromolecules upon binding to plasma proteins[43, 44].

Already 20 years ago, pioneering studies performed by Korbelik *et al*., demonstrated the importance of an intact immune system for the efficacy of PDT[45]. A comparison of the efficacy of PDT in immune-compromised and in immune-competent mice in the present study confirmed the important findings of Korbelik *et al*. PDT with Foscan and Foslip only transiently inhibited the growth of intratibial 143B cell line-derived tumors in SCID mice and had no significant effect on lung metastasis. In immune-competent BALB/c mice, however, the growth of K7M2L2 cell line-derived primary tumors was persistently suppressed and the formation of both micro- and macro-metastases significantly inhibited by PDT with the two PS formulations. Altogether, the findings confirmed the important impact of an intact immune system on PDT efficacy reported by Korbelik *et al.* and may need to be further explored.

Analysis of tumor vascularization and perfusion in the K7M2L2/BALB/c model demonstrated a pronounced, however mainly transient inhibitory effect of the here applied PDT on the blood supply of the primary tumor. These observations are consistent with reported toxic and inhibitory effects of PDT on endothelial cells and platelet formation, respectively, leading to vascular leakage and collapse[11, 46, 47]. Since angiogenesis plays a major role in tumor progression, targeting tumor vascularization by PDT has an additional beneficial tumor suppressive effect[48].

Interestingly, in the 143B/SCID model, Foslip was more effective than Foscan, presumably due to the observed higher amounts of mTHPC accumulating in tumors of Foslip than of Foscan-treated mice and to previously reported higher concentrations of monomeric mTHPC achieved with liposomal formulations, as hydrophobic PS (Foscan) strongly aggregate in aqueous media weakening their photosensitizing efficacy[38, 43].

Differences in efficacy between Foscan- based and Foslip-based PDT was only observed in the xenograft mouse model, further studies are needed to evaluate additional treatment setting for both mTHPC formulations. The relation of the liposomal carrier system and their pharmacokinetics to PDT efficacy is still under debate. Previous studies in preclinical mammary carcinoma and fibrosarcoma models showed no correlation of the PS concentrations in the tumor and PDT efficacy, indicating a correlation between PDT efficacy and PS concentration in endothelial cells 49, 50. On the other side, d`Hallewin *et al*. demonstrated the

importance of Foslip accumulation in the tumor tissue, giving rise to the highest amount of tumor necrosis with the highest PS concentration in the tumor51. Our results provide a first hint that in osteosarcoma, Foslip is equally potent compared to Foscan, but to truly compare the PDT efficiency between both compounds, further studies are needed.

In summary, this study demonstrates potent primary tumor and, even more important in osteosarcoma, lung metastasis suppressive action of mTHPC-mediated PDT in animals in two clinically relevant intratibial mouse models of osteosarcoma with an intact immune system. Considering that PDT has a relatively low systemic toxicity, repetitive application is possible. Consequently, it is an interesting novel option for the treatment of osteosarcoma, even in combination with current standards of care neoadjuvant chemotherapy.

Acknowledgments

The authors thank Matthias JE Arlt for his help with intratibial injections of tumor cells and Tojo Razafiarison for confocal microscopy and statistical analysis. Our work was supported by the University of Zurich, the Schweizerischer Verein Balgrist (Zurich, Switzerland), the Walter L. & Johanna Wolf Foundation (Zurich, Switzerland), the Highly Specialized Medicine for Musculoskeletal Oncology program of the Canton of Zurich, the Zurcher Krebsliga (Zurich, Switzerland), the Swiss National Science Foundation SNF Nr.310030_149649 and the EuroNanoMed ERA-NET grant.

Authors' Contributions

Conception and design: DM, SMB, WB; Development of methodology: DM, SMB, CC; Contributed material: SG; Acquisition of data: DM, SMB, GP, CC, BR; Analysis and interpretation of data (e.g. statistical analysis, biostatistics, computational analysis): DM, GP, SMB; Writing, review, and/or revision of the manuscript: DM, SMB, GP, BR, SG, WB, BF; Study supervision: SMB, BF

References

1. Rainusso N, Wang LL, Yustein JT. The adolescent and young adult with cancer: state of the art -- bone tumors. Curr Oncol Rep 2013;15:296-307.
2. Ward E, DeSantis C, Robbins A, Kohler B, Jemal A. Childhood and adolescent cancer statistics, 2014. CA: a cancer journal for clinicians 2014;64:83-103.
3. Mirabello L, Troisi RJ, Savage SA. Osteosarcoma incidence and survival rates from 1973 to 2004: data from the Surveillance, Epidemiology, and End Results Program. Cancer 2009;115:1531-43.
4. Allison DC, Carney SC, Ahlmann ER, Hendifar A, Chawla S, Fedenko A, Angeles C, Menendez LR. A meta-analysis of osteosarcoma outcomes in the modern medical era. Sarcoma 2012;2012:704872.
5. Miller BJ, Cram P, Lynch CF, Buckwalter JA. Risk factors for metastatic disease at presentation with osteosarcoma: an analysis of the SEER database. J Bone Joint Surg Am 2013;95:e89.
6. Whelan JS, Bielack SS, Marina N, Smeland S, Jovic G, Hook JM, Krailo M, Anninga J, Butterfass-Bahloul T, Bohling T, Calaminus G, Capra M, et al. EURAMOS-1, an international randomised study for osteosarcoma: results from pre-randomisation treatment. Annals of oncology : official journal of the European Society for Medical Oncology / ESMO 2015;26:407-14.
7. Janeway KA, Grier HE. Sequelae of osteosarcoma medical therapy: a review of rare acute toxicities and late effects. The Lancet. Oncology 2010;11:670-8.
8. He H, Ni J, Huang J. Molecular mechanisms of chemoresistance in osteosarcoma (Review). Oncology letters 2014;7:1352-62.
9. Botter SM, Neri D, Fuchs B. Recent advances in osteosarcoma. Curr Opin Pharmacol 2014;16:15-23.
10. Fayter D, Corbett M, Heirs M, Fox D, Eastwood A. A systematic review of photodynamic therapy in the treatment of pre-cancerous skin conditions, Barrett's oesophagus and cancers of the biliary tract, brain, head and neck, lung, oesophagus and skin. Health Technol Assess 2010;14:1-288.
11. Agostinis P, Berg K, Cengel KA, Foster TH, Girotti AW, Gollnick SO, Hahn SM, Hamblin MR, Juzeniene A, Kessel D, Korbelik M, Moan J, et al. Photodynamic therapy of cancer: an update. CA Cancer J Clin 2011;61:250-81.
12. Zhang X, Liu T, Li Z. Progress of photodynamic therapy applications in the treatment of musculoskeletal sarcoma (Review). Oncology letters 2014;8:1403-8.
13. Usuda J, Kato H, Okunaka T, Furukawa K, Tsutsui H, Yamada K, Suga Y, Honda H, Nagatsuka Y, Ohira T, Tsuboi M, Hirano T. Photodynamic therapy (PDT) for lung cancers. J Thorac Oncol 2006;1:489-93.
14. Gomer CJ, Ferrario A, Murphree AL. The effect of localized porphyrin photodynamic therapy on the induction of tumour metastasis. British journal of cancer 1987;56:27-32.
15. Kabingu E, Oseroff AR, Wilding GE, Gollnick SO. Enhanced systemic immune reactivity to a Basal cell carcinoma associated antigen following photodynamic therapy. Clinical cancer research : an official journal of the American Association for Cancer Research 2009;15:4460-6.

16. Thong PS, Ong KW, Goh NS, Kho KW, Manivasager V, Bhuvaneswari R, Olivo M, Soo KC. Photodynamic-therapy-activated immune response against distant untreated tumours in recurrent angiosarcoma. The Lancet. Oncology 2007;8:950-2.
17. Lorenz KJ, Maier H. Photodynamic therapy with meta-tetrahydroxyphenylchlorin (Foscan) in the management of squamous cell carcinoma of the head and neck: experience with 35 patients. Eur Arch Otorhinolaryngol 2009;266:1937-44.
18. Bredell MG, Besic E, Maake C, Walt H. The application and challenges of clinical PD-PDT in the head and neck region: a short review. Journal of photochemistry and photobiology. B, Biology 2010;101:185-90.
19. Reidy K, Campanile C, Muff R, Born W, Fuchs B. mTHPC-Mediated Photodynamic Therapy is Effective in the Metastatic Human 143B Osteosarcoma Cells. Photochem Photobiol 2012;88:721-7.
20. Kusuzaki K, Minami G, Takeshita H, Murata H, Hashiguchi S, Nozaki T, Ashihara T, Hirasawa Y. Photodynamic inactivation with acridine orange on a multidrug-resistant mouse osteosarcoma cell line. Jpn J Cancer Res 2000;91:439-45.
21. Yanase S, Nomura J, Matsumura Y, Watanabe Y, Tagawa T. Synergistic increase in osteosarcoma cell sensitivity to photodynamic therapy with aminolevulinic acid hexyl ester in the presence of hyperthermia. Photomed Laser Surg 2009;27:791-7.
22. Meier D, Campanile C, Botter SM, Born W, Fuchs B. Cytotoxic efficacy of photodynamic therapy in osteosarcoma cells in vitro. Journal of visualized experiments : JoVE 2014.
23. Nomura J, Yanase S, Matsumura Y, Nagai K, Tagawa T. Efficacy of combined photodynamic and hyperthermic therapy with a new light source in an in vivo osteosarcoma tumor model. J Clin Laser Med Surg 2004;22:3-8.
24. Sun M, Zhou C, Zeng H, Puebla-Osorio N, Damiani E, Chen J, Wang H, Li G, Yin F, Shan L, Zuo D, Liao Y, et al. Hiporfin-Mediated Photodynamic Therapy in Preclinical Treatment of Osteosarcoma. Photochem Photobiol 2015.
25. Burch S, London C, Seguin B, Rodriguez C, Wilson BC, Bisland SK. Treatment of canine osseous tumors with photodynamic therapy: a pilot study. Clin Orthop Relat Res 2009;467:1028-34.
26. Senge MO, Brandt JC. Temoporfin (Foscan(R), 5,10,15,20-tetra(m-hydroxyphenyl)chlorin)--a second-generation photosensitizer. Photochemistry and photobiology 2011;87:1240-96.
27. Buchholz J, Wergin M, Walt H, Grafe S, Bley CR, Kaser-Hotz B. Photodynamic therapy of feline cutaneous squamous cell carcinoma using a newly developed liposomal photosensitizer: preliminary results concerning drug safety and efficacy. J Vet Intern Med 2007;21:770-5.
28. Reshetov V, Lassalle HP, Francois A, Dumas D, Hupont S, Grafe S, Filipe V, Jiskoot W, Guillemin F, Zorin V, Bezdetnaya L. Photodynamic therapy with conventional and PEGylated liposomal formulations of mTHPC (temoporfin): comparison of treatment efficacy and distribution characteristics in vivo. Int J Nanomedicine 2013;8:3817-31.
29. Reshetov V, Kachatkou D, Shmigol T, Zorin V, D'Hallewin MA, Guillemin F, Bezdetnaya L. Redistribution of meta-tetra(hydroxyphenyl)chlorin (m-THPC) from conventional and PEGylated liposomes to biological substrates. Photochemical & photobiological sciences : Official journal of the European Photochemistry Association and the European Society for Photobiology 2011;10:911-9.

30. Arlt MJ, Banke IJ, Walters DK, Puskas GJ, Steinmann P, Muff R, Born W, Fuchs B. LacZ transgene expression in the subcutaneous Dunn/LM8 osteosarcoma mouse model allows for the identification of micrometastasis. J Orthop Res 2011;29:938-46.
31. Sabile AA, Arlt MJ, Muff R, Bode B, Langsam B, Bertz J, Jentzsch T, Puskas GJ, Born W, Fuchs B. Cyr61 expression in Osteosarcoma indicates poor prognosis and promotes intratibial growth and lung metastasis in mice. J Bone Miner Res 2011.
32. Fidler IJ, Naito S, Pathak S. Orthotopic implantation is essential for the selection, growth and metastasis of human renal cell cancer in nude mice [corrected]. Cancer metastasis reviews 1990;9:149-65.
33. Arlt MJ, Born W, Fuchs B. Improved Visualization of Lung Metastases at Single Cell Resolution in Mice by Combined In-situ Perfusion of Lung Tissue and X-Gal Staining of lacZ-Tagged Tumor Cells. J Vis Exp 2012.
34. Wang D, Stockard CR, Harkins L, Lott P, Salih C, Yuan K, Buchsbaum D, Hashim A, Zayzafoon M, Hardy RW, Hameed O, Grizzle W, et al. Immunohistochemistry in the evaluation of neovascularization in tumor xenografts. Biotech Histochem 2008;83:179-89.
35. Bressenot A, Marchal S, Bezdetnaya L, Garrier J, Guillemin F, Plenat F. Assessment of apoptosis by immunohistochemistry to active caspase-3, active caspase-7, or cleaved PARP in monolayer cells and spheroid and subcutaneous xenografts of human carcinoma. J Histochem Cytochem 2009;57:289-300.
36. Kiesslich T, Berlanda J, Plaetzer K, Krammer B, Berr F. Comparative characterization of the efficiency and cellular pharmacokinetics of Foscan- and Foslip-based photodynamic treatment in human biliary tract cancer cell lines. Photochemical & photobiological sciences : Official journal of the European Photochemistry Association and the European Society for Photobiology 2007;6:619-27.
37. Svensson J, Johansson A, Grafe S, Gitter B, Trebst T, Bendsoe N, Andersson-Engels S, Svanberg K. Tumor selectivity at short times following systemic administration of a liposomal temoporfin formulation in a murine tumor model. Photochemistry and photobiology 2007;83:1211-9.
38. Reshetov V, Zorin V, Siupa A, D'Hallewin MA, Guillemin F, Bezdetnaya L. Interaction of liposomal formulations of meta-tetra(hydroxyphenyl)chlorin (temoporfin) with serum proteins: protein binding and liposome destruction. Photochemistry and photobiology 2012;88:1256-64.
39. Guo D, Bell EH, Mischel P, Chakravarti A. Targeting SREBP-1-driven lipid metabolism to treat cancer. Curr Pharm Des 2014;20:2619-26.
40. Fang J, Nakamura H, Maeda H. The EPR effect: Unique features of tumor blood vessels for drug delivery, factors involved, and limitations and augmentation of the effect. Advanced drug delivery reviews 2011;63:136-51.
41. Greish K. Enhanced permeability and retention of macromolecular drugs in solid tumors: a royal gate for targeted anticancer nanomedicines. J Drug Target 2007;15:457-64.
42. de Visscher SA, Kascakova S, de Bruijn HS, van den Heuvel A, Amelink A, Sterenborg HJ, Robinson DJ, Roodenburg JL, Witjes MJ. Fluorescence localization and kinetics of mTHPC and liposomal formulations of mTHPC in the window-chamber tumor model. Lasers in surgery and medicine 2011;43:528-36.

43. Derycke AS, de Witte PA. Liposomes for photodynamic therapy. Adv Drug Deliv Rev 2004;56:17-30.
44. Konan YN, Gurny R, Allemann E. State of the art in the delivery of photosensitizers for photodynamic therapy. Journal of photochemistry and photobiology. B, Biology 2002;66:89-106.
45. Korbelik M, Krosl G, Krosl J, Dougherty GJ. The role of host lymphoid populations in the response of mouse EMT6 tumor to photodynamic therapy. Cancer Res 1996;56:5647-52.
46. Gomer CJ, Rucker N, Murphree AL. Differential cell photosensitivity following porphyrin photodynamic therapy. Cancer research 1988;48:4539-42.
47. Star WM, Marijnissen HP, van den Berg-Blok AE, Versteeg JA, Franken KA, Reinhold HS. Destruction of rat mammary tumor and normal tissue microcirculation by hematoporphyrin derivative photoradiation observed in vivo in sandwich observation chambers. Cancer research 1986;46:2532-40.
48. Bergers G, Benjamin LE. Tumorigenesis and the angiogenic switch. Nature reviews. Cancer 2003;3:401-10.
49. Jones HJ, Vernon DI, Brown SB. Photodynamic therapy effect of m-THPC (Foscan) in vivo: correlation with pharmacokinetics. Br J Cancer 2003;89:398-404.
50. Lassalle HP, Dumas D, Grafe S, D'Hallewin MA, Guillemin F, Bezdetnaya L. Correlation between in vivo pharmacokinetics, intratumoral distribution and photodynamic efficiency of liposomal mTHPC. J Control Release 2009;134:118-24.
51. D'Hallewin MA, Kochetkov D, Viry-Babel Y, Leroux A, Werkmeister E, Dumas D, Grafe S, Zorin V, Guillemin F, Bezdetnaya L. Photodynamic therapy with intratumoral administration of Lipid-Based mTHPC in a model of breast cancer recurrence. Lasers Surg Med 2008;40:543-9.

Figure Legends

Figure 1. Dose- and time-dependent uptake of Foscan and Foslip in 143B and K7M2L2 osteosarcoma cells. Cells were incubated in the dark with either Foscan (■) or Foslip (●) with the indicated concentrations of mTHPC for 5 h (a) or with 0.6 µg/ml mTHPC for indicated time periods (b). After washing with PBS, mTHPC fluorescence intensity (indicated as relative fluorescence unit (RFU)) was measured at 652 nm after excitation at 452 nm. * $P < 0.05$, ** $P < 0.01$, Foscan compared with Foslip. (c) Representative images of cellular localization of mTHPC by confocal laser scanning microscopy in 143B and K7M2L2 cells. mTHPC fluorescence appeared red and nuclei stained with Hoechst appeared blue, 20-fold magnification, scale bar, 100 µm.

Figure 2. Dark- and photo-toxicity of Foscan and Foslip in 143B and K7M2L2 osteosarcoma cells, and PDT induced apoptosis. (a) Dose-dependent dark-toxicity. 143B (left panel) and K7M2L2 (right panel) cells (2000 cells/ well) were incubated in the dark in the absence (control, set to 100%) or in the presence of indicated concentrations of mTHPC (Foscan ■, Foslip ●) for 5 h. Cell viability was assessed in a WST-1 assay. (b) Dose-dependent photo-toxicity. 143B (left panel) and K7M2L2 (right panel) cells (800 cells/ well) were incubated in the dark in the absence (control, set to 100%) or in the presence of indicated concentrations of mTHPC for 5 h and subsequently illuminated with doses of 1 J/cm^2 (Foscan □, Foslip ○) or 5 J/cm^2 (Foscan ■, Foslip ●) of 652 nm laser light. The cell viability was determined as in (a). (c) Inhibition of PDT-induced PARP cleavage by Z-VAD-FMK in 143B cells. The cells were pre-incubated in the absence or presence of Z-VAD-FMK or DMSO and treated with Foscan (left panel) or Foslip (right panel) at indicated concentrations and subjected to PDT as described in Materials and Methods. (d) Inhibition of PARP cleavage by Z-VAD-FMK in K7M2L2 subjected to PDT as described in (c). GAPDH was used as protein loading controls.

Figure 3. Uptake of Foscan or Foslip by intratibial human xenograft 143B cell line-derived tumors in SCID mice and by intratibial mouse K7M2L2 cell line-derived tumors in syngeneic BALB/c mice. SCID and BALB/c mice with tumors > 50 mm^3 were i.v. injected with Foscan or Foslip equivalent to 1.5 mg/kg mTHPC and the uptake of the mTHPC formulations by tumor tissue over time was assessed with a fluorimeter as described in Materials and Methods. Fluorescence measurements were corrected for background fluorescence of tumor tissue, assessed in non-injected mice (no mTHPC). (a) Mean (± SEM) uptake (indicated as RFU) *in vivo* of listed mTHPC formulations at indicated time points by 143B cell line-derived tumors

(n=10) and (b) by K7M2L2 cell line-derived tumors (n=14). .* $P < 0.05$, ** $P < 0.01$, *** $P < 0.001$ Foslip compared to Foscan (2-way ANOVA, Bonferroni post-test). (c) Mean (± SEM) uptake (RFU) of indicated formulations assessed *ex vivo* 48 h after PS injection in 143B cell line-derived tumors (n=10) and in corresponding healthy leg tissue (control leg) and (d) in K7M2L2 cell line-derived tumors (n=14) and in control legs. * $P < 0.05$, ** $P < 0.01$, *** $P < 0.001$ tumor leg compared to control leg, n.s.: not significant (1-way ANOVA, Bonferroni post-test). (e) *Ex vivo* visualization of mTHPC (red) in cryosections (fluorescence filter ~620nm) of indicated primary tumor tissue of Foscan- or Foslip- and non-injected mice. White arrows point to muscle tissue. Scale bar, 200 µm.

Figure 4. Inhibition of osteosarcoma primary tumor growth in two intratibial osteosarcoma mouse models in response to Foscan or Foslip based PDT (i.v. PS administration equivalent to 0.15 mg/kg mTHPC, 20 J/cm^2). (a) Mean (± SEM) fold change in size of intratibial human 143B cell line-derived tumors in SCID mice (10 control, 7 Foscan and 7 Foslip-treated mice) and (b) of intratibial mouse K7M2L2 cell line-derived tumors in syngeneic BALB/c mice (15 control, 8 Foscan and 9 Foslip-treated mice) assessed on indicated days after PDT by caliper measurements and normalized to the tumor size in individual mice measured on the day of PDT treatment. The control groups of mice received PS but no laser light illumination (control). (c) Photographs taken on indicated days from representative SCID mice with intratibial 143B cell line-derived tumors and (d) from representative BALB/c mice with intratibial K7M2L2 cell line-derived tumors in the right hind limb. The mice were treated as indicated. + $P < 0.05$, +++ $P < 0.001$ Foscan PDT vs. control, *** $P < 0.001$ Foslip PDT vs. control. (e) Representative images of 10 µm sections of K7M2L2 cell line-derived intratibial tumors collected two days after PDT from BALB/c mice treated as indicated. The sections were stained with hematoxylin and eosin (HE) for histological examination and immunostained for cleaved caspase 3 (CC3) indicating apoptotic tissue areas. N: necrosis, V: viable tumor, black arrows indicate apoptotic cells. Scale bars: top panel, 1 mm, bottom panel, 100 µm.

Figure 5. Effect of intratibial primary tumor treatment by PDT on pulmonary metastases in the human xenograft 143B/SCID and the syngeneic K7M2L2/BALB/c osteosarcoma mouse models. (a) *Ex vivo* quantification of X-Gal stained 143B/*LacZ* cell-derived metastases on the surface of whole mounts of lungs collected from SCID mice at sacrifice 14 days after PDT. The data indicate the numbers of pulmonary micrometastases per lung (diameter < 0.1mm, left panel) and of pulmonary macrometastases (diameter > 0.1mm, right panel) in individual

mice of the indicated treatment groups. The numbers of lungs analyzed in the different experimental groups are shown by the number of corresponding symbols in the figures. (b) Representative images of blue X-gal–stained metastatic nodules on whole mounts of lungs of SCID mice analyzed as described in (a). Scale bar, 200 µm. (c) *Ex vivo* quantification of X-Gal stained K7M2L2/*LacZ* cells on whole mounts of lungs collected from BALB/c mice at sacrifice 10 days after treatment. The mice of the indicated treatment groups were analyzed and the data are presented as described in (a), ** $P < 0.01$, *** $P < 0.001$, PDT-treated groups vs. control, n.s.: not significant. (d) Representative images of blue X-Gal–stained metastases on whole mounts of lungs of BALB/c mice analyzed as described in (c). Scale bar, 200 µm. Black arrows point to pulmonary micrometastases and the open black arrow to a macrometastasis.

Figure 6. Effect of primary tumor treatment by Foscan or Foslip-based PDT on hind limb blood flow in the syngeneic K7M2L2/BALB/c osteosarcoma mouse model. (a) Blood flow in control and tumor-bearing hind limbs was measured with a laser Doppler perfusion imager in the regions of interest (ROI) (as indicated in b), and the data collected from 12 mice per treatment group on indicated experimental days are presented as percent change in perfusion (flux) of tumor compared to normal tissue, *** $P < 0.001$ PDT- treated vs. control. (b) Images of hind limb perfusion taken on indicated experimental days from representative mice of the different experimental groups. White circles indicate ROI for laser Doppler image analysis. (c) Representative images of CD31 immunostained 10 µm sections of intratibial tumors collected from representative mice of the indicated treatment groups on day 2 after PDT. Black arrows point to CD31-stained endothelial cells, scale bar 250 µm.

Supporting Information Table 1. Half-maximal cell viability inhibitory doses (IC_{50}) of Foscan and Foslip in 143B and K7M2L2 osteosarcoma cells subjected to PDT with light energy doses of 1J/cm^2 or 5 J/cm^2 as indicated.

Supporting Information Figure 1. 10^6 143B (a) or K7M2L2 (b) cells were incubated for 5 h with Foscan or Foslip at indicated mTHPC concentrations. Osteosarcoma cells were illuminated (as described in Material and Methods) or kept in the dark. Cell lysates were analyzed with antibodies to cleaved caspase 3 (1:1000, Cell Signaling Technology, Danvers, MA), to cleaved caspase 7 (1:1000, Cell Signaling Technology), to caspase 9 and cleaved caspase 9 (1:1000, Cell Signaling Technology), to PARP and cleaved PARP (1:1000, Cell Signaling Technology), to GAPDH (1:3000 Santa Cruz Biotechnologies) and to Actin

(1:10`000, Millipore Darmstadt, Germany). GAPDH and Actin were used as protein loading controls.

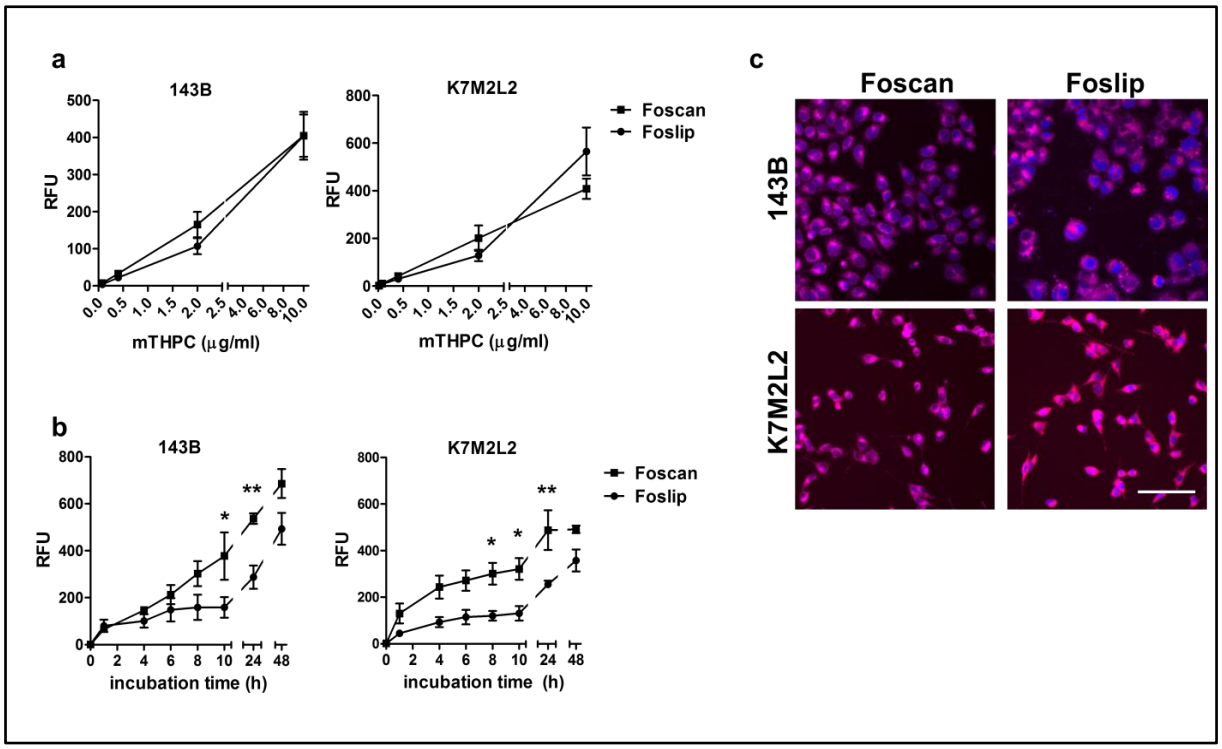
a
143B
K7M2L2
RFU
mTHPC (μg/ml)
Foscan
Foslip
b
143B
K7M2L2
RFU
incubation time (h)
Foscan
Foslip
c
Foscan
Foslip
143B
K7M2L2

Figure 1.

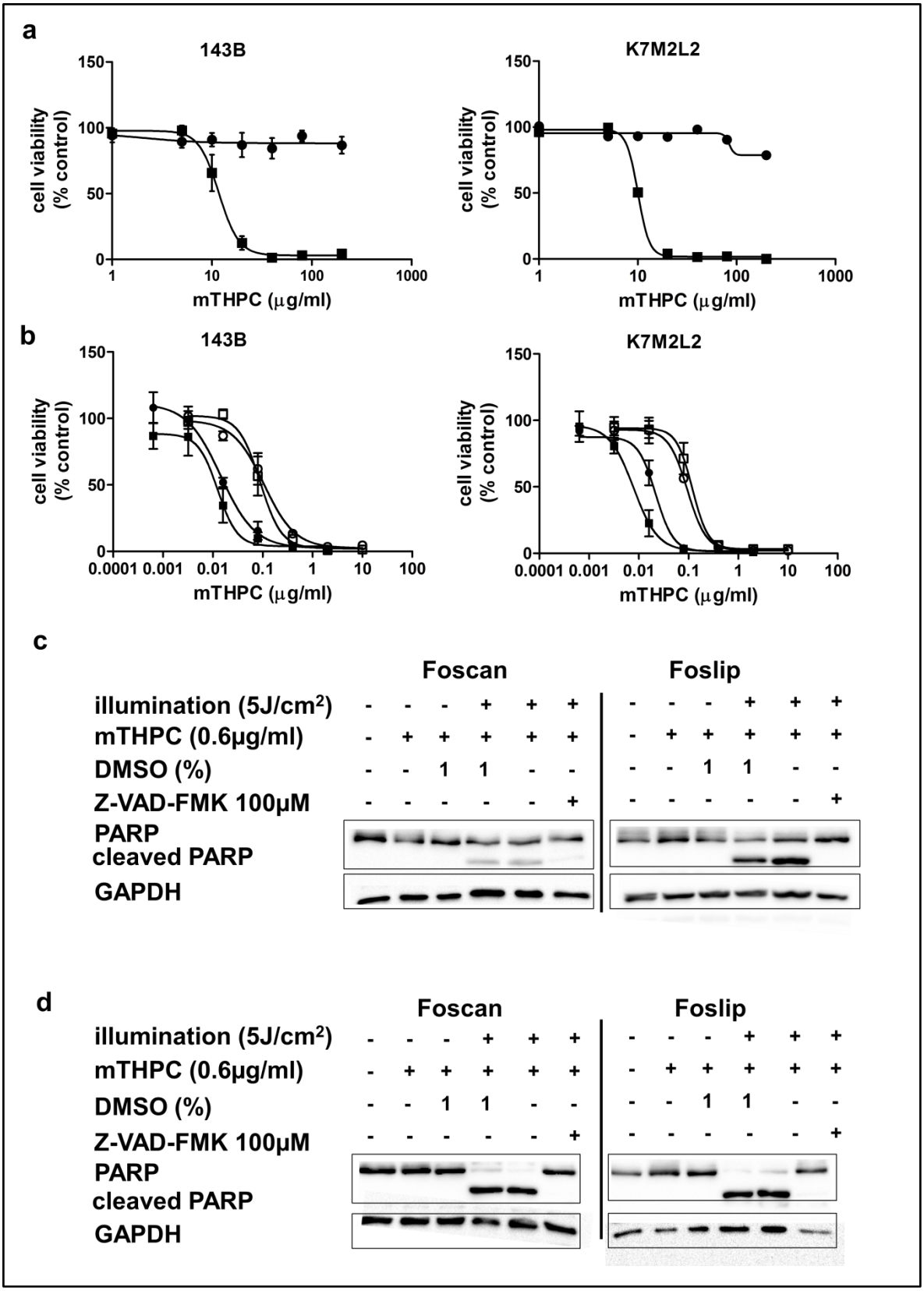
a
143B
K7M2L2
cell viability (% control)
mTHPC (μg/ml)
b
143B
K7M2L2
cell viability (% control)
mTHPC (μg/ml)
c
Foscan
Foslip
illumination (5J/cm²)
mTHPC (0.6μg/ml)
DMSO (%)
Z-VAD-FMK 100μM
PARP
cleaved PARP
GAPDH
d
Foscan
Foslip
illumination (5J/cm²)
mTHPC (0.6μg/ml)
DMSO (%)
Z-VAD-FMK 100μM
PARP
cleaved PARP
GAPDH

Figure 2.

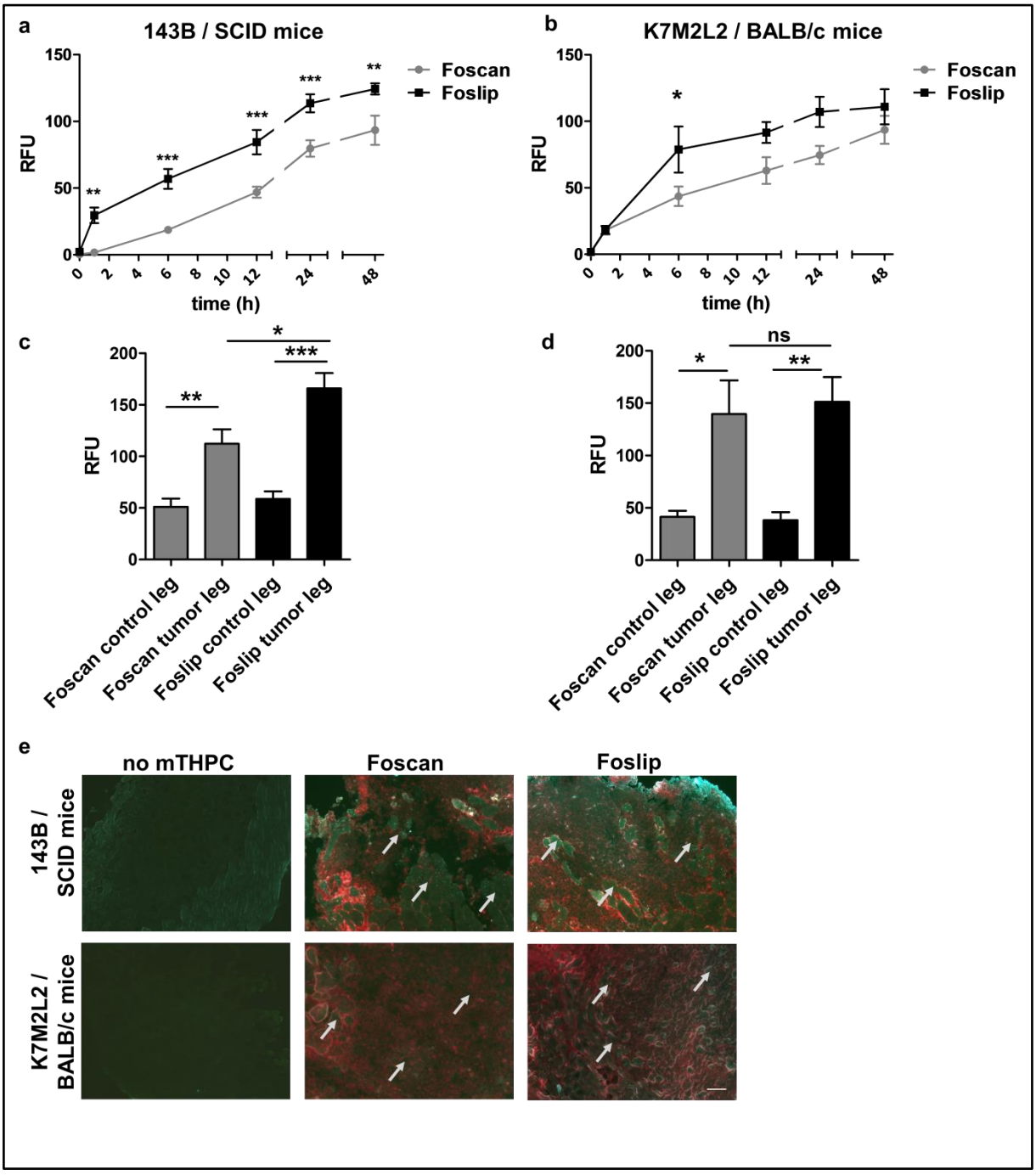
a
143B / SCID mice
RFU
time (h)
Foscan
Foslip
b
K7M2L2 / BALB/c mice
RFU
time (h)
Foscan
Foslip
c
RFU
Foscan control leg
Foscan tumor leg
Foslip control leg
Foslip tumor leg
d
RFU
ns
Foscan control leg
Foscan tumor leg
Foslip control leg
Foslip tumor leg
e
no mTHPC
Foscan
Foslip
143B / SCID mice
K7M2L2 / BALB/c mice

Figure 3.

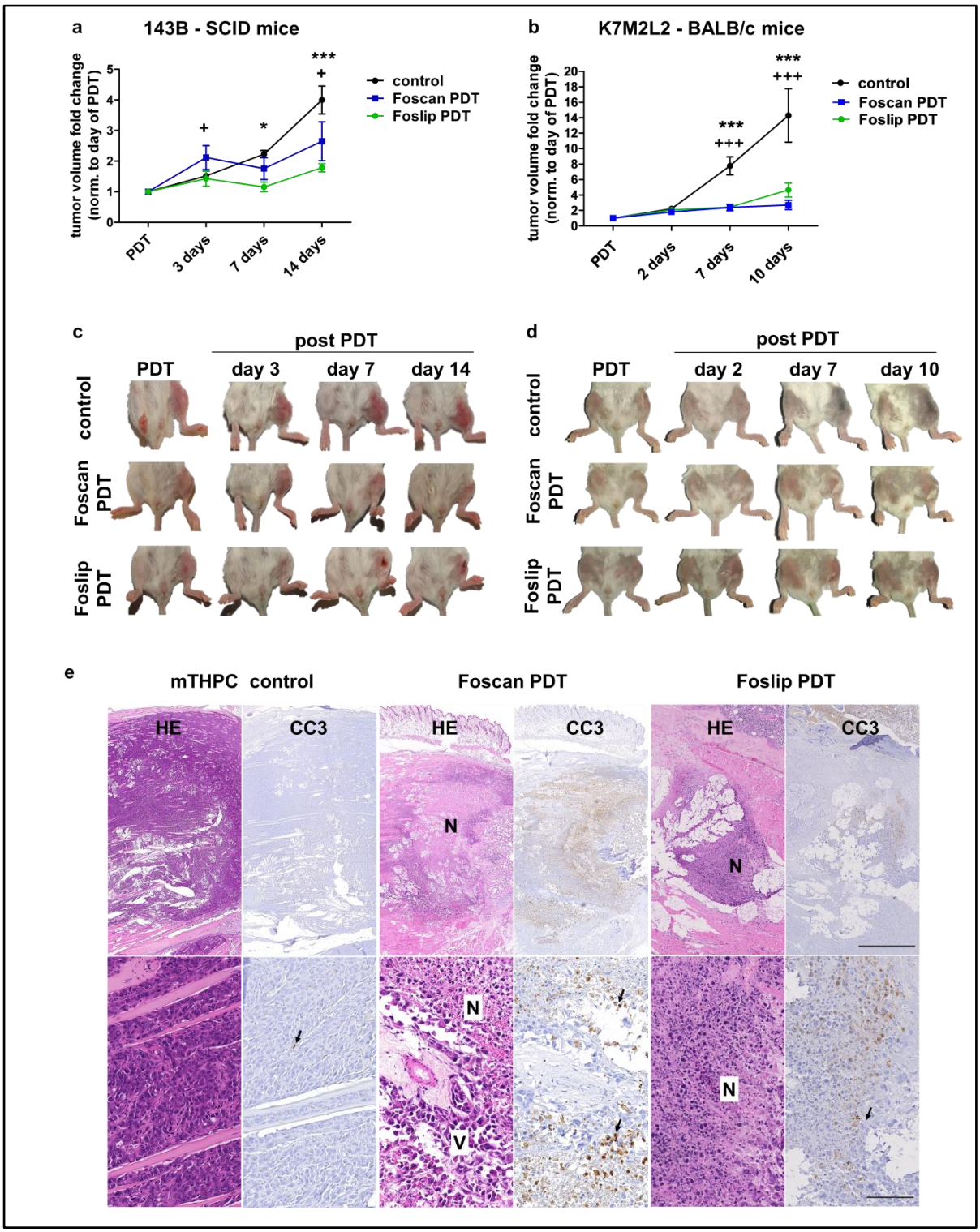
a
143B - SCID mice
tumor volume fold change (norm. to day of PDT)
control
Foscan PDT
Foslip PDT
PDT
3 days
7 days
14 days
b
K7M2L2 - BALB/c mice
tumor volume fold change (norm. to day of PDT)
control
Foscan PDT
Foslip PDT
PDT
2 days
7 days
10 days
c
post PDT
PDT
day 3
day 7
day 14
control
Foscan PDT
Foslip PDT
d
post PDT
PDT
day 2
day 7
day 10
control
Foscan PDT
Foslip PDT
e
mTHPC control
Foscan PDT
Foslip PDT
HE
CC3
N
V

Figure 4.

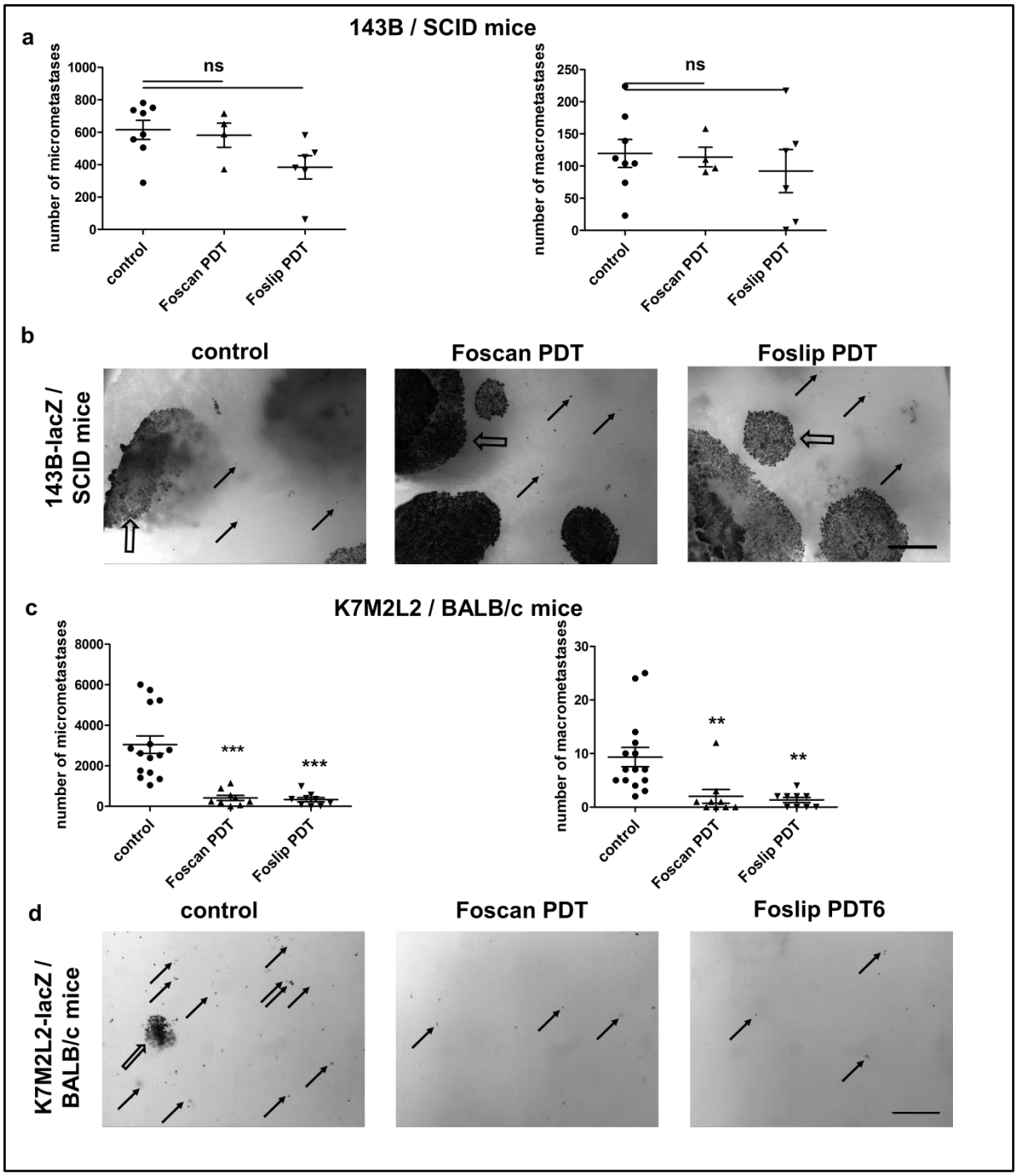
143B / SCID mice
a
number of micrometastases
ns
control
Foscan PDT
Foslip PDT
number of macrometastases
ns
b
control
Foscan PDT
Foslip PDT
143B-lacZ / SCID mice
c
K7M2L2 / BALB/c mice
number of micrometastases
***
***
number of macrometastases
**
**
d
control
Foscan PDT
Foslip PDT6
K7M2L2-lacZ / BALB/c mice

Figure 5.

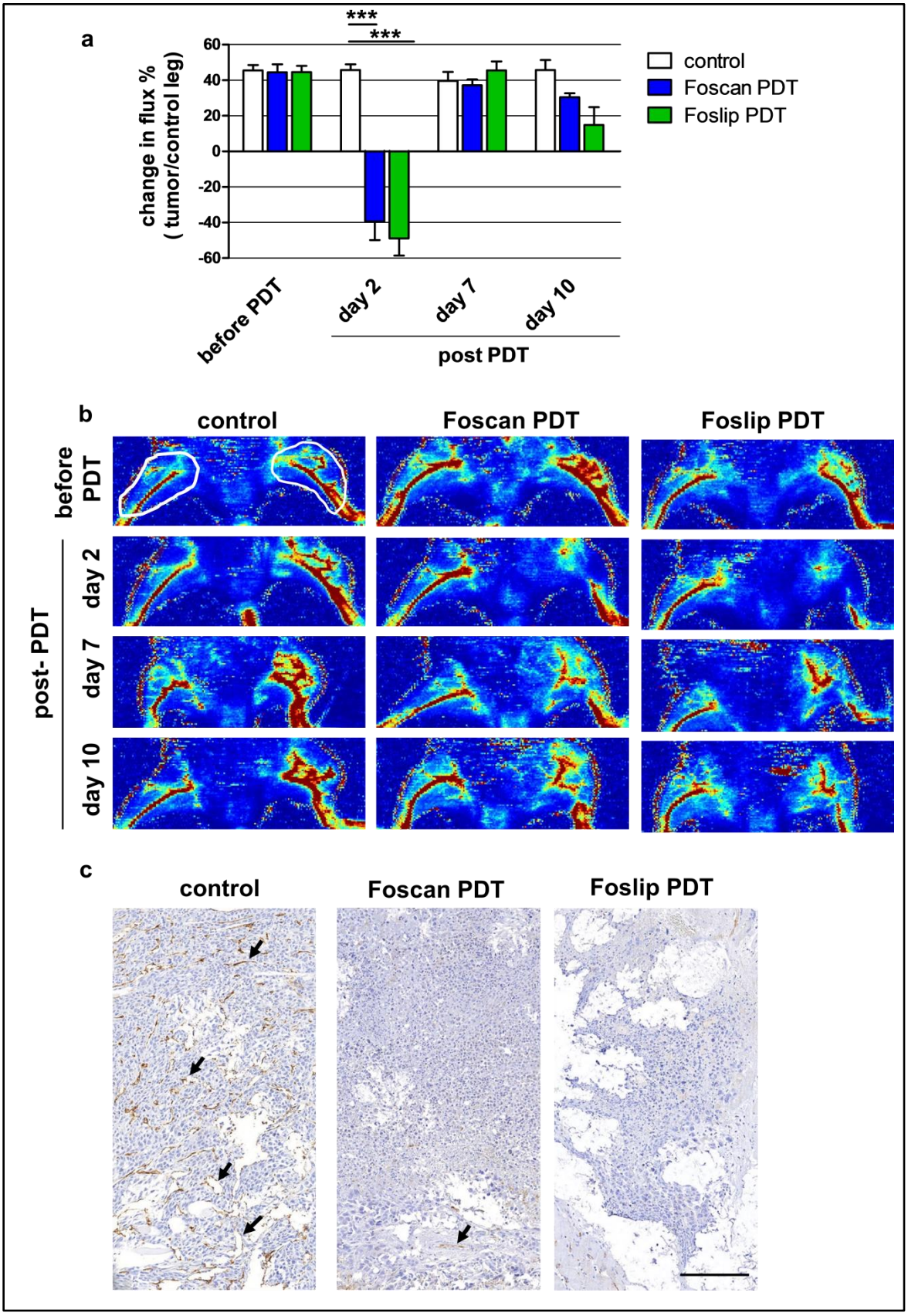
a
***
***
change in flux %
(tumor/control leg)
60
40
20
0
-20
-40
-60
before PDT
day 2
day 7
day 10
post PDT
control
Foscan PDT
Foslip PDT
b
control
Foscan PDT
Foslip PDT
before PDT
post- PDT
day 2
day 7
day 10
c
control
Foscan PDT
Foslip PDT

Figure 6.

Supporting Information Table 1

	IC50 (µg/ml)			
cell lines	Foscan (1 J/cm²)	Foscan (5 J/cm²)	Foslip (1 J/cm²)	Foslip (5 J/cm²)
143B	0.1059	0.01445	0.08914	0.01255
K7M2L2	0.1195	0.0079	0.09498	0.02192

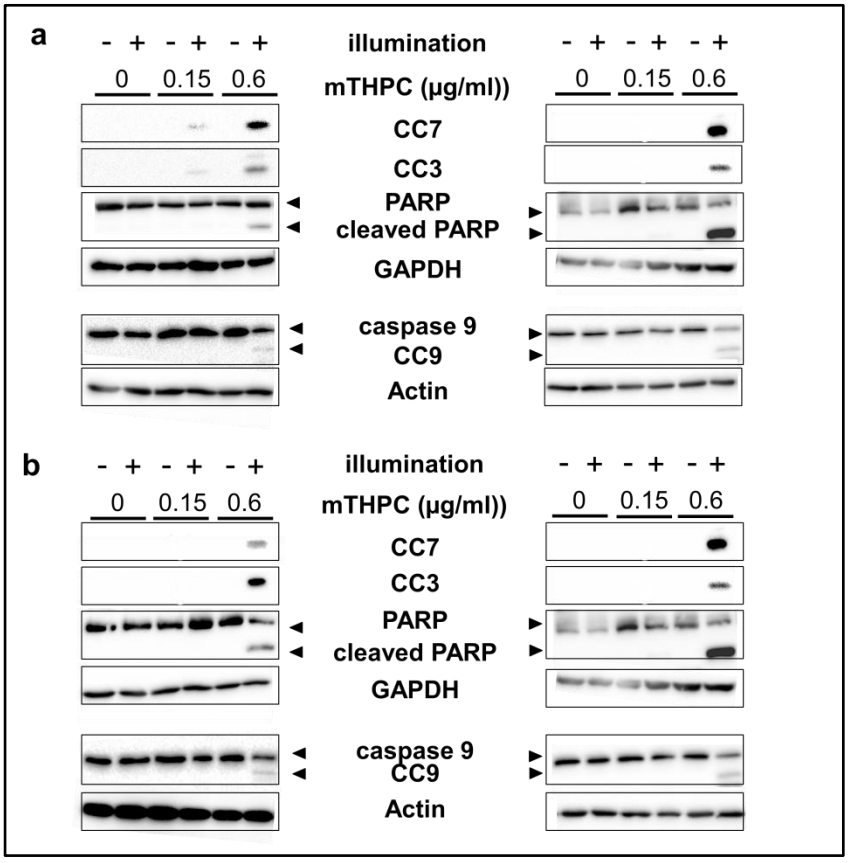

Supporting Information Figure 1

6.4 Additional Study: lipid nanoparticles as novel carriers for mTHPC

6.4.1 Results

In addition to Foscan and the liposomal formulation of mTHPC, Foslip, also lipid nanoparticles (LNP) loaded with mTHPC were investigated and the data are presented here. LNP (or lipidots®) consist of a lipid core loaded with mTHPC, surrounded by phospholipids and pegylated surfactants. LNP were tested for their PDT efficacy *in vitro* and *in vivo* in the human 143B OS cell line and in a 143B cell line-derived intratibial metastasizing OS model in SCID mice (143B/SCID), respectively.

Cellular uptake and cytotoxicity of Foscan and LNP (mTHPC)

The uptake of mTHPC in the Foscan formulation and its lipid nanoparticle formulation LNP was determined in the 143B cell line. A significantly higher time-dependent uptake was observed for Foscan than for LNP (mTHPC) at 24 h and 48 h of incubation. Conversely after 72 h of incubation, uptake of the LNP was significantly higher than that of Foscan (**Fig. A1 A**).

Dark-toxicity, examined in 143B cells was not observed at the indicated concentrations up to 20 µg/ml of mTHPC. Photo-toxicity, however, occurred in the 143B cell line at concentrations as low as 0.0032 µg/ml mTHPC (**Fig. A1 B**).

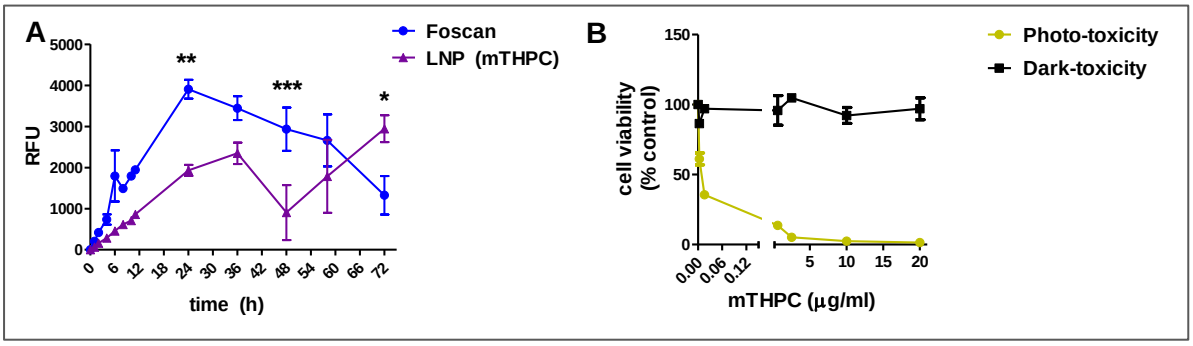

Figure A1: Cellular uptake and cytotoxicity of mTHPC containing lipid nanoparticles (LNP). (A) Time dependent uptake of Foscan and LNP (mTHPC) by 143B OS cells. Cells were incubated in the dark with either Foscan (blue) or LNP (violet) with 2.5 µg/ml mTHPC for indicated time periods. After replacing the medium, mTHPC fluorescence intensity was measured at 652 nm after excitation at 417 nm. ** $P < 0.01$, *** $P < 0.001$ Foscan treated vs. LNP (mTHPC) treated. (B) Photo- and dark-toxicity of LNP (mTHPC) in 143B cells. Cells were incubated in the dark in the absence (control) or in the presence of LNP (mTHPC) at indicated concentrations of mTHPC for 5 h and illuminated with laser light of 652 nm wavelength at doses of 5 J/cm^2. To determine dark-toxicity, the cells were kept in the dark until harvested. Metabolic activity was assessed after 24 h. Results are the mean ± SEM of three independent experiments.

LNP uptake *in vivo* in the 143B/SCID model

Uptake of the mTHPC formulations Foscan, Foslip and LNP (mTHPC) was investigated in an orthotopic 143B osteosarcoma mouse model and the data are illustrated in Figure A2. All mTHPC formulations were taken up by the tumor tissue in a time-dependent manner. Since the results of the Foslip uptake were already evaluated and discussed in the third manuscript (Chapter 6.3), the focus in this section of the thesis is on the uptake of LNP in relation to Foscan and Foslip.

Although the injection of Foslip resulted in the highest mTHPC signal in the tumor bearing leg, the injection of LNP with mTHPC in the lipid core revealed also a statistically significant higher mTHPC uptake than that observed with `naked` mTHPC in the Foscan formulation (**Fig. A2 A**). *Ex vivo* measurements of mTHPC fluorescence in tumor and control tissue in mice that received LNP loaded with mTHPC showed a 2.5-fold higher accumulation of mTHPC in the tumor tissue than in corresponding healthy control tissue dissected form contralateral hind limb (**Fig. A2 B**).

In order to investigate in more detail the *in vivo* uptake and tissue distribution of LNP in the 143B/SCID model, LNP were loaded with a near-infrared fluorescent dye (NIR) and their distribution in tumor and healthy tissue analyzed in 3D in a fluorescence molecular tomograph (FMT). Results are presented as the concentration of mTHPC (pmol) within the tumor tissue and in the corresponding ROI in the control leg at the indicated time points (**Fig. A2 C**). The results confirmed the *ex vivo* measured significant difference in LNP (mTHPC) uptake between the tumor-bearing and the healthy contralateral leg. A significant higher uptake in the tumor than in the control leg was observed during the entire experimental period of 48 h. **Figure A2 D** shows representative FMT pictures of the LNP (NIR) uptake in the ROI in the tumor-bearing leg, with the color scale indicating the concentration of NIR within the tissue.

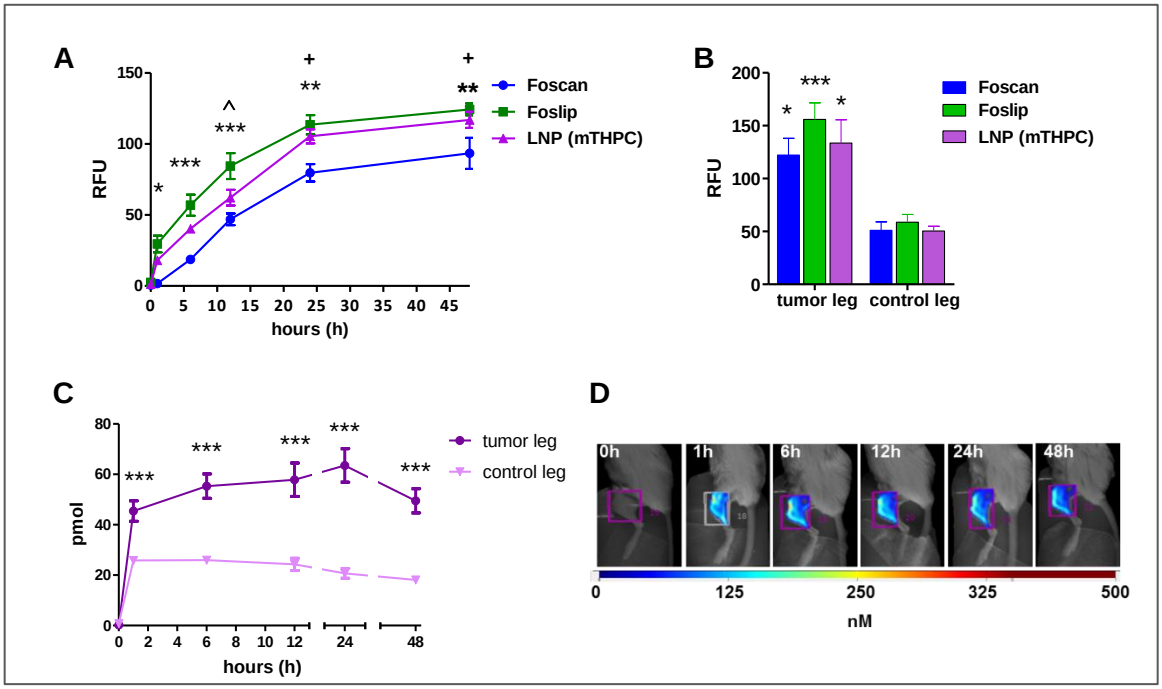

Figure A2: Uptake of Foscan, Foslip and LNP in the 143B/SCID model. Mice with intratibial tumors > 50 mm^3 were injected with or without indicated photosensitizer formulations equivalent to 1.5 mg/kg mTHPC. (A) *In vivo* photosensitizer uptake in the 143B tumor leg was assessed with a fluorimeter over time as described in Materials and Methods. (B) mTHPC fluorescence 48 h after injection was measured *ex vivo* within the primary tumor tissue with the fluorimeter. * $P < 0.05$, ** $P < 0.01$, *** $P < 0.001$ Foslip vs. Foscan, $^{+}P < 0.05$ LNP vs. Foscan, ^ $P < 0.05$ Foslip vs. LNP (mTHPC). (C) *In vivo* uptake of LNP containing a near-infrared fluorescent dye (LNP (NIR)) measured with a FMT (FMT 2500, Perkin Elmer), *** < 0.001 tumor leg vs. control leg. Results are the mean ± SEM of three independent experiments.

Tumor-suppressive efficacy of LNP (mTHPC) based photodynamic therapy in the 143B/SCID model

The change in tumor volume in mice subjected to LNP (mTHPC) mediated PDT was not significantly different compared to that in control animals (**Fig A3 A, B**). There was however a tendency for larger tumors in treated than in control mice two weeks after illumination; at that time point, the treated mice had on average a 9.4-fold larger volume than on the day of treatment whereas the tumors in the control group were only 4.1-fold larger. No difference in the fold change of tumor volume was observed between the Foscan and LNP (mTHPC) injected control (no illumination) mice (**Fig. A3, A, B**). It is important to note that 1 out of 6 control mice (17%) compared to 4 out of 8 LNP (mTHPC)-based PDT treated mice had to be sacrificed before the end the treatment study.

The counting of pulmonary metastases on the lung surface revealed no significant difference in the number of macrometastases in treated and non-treated mice (**Fig A4 A**), but a significant increase in the number of micrometastases in the PDT treated compared to non-treated mice (**Fig. A4 B**).

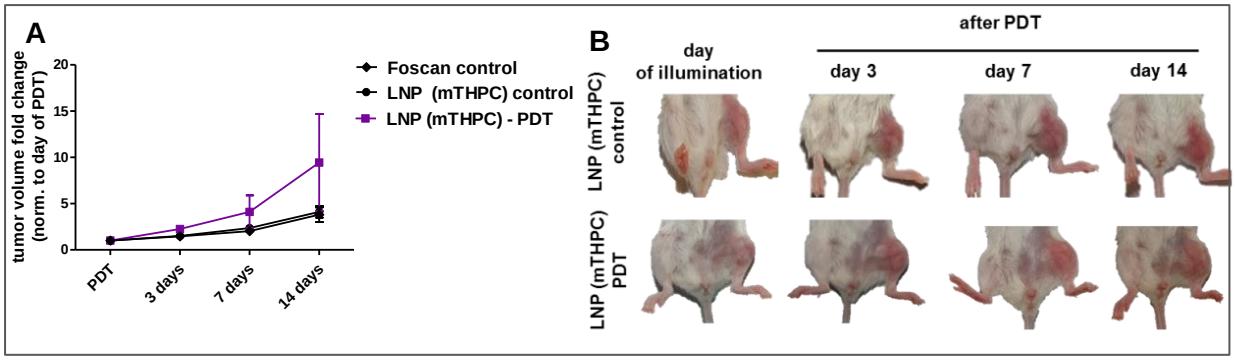

Figure A3: Osteosarcoma primary tumor growth in the 143B/SCID model upon LNP (mTHPC) based PDT (0.15 mg/kg mTHPC, 20 J/cm^2). (A) Intratibial tumor growth in 143B/SCID mice on the day of laser light illumination and 3, 7 and 14 days after illumination. Tumor volume was measured with a caliper ruler and is shown as the fold change compared to the tumor volume measured on the day of laser light illumination. The control group received i.v. Foscan and LNP (mTHPC) but no laser light illumination. (B) Representative photographs of the hind limbs of control and PDT treated 143B/SCID mice. Results are the mean ± SEM of three independent experiments.

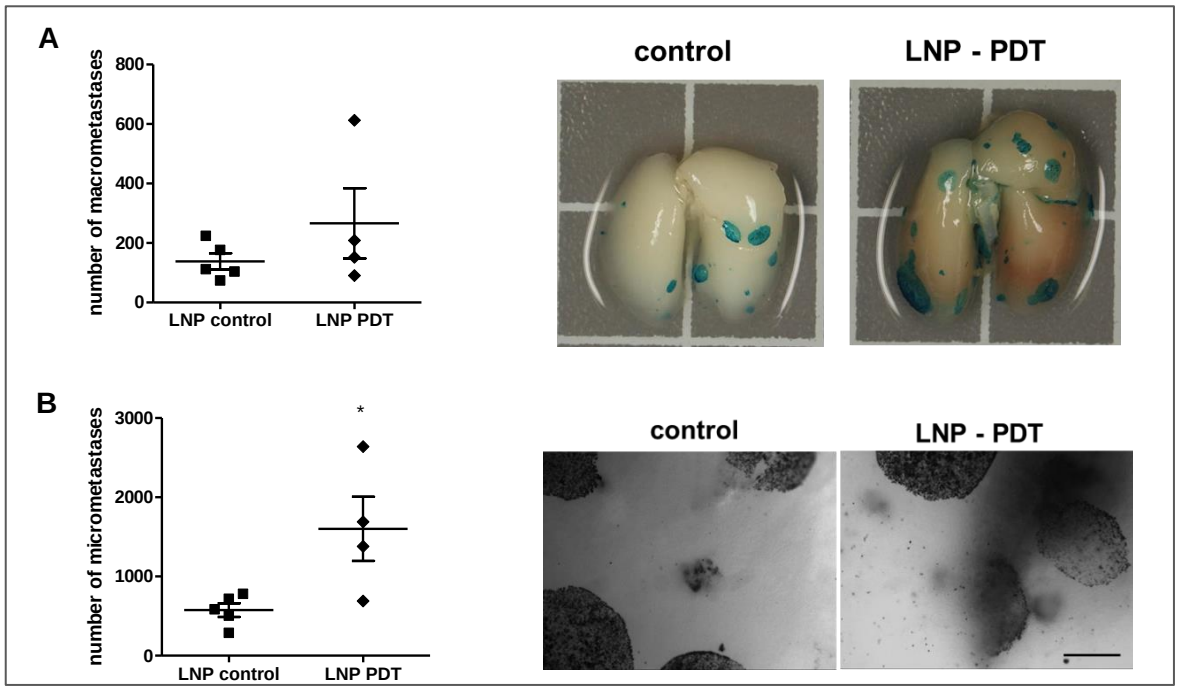

Figure A4: Effect of LNP (mTHPC) - based PDT on pulmonary metastases in the 143B/SCID model. (A, B) *Ex vivo* quantification of X-Gal stained 143B/LacZ cells on the surface of the entire lung. (A) Number of pulmonary macrometastases (diameter > 0.1mm) (left panel) and representative images of blue X-gal–stained macrometastases on the lung surface (right panel). (B) Number of pulmonary micrometastases (diameter < 0.1mm) (left panel) and representative images of blue X-Gal–stained micrometastases in the lungs observed at 4-fold magnification under the microscope, scale bar, 200 µm (right panel).* $P < 0.05$, LNP (mTHPC) PDT-treated group vs. control group. Results are the mean ± SEM of three independent experiments.

6.4.2 Discussion

This study shows the *in vitro* and *in vivo* efficacy of PDT with mTHPC incorporated into LNP. The *in vitro* results demonstrated an effective uptake and cytotoxicity in osteosarcoma cell lines. All components of the LNP are biocompatible, biodegradable and are FDA approved, which makes them an interesting novel carrier for mTHPC (Delmas, Couffin et al. 2011). Navarro et al., already demonstrated that the encapsulation of mTHPC into solid LNP does not affect the generation of oxygen radical and the LNP showed good colloidal stability and increased significantly the solubility of the photosensitizer compared to the hydrophobic Foscan formulation of mTHPC (Navarro, Creusat et al. 2014).

Cellular uptake of LNP (mTHPC) was shown to be slightly delayed when compared to Foscan in the first hours, probably due to a delay in the release from the inner oil core of the LNP. The LNP provoked also striking cytotoxicity at low mTHPC doses, which is comparable to previously published data (Reidy, Campanile et al. 2012) and results shown in the third manuscript (Chapter 6.3, Results). Similar to Foslip, a reduction in dark-toxicity was also demonstrated and the findings are in line with previous observations in breast cancer cells (Navarro, Creusat et al. 2014).

Based on these promising *in vitro* results, the LNP were further tested in an intratibial xenograft osteosarcoma mouse model, which largely reproduces the clinical situation in patients, including metastatic spread to the lungs. Comparable to the already described data in the results part of the third manuscript (Chapter 6.3, Results), the LNP showed an efficient uptake by the tumor tissue compared to healthy tissue. These data were also confirmed by FMT imaging using LNP that contained a near-infrared fluorescent dye, which allowed not only an epifluorescence measurement but a three-dimensional measurement of the mTHPC uptake in the tumor tissue (Ntziachristos, Tung et al. 2002; Jacquart, Keramidas et al. 2013). The LNP mediated uptake of mTHPC in the tumor tissue was higher than that of Foscan. Likely explanations for the higher LNP uptake are an enhanced permeability and retention (ERP) effect (Fang, Nakamura et al. 2011), but also the PEGylated shell of the LNP, which reduces the recognition by the mononuclear phagocyte system and thereby enhances the half-life in the circulation (Caliceti and Veronese 2003; Jokerst, Lobovkina et al. 2011; Perry, Reuter et al. 2012).

Despite the proof of uptake and cytotoxic activity *in vitro* and LNP uptake by primary tumor tissue *in vivo*, the present study showed no effect of the LNP (mTHPC)-based PDT in the osteosarcoma mouse model. Both, primary tumor growth and metastatic spread were not

inhibited, and there was even a tendency for more aggressive tumor progression and metastasis in treated than in non-treated mice. The components of mTHPC loaded LNP unlikely induced tumor progression because tumors in mice that received LNP (mTHPC) or Foscan without illumination showed no difference in progression. Therefore, further studies are needed to investigate unknown processes that lead to the failure of LNP (mTHPC)-based PDT in the osteosarcoma mouse used in this study.

6.4.3 Material and Methods

Lipid nanoparticles

Lipid nanoparticles (LNP) also called Lipidots® were prepared as reported (Delmas, Couffin et al. 2011). LNP consist of a lipid core (soybean oil and suppocire NB), which is surrounded by a lecithin layer (lipoid s75) decorated with pegylated surfactants and are kept in suspension in an aqueous buffer such as PBS. 50 nm sized LNP were designed due to their suitable weight ratios of core/shell excipients. The LNP were then loaded with mTHPC PS accodring to Navarro et al. (Navarro, Creusat et al. 2014) aiming at a content of 920 molecules of mTHPC per LNP.

For in vivo fluorescence imaging, the lipid core of LNP was loaded with the near-infrared fluorescent dye IRO-780-Oleyl (LNP-NIR) as previously described (Jacquart, Keramidas et al. 2013).

***In vitro* photosensitizer uptake**

143B cells were seeded in six well plates (800 cells / well) and allowed to adhere overnight. Either Foscan or LNP (mTHPC) were added (25 µl/well; 0.6 µg/ml mTHPC) in a time dependent manner (0 - 48 h) and the cells kept in the dark. PS uptake was stopped by washing the cells twice with 100 µl PBS. The fluorescence of the cells in 100 µl PBS was measured at 652 nm after excitation at 417 nm with a Spectramax Gemini XS plate reader (Molecular Devices, Sunnyvale, CA).

Dark- and phototoxicity of LNP (mTHPC)

143B were incubated with indicated concentrations of LNP, equivalent to 0 - 200 µg/ml mTHPC, for 5 h, and subsequently illuminated with an energy dose of 5 J/cm^2 at 652 nm (21.88 mW/cm2, 230sec) as described previously (Reidy, Campanile et al. 2012). The remaining cell metabolic activity was then measured with the water-soluble tetrazolium (WST-1) assay according to the manufacturer's protocol.

Intratibial human xenograft OS mouse model

All studies were conducted with the approval of the Veterinary Office Kanton Zurich, Switzerland (animal application license 167/2012), in accordance with the guidelines of the Swiss Federal Veterinary Office. A highly metastatic 143B cell line derived intratibial xenograft model in SCID mice (143B/SCID) was used as described in previously (Sabile, Arlt et al. 2011).

In vivo uptake of different mTHPC formulations

Upon formation of a tumor larger than > 50 mm^3, Foscan (10 mice), Foslip (10 mice) or LNP (mTHPC) (11 mice) (mTHPC 1.5 mg/kg) was i.v. administered. mTHPC uptake was measured using a PDT fluorometer as described in the Materials and Methods of the third manuscript (Chapter 6.3).

LNP containing the near-infrared fluorescent dye LNP (NIR) were used for 3D biodistribution imaging of LNP in a fluorescence molecular tomograph (FMT2500, Perkin Elmer Inc., Boston, USA). The FMT was calibrated for the LNP (NIR), following the guidelines of the TrueQuant™ Operator Manual 2011.

SCID mice were i.v. injected with 200µl of LNP (10 µM NIR) and imaged 0, 1, 6, 12, 24 and 48 h after injection. Before imaging, mice were shaved and anesthetized with 1-5% isoflurane. The anesthetized mice were placed in the imaging cassette to restrain the mouse and adjust the position. The imaging cassette with the mouse was inserted into the heated docking system in the FMT machine. A trans-illumination laser using an excitation filter at 790 nm and an emission filter above 805 nm were used for signal detection. The fluorescence data were reconstructed using the TrueQuant 3.1 PerkinElmer Software. Three-dimensional regions of interest (ROI) were marked around the hind limbs. The mTHPC uptake in the tumor tissue was calculated as the concentration of mTHPC in the ROI and in the corresponding ROI in the non-tumor bearing leg (control leg).

***In vivo* PDT protocol with LNP (mTHPC)**

The PDT treatment using LNP (mTHPC) and measurements of tumor growth and pulmonary metastases were performed in the same study as described in the Materials and Methods of the third manuscript (Chapter 6.3). Mice were randomly assigned into three groups; control (with LNP (mTHPC) or Foscan, without illumination, n= 6) and LNP (mTHPC) (n=8) PDT treated mice.

7 Conclusion and Outlook

Current protocols for the treatment of OS, developed in recent decades and combining neoadjuvant chemotherapy and refined tumor surgical techniques, no longer improve the outcome of the patients and their quality of life. Many patients suffer from severe side effects of multimodal drug therapy and the development of chemoresistance during treatment. Thus, novel drugs that strictly and specifically target local OS specific pathophysiological processes with minimal side effects are needed to complement or even replace current therapies.

Consequently, aim 1 of the thesis presented here focused on targeting, in clinically relevant experimental OS mouse models, key mechanisms in the "vicious cycle" of the interaction between the primary tumor in the bone and its microenvironment that causes pathological, abnormal regulation of local bone remodeling in favor of the tumor. Similarly, in aim 2, we investigated in experimental metastasizing OS in immunocompromised and immunocompetent mice, the potential of minimally toxic PDT, shown to be effective in many other tumor types, for supplementary treatment of metastasizing OS with minimal side effects.

The data of the studies carried out under aim 1 provide solid evidence for aberrant regulation of local bone remodeling in favor of tumor development, considered as the "vicious cycle", as an essential pathophysiological mechanism in OS progression. The studies identified activin A as an important regulator in this cycle. The inhibition of activin A lead to a disruption of tumor-promoted osteoclast-mediated bone resorption and osteoblast-mediated bone formation and a marked suppression of OS primary tumor progression. Our results highlight activin A inhibitors also in combination with the gold-standard in the inhibition of bone remodeling, zoledronic acid, as a promising therapeutic intervention in OS.

Future studies that further investigate the biological relevance of activin A in the osteosarcoma bone microenvironment are of great interest. These studies need to address the communication between the osteosarcoma cells and the different cell types in the bone microenvironment such as the osteoclasts, osteoblasts, mesenchymal stem cells or endothelial cells and they need to further elucidate the role of activin A in these interactions.

The studies carried out under aim 2 proofed the principle of PDT, being effective in clinically relevant metastasizing OS with minimal side effects as reported for a variety of

other tumor types. These findings, including low toxicity of PDT, are particularly important for the treatment of rapidly growing pediatric patients. These patients are most sensitive to treatment-associated side effects, which affect their normal development. We consider PDT as an intraoperative approach with the aim to save vital local anatomical structures and to suppress metastasis by inducing an anti-tumor immune response, the main cause of death in OS patients. The results of the *in vitro* experiments demonstrate high sensitivity of OS cells to PDT with Foscan and indicate a considerable efficacy-enhancing potential of liposomal and lipid nanoparticle formulations. Importantly, the findings were confirmed *in vivo* in the two clinically relevant OS mouse models for Foscan and Foslip, whereas the treatment with the LNP formulation of Foscan failed for, at the moment, unknown reasons. The results also highlight the importance of an intact immune system for PDT potency and a therapeutic immune response-dependent effect on lung metastasis.

To further improve PDT efficacy, a targeted approach is of great interest. Our results confirm a passive targeting of the tumor tissue, probably mainly due to the EPR effect, but its limitations are obvious. Changes in permeability and retention of PS within the tumor or limited PS uptake by smaller tumors that might not exhibit a leaky vasculature likely can hamper PS efficacy. Accordingly, current research investigates novel PS carriers with targeting moieties, such as PEGylated liposomes decorated with receptor-ligands, antibodies or other tumor targeting proteins (Goutayer, Dufort et al. 2010; Pereira, Korsak et al. 2015). Although OS is missing a common marker, potential targets in OS include EGFRs, playing an important role in tumor proliferation of different sarcomas (Wen, Koeppen et al. 2007), the CXCR4 chemokine receptor, involved in chemotaxis, invasion, angiogenesis and proliferation and associated with poor survival when upregulated in OS (Brennecke, Arlt et al. 2013; Zhao, Guo et al. 2015), VEGF, playing an important role in tumor angiogenesis; avβ3, an integrin receptor expressed in osteosarcoma tumor tissue (Gvozdenovic A., et al. submitted to Oncotarget, May 2016). Of great therapeutic interest is also the combination of PDT with established chemotherapeutics with the aim to potentiate treatment efficacy while reducing the doses of currently used toxic drugs. Preclinical studies already revealed additive tumor-suppressive effects of cisplatin and doxorubicin administered at low non-therapeutic doses in combination with PDT (Canti, Nicolin et al. 1998; Kirveliene, Grazeliene et al. 2006). Co-delivery of both, chemotherapeutics and PS within nanoparticles has already been investigated (Wang, Ma et al. 2015).

Altogether, based on the results presented in thesis and those reported by Akens MK et al., even a combination of activin A inhibitors and photodynamic therapy can be considered

for the treatment of metastasizing OS. The recent study performed by Akens MK et al. reported a combination of ZOL with Verteporfin-based PDT as a safe treatment for experimental bone-metastatic breast cancer (Akens, Wise-Milestone et al. 2014). In conclusion, this thesis shows novel routes for effective treatment of metastatic OS that target the primary tumor together with its microenvironment, which supports tumor progression. Moreover, applications of these novel treatment modalities in combination with currently used drugs can be envisaged.

8 References

Abdulkadyrov, K. M., G. N. Salogub, et al. (2014). "Sotatercept in patients with osteolytic lesions of multiple myeloma." British journal of haematology 165(6): 814-823.

Abe, Y., T. Minegishi, et al. (2004). "Activin receptor signaling." Growth factors 22(2): 105-110.

Agostinis, P., K. Berg, et al. (2011). "Photodynamic therapy of cancer: an update." CA Cancer J Clin 61(4): 250-281.

Akens, M. K., L. Wise-Milestone, et al. (2014). "In vitro and in vivo effects of photodynamic therapy on metastatic breast cancer cells pre-treated with zoledronic acid." Photodiagnosis and photodynamic therapy 11(3): 426-433.

Akiyama, T., C. R. Dass, et al. (2008). "Novel therapeutic strategy for osteosarcoma targeting osteoclast differentiation, bone-resorbing activity, and apoptosis pathway." Mol Cancer Ther 7(11): 3461-3469.

Alfranca, A., L. Martinez-Cruzado, et al. (2015). "Bone microenvironment signals in osteosarcoma development." Cellular and molecular life sciences : CMLS 72(16): 3097-3113.

Allison, R. R., G. H. Downie, et al. (2004). "Photosensitizers in clinical PDT." Photodiagnosis and photodynamic therapy 1(1): 27-42.

Alves, R. D., M. Eijken, et al. (2013). "Activin A suppresses osteoblast mineralization capacity by altering extracellular matrix (ECM) composition and impairing matrix vesicle (MV) production." Mol Cell Proteomics 12(10): 2890-2900.

Anderson, H. C. (1995). "Molecular biology of matrix vesicles." Clinical orthopaedics and related research(314): 266-280.

Antsiferova, M. and S. Werner (2012). "The bright and the dark sides of activin in wound healing and cancer." Journal of cell science 125(Pt 17): 3929-3937.

Aung, L., R. G. Gorlick, et al. (2002). "Second malignant neoplasms in long-term survivors of osteosarcoma: Memorial Sloan-Kettering Cancer Center Experience." Cancer 95(8): 1728-1734.

Aviles, A., N. Neri, et al. (2013). "Randomized clinical trial of zoledronic acid in multiple myeloma patients undergoing high-dose chemotherapy and stem-cell transplantation." Current oncology 20(1): e13-20.

Avnet, S., A. Longhi, et al. (2008). "Increased osteoclast activity is associated with aggressiveness of osteosarcoma." International journal of oncology 33(6): 1231-1238.

Bacci, G., S. Ferrari, et al. (2002). "Osteosarcoma of the limb. Amputation or limb salvage in patients treated by neoadjuvant chemotherapy." The Journal of bone and joint surgery. British volume 84(1): 88-92.

Bao, Y. L., K. Tsuchida, et al. (2005). "Synergistic activity of activin A and basic fibroblast growth factor on tyrosine hydroxylase expression through Smad3 and ERK1/ERK2 MAPK signaling pathways." The Journal of endocrinology 184(3): 493-504.

Bashir, M., S. Damineni, et al. (2015). "Activin-A signaling promotes epithelial–mesenchymal transition, invasion, and metastatic growth of breast cancer." Npj Breast Cancer 1: 15007.

Berenson, J. R., L. S. Rosen, et al. (2001). "Zoledronic acid reduces skeletal-related events in patients with osteolytic metastases." Cancer 91(7): 1191-1200.

Bergers, G. and L. E. Benjamin (2003). "Tumorigenesis and the angiogenic switch." Nature reviews. Cancer 3(6): 401-410.

Beristain, A. G., S. R. Narala, et al. (2012). "Homotypic RANK signaling differentially regulates proliferation, motility and cell survival in osteosarcoma and mammary epithelial cells." Journal of cell science 125(Pt 4): 943-955.

Bielack, S. S., B. Kempf-Bielack, et al. (2002). "Prognostic factors in high-grade osteosarcoma of the extremities or trunk: an analysis of 1,702 patients treated on neoadjuvant cooperative osteosarcoma study group protocols." Journal of clinical oncology : official journal of the American Society of Clinical Oncology 20(3): 776-790.

Black, D. M., P. D. Delmas, et al. (2007). "Once-yearly zoledronic acid for treatment of postmenopausal osteoporosis." The New England journal of medicine 356(18): 1809-1822.

Bonewald, L. F. (2011). "The amazing osteocyte." Journal of bone and mineral research : the official journal of the American Society for Bone and Mineral Research 26(2): 229-238.

Bown, S. G., A. Z. Rogowska, et al. (2002). "Photodynamic therapy for cancer of the pancreas." Gut 50(4): 549-557.
Boyle, W. J., W. S. Simonet, et al. (2003). "Osteoclast differentiation and activation." Nature 423(6937): 337-342.
Braathen, L. R., R. M. Szeimies, et al. (2007). "Guidelines on the use of photodynamic therapy for nonmelanoma skin cancer: an international consensus. International Society for Photodynamic Therapy in Dermatology, 2005." Journal of the American Academy of Dermatology 56(1): 125-143.
Bramer, J. A., A. A. Abudu, et al. (2007). "Do pathological fractures influence survival and local recurrence rate in bony sarcomas?" European journal of cancer 43(13): 1944-1951.
Brennecke, P., M. J. Arlt, et al. (2013). "Expression of the chemokine receptor CXCR7 in CXCR4-expressing human 143B osteosarcoma cells enhances lung metastasis of intratibial xenografts in SCID mice." PloS one 8(9): e74045.
Buchholz, J., B. Kaser-Hotz, et al. (2005). "Optimizing photodynamic therapy: in vivo pharmacokinetics of liposomal meta-(tetrahydroxyphenyl)chlorin in feline squamous cell carcinoma." Clinical cancer research : an official journal of the American Association for Cancer Research 11(20): 7538-7544.
Buchholz, J., M. Wergin, et al. (2007). "Photodynamic therapy of feline cutaneous squamous cell carcinoma using a newly developed liposomal photosensitizer: preliminary results concerning drug safety and efficacy." Journal of veterinary internal medicine / American College of Veterinary Internal Medicine 21(4): 770-775.
Burch, S., C. London, et al. (2009). "Treatment of canine osseous tumors with photodynamic therapy: a pilot study." Clin Orthop Relat Res 467(4): 1028-1034.
Burger, H. G. and M. Igarashi (1988). "Inhibin: definition and nomenclature, including related substances." Endocrinology 122(4): 1701-1702.
Caliceti, P. and F. M. Veronese (2003). "Pharmacokinetic and biodistribution properties of poly(ethylene glycol)-protein conjugates." Advanced drug delivery reviews 55(10): 1261-1277.
Canti, G., A. Nicolin, et al. (1998). "Antitumor efficacy of the combination of photodynamic therapy and chemotherapy in murine tumors." Cancer letters 125(1-2): 39-44.
Cao, X. and D. Chen (2005). "The BMP signaling and in vivo bone formation." Gene 357(1): 1-8.
Castano, A. P., T. N. Demidova, et al. (2004). "Mechanisms in photodynamic therapy: part one-photosensitizers, photochemistry and cellular localization." Photodiagnosis and photodynamic therapy 1(4): 279-293.
Castano, A. P., T. N. Demidova, et al. (2005). "Mechanisms in photodynamic therapy: Part three-Photosensitizer pharmacokinetics, biodistribution, tumor localization and modes of tumor destruction." Photodiagnosis and photodynamic therapy 2(2): 91-106.
Castano, A. P., P. Mroz, et al. (2006). "Photodynamic therapy and anti-tumour immunity." Nat Rev Cancer 6(7): 535-545.
Cathomas, R., C. Rothermundt, et al. (2015). "RANK ligand blockade with denosumab in combination with sorafenib in chemorefractory osteosarcoma: a possible step forward?" Oncology 88(4): 257-260.
Cecic, I., C. S. Parkins, et al. (2001). "Induction of systemic neutrophil response in mice by photodynamic therapy of solid tumors." Photochemistry and photobiology 74(5): 712-720.
Cecic, I., B. Stott, et al. (2006). "Acute phase response-associated systemic neutrophil mobilization in mice bearing tumors treated by photodynamic therapy." International immunopharmacology 6(8): 1259-1266.
Chai, J., J. W. Wu, et al. (2003). "Features of a Smad3 MH1-DNA complex. Roles of water and zinc in DNA binding." The Journal of biological chemistry 278(22): 20327-20331.
Chambers, A. F., A. C. Groom, et al. (2002). "Dissemination and growth of cancer cells in metastatic sites." Nature reviews. Cancer 2(8): 563-572.
Chandhanayingyong, C., Y. Kim, et al. (2012). "MAPK/ERK Signaling in Osteosarcomas, Ewing Sarcomas and Chondrosarcomas: Therapeutic Implications and Future Directions." Sarcoma 2012: 404810.
Chen, Q., Z. Huang, et al. (2002). "Improvement of tumor response by manipulation of tumor oxygenation during photodynamic therapy." Photochemistry and photobiology 76(2): 197-203.
Chou, A. J. and R. Gorlick (2006). "Chemotherapy resistance in osteosarcoma: current challenges and future directions." Expert review of anticancer therapy 6(7): 1075-1085.
Clark, J. C., C. R. Dass, et al. (2008). "A review of clinical and molecular prognostic factors in osteosarcoma." J Cancer Res Clin Oncol 134(3): 281-297.

Cocolakis, E., S. Lemay, et al. (2001). "The p38 MAPK pathway is required for cell growth inhibition of human breast cancer cells in response to activin." The Journal of biological chemistry 276(21): 18430-18436.
Coleman, R., R. de Boer, et al. (2013). "Zoledronic acid (zoledronate) for postmenopausal women with early breast cancer receiving adjuvant letrozole (ZO-FAST study): final 60-month results." Ann Oncol 24(2): 398-405.
Coleman, R. E. (2006). "Clinical features of metastatic bone disease and risk of skeletal morbidity." Clinical cancer research : an official journal of the American Association for Cancer Research 12(20 Pt 2): 6243s-6249s.
Coleman, R. E., H. Marshall, et al. (2011). "Breast-cancer adjuvant therapy with zoledronic acid." N Engl J Med 365(15): 1396-1405.
Coxon, F. P. and A. Taylor (2008). "Vesicular trafficking in osteoclasts." Seminars in cell & developmental biology 19(5): 424-433.
Cramers, P., M. Ruevekamp, et al. (2003). "Foscan uptake and tissue distribution in relation to photodynamic efficacy." Br J Cancer 88(2): 283-290.
D'Cruz, A. K., M. H. Robinson, et al. (2004). "mTHPC-mediated photodynamic therapy in patients with advanced, incurable head and neck cancer: a multicenter study of 128 patients." Head & neck 26(3): 232-240.
Dass, C. R. and P. F. Choong (2007). "Zoledronic acid inhibits osteosarcoma growth in an orthotopic model." Mol Cancer Ther 6(12 Pt 1): 3263-3270.
David, E., F. Blanchard, et al. (2011). "The Bone Niche of Chondrosarcoma: A Sanctuary for Drug Resistance, Tumour Growth and also a Source of New Therapeutic Targets." Sarcoma 2011: 932451.
De Rosa, G., G. Misso, et al. (2013). "Bisphosphonates and cancer: what opportunities from nanotechnology?" Journal of drug delivery 2013: 637976.
Delmas, T., A. C. Couffin, et al. (2011). "Preparation and characterization of highly stable lipid nanoparticles with amorphous core of tuneable viscosity." Journal of colloid and interface science 360(2): 471-481.
Derycke, A. S. and P. A. de Witte (2004). "Liposomes for photodynamic therapy." Adv Drug Deliv Rev 56(1): 17-30.
Dougherty, T. J., J. E. Kaufman, et al. (1978). "Photoradiation therapy for the treatment of malignant tumors." Cancer research 38(8): 2628-2635.
Drake, M. T., B. L. Clarke, et al. (2008). "Bisphosphonates: mechanism of action and role in clinical practice." Mayo Clinic proceedings 83(9): 1032-1045.
Eijken, M., S. Swagemakers, et al. (2007). "The activin A-follistatin system: potent regulator of human extracellular matrix mineralization." FASEB J 21(11): 2949-2960.
Elmore, S. (2007). "Apoptosis: a review of programmed cell death." Toxicologic pathology 35(4): 495-516.
Endo-Munoz, L., A. Evdokiou, et al. (2012). "The role of osteoclasts and tumour-associated macrophages in osteosarcoma metastasis." Biochimica et biophysica acta 1826(2): 434-442.
Everts, V., J. M. Delaisse, et al. (2002). "The bone lining cell: its role in cleaning Howship's lacunae and initiating bone formation." Journal of bone and mineral research : the official journal of the American Society for Bone and Mineral Research 17(1): 77-90.
Ewing, J. (1928). "Neoplastic Diseases: A Treatise on Tumours. ." British Journal of Surgery 16: 174-175.
Fang, J., H. Nakamura, et al. (2011). "The EPR effect: Unique features of tumor blood vessels for drug delivery, factors involved, and limitations and augmentation of the effect." Advanced drug delivery reviews 63(3): 136-151.
Fidler, M. M., C. Frobisher, et al. (2015). "Long-term adverse outcomes in survivors of childhood bone sarcoma: the British Childhood Cancer Survivor Study." British journal of cancer 112(12): 1857-1865.
Fletcher C.D.M., U. K. K., Mertens F. (Eds.) (Lyon 2002). "World Health Organization Classification of Tumours. Pathology and Genetics of Tumours of Soft Tissue and Bone." IARC Press.
Florio, P., S. Luisi, et al. (2000). "Activin A stimulates insulin secretion in cultured human pancreatic islets." Journal of endocrinological investigation 23(4): 231-234.
Fornerod, M., M. Ohno, et al. (1997). "CRM1 is an export receptor for leucine-rich nuclear export signals." Cell 90(6): 1051-1060.
Franzen, P., C. H. Heldin, et al. (1995). "The GS domain of the transforming growth factor-beta type I receptor is important in signal transduction." Biochemical and biophysical research communications 207(2): 682-689.

Friedberg, J. S., R. Mick, et al. (2003). "A phase I study of Foscan-mediated photodynamic therapy and surgery in patients with mesothelioma." The Annals of thoracic surgery 75(3): 952-959.
Fuchs, B. and D. J. Pritchard (2002). "Etiology of osteosarcoma." Clinical orthopaedics and related research(397): 40-52.
Fuller, K., K. E. Bayley, et al. (2000). "Activin A is an essential cofactor for osteoclast induction." Biochem Biophys Res Commun 268(1): 2-7.
Gaddy-Kurten, D., J. K. Coker, et al. (2002). "Inhibin suppresses and activin stimulates osteoblastogenesis and osteoclastogenesis in murine bone marrow cultures." Endocrinology 143(1): 74-83.
Gajos-Michniewicz, A., A. W. Piastowska, et al. (2010). "Follistatin as a potent regulator of bone metabolism." Biomarkers : biochemical indicators of exposure, response, and susceptibility to chemicals 15(7): 563-574.
Garg, A. D., D. Nowis, et al. (2010). "Photodynamic therapy: illuminating the road from cell death towards anti-tumour immunity." Apoptosis 15(9): 1050-1071.
Garimella, R., L. Washington, et al. (2014). "Extracellular Membrane Vesicles Derived from 143B Osteosarcoma Cells Contain Pro-Osteoclastogenic Cargo: A Novel Communication Mechanism in Osteosarcoma Bone Microenvironment." Transl Oncol 7(3): 331-340.
Geller, D. S. and R. Gorlick (2010). "Osteosarcoma: a review of diagnosis, management, and treatment strategies." Clin Adv Hematol Oncol 8(10): 705-718.
Gomer, C. J., N. Rucker, et al. (1988). "Differential cell photosensitivity following porphyrin photodynamic therapy." Cancer research 48(16): 4539-4542.
Gomer, C. J., N. Rucker, et al. (1988). "Differential cell photosensitivity following porphyrin photodynamic therapy." Cancer Res 48(16): 4539-4542.
Goutayer, M., S. Dufort, et al. (2010). "Tumor targeting of functionalized lipid nanoparticles: assessment by in vivo fluorescence imaging." European journal of pharmaceutics and biopharmaceutics : official journal of Arbeitsgemeinschaft fur Pharmazeutische Verfahrenstechnik e.V 75(2): 137-147.
Gray, A. M. and A. J. Mason (1990). "Requirement for activin A and transforming growth factor--beta 1 pro-regions in homodimer assembly." Science 247(4948): 1328-1330.
Gray, P. C., C. A. Harrison, et al. (2003). "Cripto forms a complex with activin and type II activin receptors and can block activin signaling." Proceedings of the National Academy of Sciences of the United States of America 100(9): 5193-5198.
Green, J. R. (2004). "Bisphosphonates: preclinical review." Oncologist 9 Suppl 4: 3-13.
Guise, T. A. (2002). "The vicious cycle of bone metastases." Journal of musculoskeletal & neuronal interactions 2(6): 570-572.
Hansen, M. F., M. Seton, et al. (2006). "Osteosarcoma in Paget's disease of bone." Journal of bone and mineral research : the official journal of the American Society for Bone and Mineral Research 21 Suppl 2: P58-63.
Harrington, A. E., S. A. Morris-Triggs, et al. (2006). "Structural basis for the inhibition of activin signalling by follistatin." The EMBO journal 25(5): 1035-1045.
Hauschka, P. V., A. E. Mavrakos, et al. (1986). "Growth factors in bone matrix. Isolation of multiple types by affinity chromatography on heparin-Sepharose." The Journal of biological chemistry 261(27): 12665-12674.
He, H., J. Ni, et al. (2014). "Molecular mechanisms of chemoresistance in osteosarcoma (Review)." Oncology letters 7(5): 1352-1362.
Hedger, M. P., W. R. Winnall, et al. (2011). "The regulation and functions of activin and follistatin in inflammation and immunity." Vitamins and hormones 85: 255-297.
Henderson, B. W., S. O. Gollnick, et al. (2004). "Choice of oxygen-conserving treatment regimen determines the inflammatory response and outcome of photodynamic therapy of tumors." Cancer research 64(6): 2120-2126.
Hessle, L., K. A. Johnson, et al. (2002). "Tissue-nonspecific alkaline phosphatase and plasma cell membrane glycoprotein-1 are central antagonistic regulators of bone mineralization." Proceedings of the National Academy of Sciences of the United States of America 99(14): 9445-9449.
Hill, C. S. (2009). "Nucleocytoplasmic shuttling of Smad proteins." Cell research 19(1): 36-46.
Hogendoorn, P. C., N. Athanasou, et al. (2010). "Bone sarcomas: ESMO Clinical Practice Guidelines for diagnosis, treatment and follow-up." Annals of oncology : official journal of the European Society for Medical Oncology / ESMO 21 Suppl 5: v204-213.

Hopper, C., A. Kubler, et al. (2004). "mTHPC-mediated photodynamic therapy for early oral squamous cell carcinoma." International journal of cancer. Journal international du cancer 111(1): 138-146.
Isakoff, M. S., S. S. Bielack, et al. (2015). "Osteosarcoma: Current Treatment and a Collaborative Pathway to Success." Journal of clinical oncology : official journal of the American Society of Clinical Oncology 33(27): 3029-3035.
Jacquart, A., M. Keramidas, et al. (2013). "LipImage 815: novel dye-loaded lipid nanoparticles for long-term and sensitive in vivo near-infrared fluorescence imaging." Journal of biomedical optics 18(10): 101311.
Jaillon, S., M. R. Galdiero, et al. (2013). "Neutrophils in innate and adaptive immunity." Seminars in immunopathology 35(4): 377-394.
Jain, S., V. Gautam, et al. (2011). "Acute-phase proteins: As diagnostic tool." Journal of pharmacy & bioallied sciences 3(1): 118-127.
Janeway, K. A. and H. E. Grier (2010). "Sequelae of osteosarcoma medical therapy: a review of rare acute toxicities and late effects." The Lancet. Oncology 11(7): 670-678.
Johansson, A., J. Svensson, et al. (2007). "Fluorescence and absorption assessment of a lipid mTHPC formulation following topical application in a non-melanotic skin tumor model." Journal of biomedical optics 12(3): 034026.
Jokerst, J. V., T. Lobovkina, et al. (2011). "Nanoparticle PEGylation for imaging and therapy." Nanomedicine 6(4): 715-728.
Josefsen, L. B. and R. W. Boyle (2008). "Photodynamic therapy and the development of metal-based photosensitisers." Metal-based drugs 2008: 276109.
Josefsen, L. B. and R. W. Boyle (2008). "Photodynamic therapy: novel third-generation photosensitizers one step closer?" British journal of pharmacology 154(1): 1-3.
Kang, H. Y., H. Y. Huang, et al. (2009). "Activin A enhances prostate cancer cell migration through activation of androgen receptor and is overexpressed in metastatic prostate cancer." Journal of bone and mineral research : the official journal of the American Society for Bone and Mineral Research 24(7): 1180-1193.
Kansara, M., M. W. Teng, et al. (2014). "Translational biology of osteosarcoma." Nature reviews. Cancer 14(11): 722-735.
Karsenty, G., H. M. Kronenberg, et al. (2009). "Genetic control of bone formation." Annual review of cell and developmental biology 25: 629-648.
Kato, M. V. (2000). "A secreted tumor-suppressor, mac25, with activin-binding activity." Mol Med 6(2): 126-135.
Kato, M. V., H. Sato, et al. (1996). "A follistatin-like gene, mac25, may act as a growth suppressor of osteosarcoma cells." Oncogene 12(6): 1361-1364.
Kelly, J. F. and M. E. Snell (1976). "Hematoporphyrin derivative: a possible aid in the diagnosis and therapy of carcinoma of the bladder." The Journal of urology 115(2): 150-151.
Kirveliene, V., G. Grazeliene, et al. (2006). "Schedule-dependent interaction between Doxorubicin and mTHPC-mediated photodynamic therapy in murine hepatoma in vitro and in vivo." Cancer chemotherapy and pharmacology 57(1): 65-72.
Klein, G., J. Michaelis, et al. (2003). "Second malignant neoplasms after treatment of childhood cancer." European journal of cancer 39(6): 808-817.
Klein, M. J. and G. P. Siegal (2006). "Osteosarcoma: anatomic and histologic variants." Am J Clin Pathol 125(4): 555-581.
Korbelik, M. (2006). "PDT-associated host response and its role in the therapy outcome." Lasers in surgery and medicine 38(5): 500-508.
Korbelik, M. and I. Cecic (1999). "Contribution of myeloid and lymphoid host cells to the curative outcome of mouse sarcoma treatment by photodynamic therapy." Cancer letters 137(1): 91-98.
Korbelik, M. and G. J. Dougherty (1999). "Photodynamic therapy-mediated immune response against subcutaneous mouse tumors." Cancer research 59(8): 1941-1946.
Korbelik, M., G. Krosl, et al. (1996). "The role of host lymphoid populations in the response of mouse EMT6 tumor to photodynamic therapy." Cancer Res 56(24): 5647-5652.
Kreidl, E., D. Ozturk, et al. (2009). "Activins and follistatins: Emerging roles in liver physiology and cancer." World J Hepatol 1(1): 17-27.

Kubista, B., K. Trieb, et al. (2006). "Anticancer effects of zoledronic acid against human osteosarcoma cells." J Orthop Res 24(6): 1145-1152.
Kusuzaki, K., G. Minami, et al. (2000). "Photodynamic inactivation with acridine orange on a multidrug-resistant mouse osteosarcoma cell line." Japanese journal of cancer research : Gann 91(4): 439-445.
Lamoureux, F., P. Richard, et al. (2007). "Therapeutic relevance of osteoprotegerin gene therapy in osteosarcoma: blockade of the vicious cycle between tumor cell proliferation and bone resorption." Cancer research 67(15): 7308-7318.
Lander, E. S., L. M. Linton, et al. (2001). "Initial sequencing and analysis of the human genome." Nature 409(6822): 860-921.
Lassalle, H. P., D. Dumas, et al. (2009). "Correlation between in vivo pharmacokinetics, intratumoral distribution and photodynamic efficiency of liposomal mTHPC." J Control Release 134(2): 118-124.
Laverdiere, C., B. H. Hoang, et al. (2005). "Messenger RNA expression levels of CXCR4 correlate with metastatic behavior and outcome in patients with osteosarcoma." Clinical cancer research : an official journal of the American Association for Cancer Research 11(7): 2561-2567.
Lee, J. A., J. S. Jung, et al. (2011). "RANKL expression is related to treatment outcome of patients with localized, high-grade osteosarcoma." Pediatric blood & cancer 56(5): 738-743.
Lerch, T. F., S. Shimasaki, et al. (2007). "Structural and biophysical coupling of heparin and activin binding to follistatin isoform functions." The Journal of biological chemistry 282(21): 15930-15939.
Leto, G., L. Incorvaia, et al. (2006). "Activin A circulating levels in patients with bone metastasis from breast or prostate cancer." Clin Exp Metastasis 23(2): 117-122.
Li, S., Y. Peng, et al. (2012). "Estimated number of prevalent cases of metastatic bone disease in the US adult population." Clinical epidemiology 4: 87-93.
Lin, S. Y., R. G. Craythorn, et al. (2008). "Female infertility and disrupted angiogenesis are actions of specific follistatin isoforms." Molecular endocrinology 22(2): 415-429.
Link, M. P., A. M. Goorin, et al. (1991). "Adjuvant chemotherapy of high-grade osteosarcoma of the extremity. Updated results of the Multi-Institutional Osteosarcoma Study." Clinical orthopaedics and related research(270): 8-14.
Longhi, A., C. Errani, et al. (2006). "Primary bone osteosarcoma in the pediatric age: state of the art." Cancer treatment reviews 32(6): 423-436.
Loomans, H. A. and C. D. Andl (2014). "Intertwining of Activin A and TGFbeta Signaling: Dual Roles in Cancer Progression and Cancer Cell Invasion." Cancers 7(1): 70-91.
Luckman, S. P., D. E. Hughes, et al. (1998). "Nitrogen-containing bisphosphonates inhibit the mevalonate pathway and prevent post-translational prenylation of GTP-binding proteins, including Ras." Journal of bone and mineral research : the official journal of the American Society for Bone and Mineral Research 13(4): 581-589.
Luetke, A., P. A. Meyers, et al. (2014). "Osteosarcoma treatment - where do we stand? A state of the art review." Cancer treatment reviews 40(4): 523-532.
Luksiene, Z. (2003). "Photodynamic therapy: mechanism of action and ways to improve the efficiency of treatment." Medicina 39(12): 1137-1150.
Makanji, Y., J. Zhu, et al. (2014). "Inhibin at 90: from discovery to clinical application, a historical review." Endocrine reviews 35(5): 747-794.
Manning, G., D. B. Whyte, et al. (2002). "The protein kinase complement of the human genome." Science 298(5600): 1912-1934.
Marina, N., M. Gebhardt, et al. (2004). "Biology and therapeutic advances for pediatric osteosarcoma." The oncologist 9(4): 422-441.
Martin, J. W., J. A. Squire, et al. (2012). "The genetics of osteosarcoma." Sarcoma 2012: 627254.
Mason, A. J., L. M. Berkemeier, et al. (1989). "Activin B: precursor sequences, genomic structure and in vitro activities." Molecular endocrinology 3(9): 1352-1358.
Massague, J. (1998). "TGF-beta signal transduction." Annual review of biochemistry 67: 753-791.
Massague, J. (2008). "TGFbeta in Cancer." Cell 134(2): 215-230.
Massague, J., J. Seoane, et al. (2005). "Smad transcription factors." Genes & development 19(23): 2783-2810.
Matsuo, K. and N. Irie (2008). "Osteoclast-osteoblast communication." Archives of biochemistry and biophysics 473(2): 201-209.
Matsuyama, S., M. Iwadate, et al. (2003). "SB-431542 and Gleevec inhibit transforming growth factor-beta-induced proliferation of human osteosarcoma cells." Cancer Res 63(22): 7791-7798.

Matzuk, M. M., T. R. Kumar, et al. (1995). "Different phenotypes for mice deficient in either activins or activin receptor type II." Nature 374(6520): 356-360.
Maugain, E., S. Sasnouski, et al. (2004). "Foscan-based photodynamic treatment in vivo: correlation between efficacy and Foscan accumulation in tumor, plasma and leukocytes." Oncology reports 12(3): 639-645.
Miller, T. T. (2008). "Bone tumors and tumorlike conditions: analysis with conventional radiography." Radiology 246(3): 662-674.
Minn, A. J., G. P. Gupta, et al. (2005). "Genes that mediate breast cancer metastasis to lung." Nature 436(7050): 518-524.
Mundy, G. R. (2002). "Metastasis to bone: causes, consequences and therapeutic opportunities." Nature reviews. Cancer 2(8): 584-593.
Murakami, G., T. Watabe, et al. (2003). "Cooperative inhibition of bone morphogenetic protein signaling by Smurf1 and inhibitory Smads." Molecular biology of the cell 14(7): 2809-2817.
Nahabedian, M. Y., R. A. Cohen, et al. (1988). "Combination cytotoxic chemotherapy with cisplatin or doxorubicin and photodynamic therapy in murine tumors." Journal of the National Cancer Institute 80(10): 739-743.
Nakashima, T. and H. Takayanagi (2011). "New regulation mechanisms of osteoclast differentiation." Annals of the New York Academy of Sciences 1240: E13-18.
Navarro, F. P., G. Creusat, et al. (2014). "Preparation and characterization of mTHPC-loaded solid lipid nanoparticles for photodynamic therapy." Journal of photochemistry and photobiology. B, Biology 130: 161-169.
Nguyen, D. X., P. D. Bos, et al. (2009). "Metastasis: from dissemination to organ-specific colonization." Nature reviews. Cancer 9(4): 274-284.
Nomura, J., S. Yanase, et al. (2004). "Efficacy of combined photodynamic and hyperthermic therapy with a new light source in an in vivo osteosarcoma tumor model." Journal of clinical laser medicine & surgery 22(1): 3-8.
Ntziachristos, V., C. H. Tung, et al. (2002). "Fluorescence molecular tomography resolves protease activity in vivo." Nature medicine 8(7): 757-760.
O'Connor, A. E., W. M. Gallagher, et al. (2009). "Porphyrin and nonporphyrin photosensitizers in oncology: preclinical and clinical advances in photodynamic therapy." Photochem Photobiol 85(5): 1053-1074.
Ogawa, Y., D. K. Schmidt, et al. (1992). "Bovine bone activin enhances bone morphogenetic protein-induced ectopic bone formation." J Biol Chem 267(20): 14233-14237.
Ogino, H., S. Yano, et al. (2008). "Follistatin suppresses the production of experimental multiple-organ metastasis by small cell lung cancer cells in natural killer cell-depleted SCID mice." Clin Cancer Res 14(3): 660-667.
Onichtchouk, D., Y. G. Chen, et al. (1999). "Silencing of TGF-beta signalling by the pseudoreceptor BAMBI." Nature 401(6752): 480-485.
Ory, B., F. Blanchard, et al. (2007). "Zoledronic acid activates the DNA S-phase checkpoint and induces osteosarcoma cell death characterized by apoptosis-inducing factor and endonuclease-G translocation independently of p53 and retinoblastoma status." Molecular pharmacology 71(1): 333-343.
Ory, B., M. F. Heymann, et al. (2005). "Zoledronic acid suppresses lung metastases and prolongs overall survival of osteosarcoma-bearing mice." Cancer 104(11): 2522-2529.
Ottaviani, G. and N. Jaffe (2009). "The epidemiology of osteosarcoma." Cancer treatment and research 152: 3-13.
Paget, S. (1989). "The distribution of secondary growths in cancer of the breast. 1889." Cancer metastasis reviews 8(2): 98-101.
Pahl, J. H., S. E. Ruslan, et al. (2012). "Anti-EGFR antibody cetuximab enhances the cytolytic activity of natural killer cells toward osteosarcoma." Clinical cancer research : an official journal of the American Association for Cancer Research 18(2): 432-441.
Pereira, P. M., B. Korsak, et al. (2015). "Antibodies armed with photosensitizers: from chemical synthesis to photobiological applications." Organic & biomolecular chemistry 13(9): 2518-2529.
Perrien, D. S., N. S. Akel, et al. (2007). "Inhibin A is an endocrine stimulator of bone mass and strength." Endocrinology 148(4): 1654-1665.

Perry, J. L., K. G. Reuter, et al. (2012). "PEGylated PRINT nanoparticles: the impact of PEG density on protein binding, macrophage association, biodistribution, and pharmacokinetics." Nano letters 12(10): 5304-5310.
Persson, U., H. Izumi, et al. (1998). "The L45 loop in type I receptors for TGF-beta family members is a critical determinant in specifying Smad isoform activation." FEBS letters 434(1-2): 83-87.
Plaetzer, K., B. Krammer, et al. (2009). "Photophysics and photochemistry of photodynamic therapy: fundamental aspects." Lasers in medical science 24(2): 259-268.
Pogue, B. W., J. A. O'Hara, et al. (2003). "Photodynamic therapy with verteporfin in the radiation-induced fibrosarcoma-1 tumor causes enhanced radiation sensitivity." Cancer research 63(5): 1025-1033.
Powell, D., C. Bowler, et al. (2012). "Incidence of serious side effects with intravenous bisphosphonate: a clinical audit." QJM.
Quirk, B. J., G. Brandal, et al. (2015). "Photodynamic therapy (PDT) for malignant brain tumors--where do we stand?" Photodiagnosis and photodynamic therapy 12(3): 530-544.
Redini, F. and D. Heymann (2015). "Bone Tumor Environment as a Potential Therapeutic Target in Ewing Sarcoma." Frontiers in oncology 5: 279.
Reidy, K., C. Campanile, et al. (2012). "mTHPC-Mediated Photodynamic Therapy is Effective in the Metastatic Human 143B Osteosarcoma Cells." Photochem Photobiol 88(3): 721-727.
Reidy, K., C. Campanile, et al. (2012). "mTHPC-mediated photodynamic therapy is effective in the metastatic human 143B osteosarcoma cells." Photochemistry and photobiology 88(3): 721-727.
Risbridger, G. P., J. F. Schmitt, et al. (2001). "Activins and inhibins in endocrine and other tumors." Endocrine reviews 22(6): 836-858.
Ritter, J. and S. S. Bielack (2010). "Osteosarcoma." Ann Oncol 21 Suppl 7: vii320-325.
Robertson, C. A., D. H. Evans, et al. (2009). "Photodynamic therapy (PDT): a short review on cellular mechanisms and cancer research applications for PDT." Journal of photochemistry and photobiology. B, Biology 96(1): 1-8.
Rosen, L. S., D. Gordon, et al. (2004). "Long-term efficacy and safety of zoledronic acid in the treatment of skeletal metastases in patients with nonsmall cell lung carcinoma and other solid tumors: a randomized, Phase III, double-blind, placebo-controlled trial." Cancer 100(12): 2613-2621.
Ruckle, J., M. Jacobs, et al. (2009). "Single-dose, randomized, double-blind, placebo-controlled study of ACE-011 (ActRIIA-IgG1) in postmenopausal women." J Bone Miner Res 24(4): 744-752.
Saad, F., D. M. Gleason, et al. (2004). "Long-term efficacy of zoledronic acid for the prevention of skeletal complications in patients with metastatic hormone-refractory prostate cancer." Journal of the National Cancer Institute 96(11): 879-882.
Sabile, A. A., M. J. Arlt, et al. (2011). "Cyr61 expression in Osteosarcoma indicates poor prognosis and promotes intratibial growth and lung metastasis in mice." J Bone Miner Res.
Sakai, R., Y. Eto, et al. (1993). "Activin enhances osteoclast-like cell formation in vitro." Biochemical and biophysical research communications 195(1): 39-46.
Sakai, R., K. Miwa, et al. (1999). "Local administration of activin promotes fracture healing in the rat fibula fracture model." Bone 25(2): 191-196.
Sasaki, K., T. Hitora, et al. (2011). "The role of MAPK pathway in bone and soft tissue tumors." Anticancer research 31(2): 549-553.
Schafer, M. and S. Werner (2008). "Cancer as an overhealing wound: an old hypothesis revisited." Nature reviews. Molecular cell biology 9(8): 628-638.
Schmierer, B. and C. S. Hill (2007). "TGFbeta-SMAD signal transduction: molecular specificity and functional flexibility." Nature reviews. Molecular cell biology 8(12): 970-982.
Sharma, A., S. Chatterjee, et al. (2013). "Risk of serious atrial fibrillation and stroke with use of bisphosphonates: evidence from a meta-analysis." Chest 144(4): 1311-1322.
Shi, Y. and J. Massague (2003). "Mechanisms of TGF-beta signaling from cell membrane to the nucleus." Cell 113(6): 685-700.
Snyder, J. W., W. R. Greco, et al. (2003). "Photodynamic therapy: a means to enhanced drug delivery to tumors." Cancer research 63(23): 8126-8131.
Star, W. M., H. P. Marijnissen, et al. (1986). "Destruction of rat mammary tumor and normal tissue microcirculation by hematoporphyrin derivative photoradiation observed in vivo in sandwich observation chambers." Cancer research 46(5): 2532-2540.

Stephens, P. J., C. D. Greenman, et al. (2011). "Massive genomic rearrangement acquired in a single catastrophic event during cancer development." Cell 144(1): 27-40.
Sugino, K., N. Kurosawa, et al. (1993). "Molecular heterogeneity of follistatin, an activin-binding protein. Higher affinity of the carboxyl-terminal truncated forms for heparan sulfate proteoglycans on the ovarian granulosa cell." The Journal of biological chemistry 268(21): 15579-15587.
Sun, M., C. Zhou, et al. (2015). "Hiporfin-Mediated Photodynamic Therapy in Preclinical Treatment of Osteosarcoma." Photochem Photobiol.
Sun, P. D. and D. R. Davies (1995). "The cystine-knot growth-factor superfamily." Annual review of biophysics and biomolecular structure 24: 269-291.
Terpos, E., E. Kastritis, et al. (2012). "Circulating activin-A is elevated in patients with advanced multiple myeloma and correlates with extensive bone involvement and inferior survival; no alterations post-lenalidomide and dexamethasone therapy." Ann Oncol.
Thompson, T. B., T. F. Lerch, et al. (2005). "The structure of the follistatin:activin complex reveals antagonism of both type I and type II receptor binding." Developmental cell 9(4): 535-543.
Thompson, T. B., T. K. Woodruff, et al. (2003). "Structures of an ActRIIB:activin A complex reveal a novel binding mode for TGF-beta ligand:receptor interactions." The EMBO journal 22(7): 1555-1566.
Thong, P. S., K. W. Ong, et al. (2007). "Photodynamic-therapy-activated immune response against distant untreated tumours in recurrent angiosarcoma." The Lancet. Oncology 8(10): 950-952.
Tortoriello, D. V., Y. Sidis, et al. (2001). "Human follistatin-related protein: a structural homologue of follistatin with nuclear localization." Endocrinology 142(8): 3426-3434.
Trinchieri, G. (2012). "Cancer and inflammation: an old intuition with rapidly evolving new concepts." Annual review of immunology 30: 677-706.
Uhlen, M., L. Fagerberg, et al. (2015). "Proteomics. Tissue-based map of the human proteome." Science 347(6220): 1260419.
Usuda, J., H. Kato, et al. (2006). "Photodynamic therapy (PDT) for lung cancers." Journal of thoracic oncology : official publication of the International Association for the Study of Lung Cancer 1(5): 489-493.
Valastyan, S. and R. A. Weinberg (2011). "Tumor metastasis: molecular insights and evolving paradigms." Cell 147(2): 275-292.
Vale, W., J. Rivier, et al. (1986). "Purification and characterization of an FSH releasing protein from porcine ovarian follicular fluid." Nature 321(6072): 776-779.
Vallet, S., S. Mukherjee, et al. (2010). "Activin A promotes multiple myeloma-induced osteolysis and is a promising target for myeloma bone disease." Proc Natl Acad Sci U S A 107(11): 5124-5129.
Wang, H. W., T. C. Zhu, et al. (2005). "Broadband reflectance measurements of light penetration, blood oxygenation, hemoglobin concentration, and drug concentration in human intraperitoneal tissues before and after photodynamic therapy." Journal of biomedical optics 10(1): 14004.
Wang, Z., R. Ma, et al. (2015). "Combined chemotherapy and photodynamic therapy using a nanohybrid based on layered double hydroxides to conquer cisplatin resistance." Chemical communications 51(58): 11587-11590.
Ward, E., C. DeSantis, et al. (2014). "Childhood and adolescent cancer statistics, 2014." CA: a cancer journal for clinicians 64(2): 83-103.
Weiss, A. and L. Attisano (2013). "The TGFbeta superfamily signaling pathway." Wiley interdisciplinary reviews. Developmental biology 2(1): 47-63.
Welt, C., Y. Sidis, et al. (2002). "Activins, inhibins, and follistatins: from endocrinology to signaling. A paradigm for the new millennium." Experimental biology and medicine 227(9): 724-752.
Wen, Y. H., H. Koeppen, et al. (2007). "Epidermal growth factor receptor in osteosarcoma: expression and mutational analysis." Human pathology 38(8): 1184-1191.
Werner, S. and C. Alzheimer (2006). "Roles of activin in tissue repair, fibrosis, and inflammatory disease." Cytokine & growth factor reviews 17(3): 157-171.
West, C. M., D. C. West, et al. (1990). "A comparison of the sensitivity to photodynamic treatment of endothelial and tumour cells in different proliferative states." International journal of radiation biology 58(1): 145-156.
Whelan, J. S., S. S. Bielack, et al. (2015). "EURAMOS-1, an international randomised study for osteosarcoma: results from pre-randomisation treatment." Annals of oncology : official journal of the European Society for Medical Oncology / ESMO 26(2): 407-414.

Wolf, R. E. and W. F. Enneking (1996). "The staging and surgery of musculoskeletal neoplasms." The Orthopedic clinics of North America 27(3): 473-481.
Xia, Y. and A. L. Schneyer (2009). "The biology of activin: recent advances in structure, regulation and function." J Endocrinol 202(1): 1-12.
Xu, L., Y. Kang, et al. (2002). "Smad2 nucleocytoplasmic shuttling by nucleoporins CAN/Nup214 and Nup153 feeds TGFbeta signaling complexes in the cytoplasm and nucleus." Molecular cell 10(2): 271-282.
Yanase, S., J. Nomura, et al. (2009). "Synergistic increase in osteosarcoma cell sensitivity to photodynamic therapy with aminolevulinic acid hexyl ester in the presence of hyperthermia." Photomedicine and laser surgery 27(5): 791-797.
Yang, D., G. de la Rosa, et al. (2009). "Alarmins link neutrophils and dendritic cells." Trends in immunology 30(11): 531-537.
Yoneda, T. and T. Hiraga (2005). "Crosstalk between cancer cells and bone microenvironment in bone metastasis." Biochemical and biophysical research communications 328(3): 679-687.
Yu, J., L. E. Shao, et al. (1987). "Importance of FSH-releasing protein and inhibin in erythrodifferentiation." Nature 330(6150): 765-767.
Zawel, L., J. L. Dai, et al. (1998). "Human Smad3 and Smad4 are sequence-specific transcription activators." Molecular cell 1(4): 611-617.
Zeitouni, N. C., S. Shieh, et al. (2001). "Laser and photodynamic therapy in the management of cutaneous malignancies." Clinics in dermatology 19(3): 328-338.
Zhang, J., X. H. Yu, et al. (2015). "PI3K/Akt signaling in osteosarcoma." Clinica chimica acta; international journal of clinical chemistry 444: 182-192.
Zhang, X. H., X. Jin, et al. (2013). "Selection of bone metastasis seeds by mesenchymal signals in the primary tumor stroma." Cell 154(5): 1060-1073.
Zhang, Y., C. Chang, et al. (2001). "Regulation of Smad degradation and activity by Smurf2, an E3 ubiquitin ligase." Proceedings of the National Academy of Sciences of the United States of America 98(3): 974-979.
Zhang, Y. E. (2009). "Non-Smad pathways in TGF-beta signaling." Cell research 19(1): 128-139.
Zhao, H., L. Guo, et al. (2015). "CXCR4 over-expression and survival in cancer: a system review and meta-analysis." Oncotarget 6(7): 5022-5040.
Zhu, J., F. Liu, et al. (2015). "Activin A regulates proliferation, invasion and migration in osteosarcoma cells." Mol Med Rep 11(6): 4501-4507.

9 Curriculum Vitae

Name	MEIER Daniela
Date of Birth	05.10.1985
Place of origin	Würenlingen, AG
E-mail	Dani.Meier.85@gmail.com

Education

Mar 2012 - Jul 2016	PhD Study in the Laboratory for Orthopedic Research, Balgrist University Hospital, Zurich, Switzerland within the "Cancer Biology" PhD Program of Life Science Zurich Graduate School, Faculty of Science, University of Zurich
Oct 2009 - Dec 2011	MSc in Human Biology, Faculty of Science, University of Zurich Thesis Title: "Disturbed eating at high altitude"
Sep 2006 - Jan 2010	BSc in Biology, Faculty of Science, University of Zurich
Aug 2001 - Jun 2005	Eidgenössische Maturität, Kantonsschule Baden, AG

Publications

- Targeting αvβ3 and αvβ5 integrins inhibits pulmonary metastasis in an intratibial xenograft osteosarcoma mouse model

  *Gvozdenovic A, Boro A, **Meier D**, Bode-Lesniewska B, Born W, Muff R, and Fuchs B (under revision; March 2016, Oncotarget)*

- Cytotoxic efficacy of photodynamic therapy in osteosarcoma cells *in vitro*.

  ***Meier D**, Campanile C, Botter SM, Born W, Fuchs B. (J Vis Exp. 2014 Mar 18).*

10 Acknowledgments

I would like to express my sincere gratitude to Prof. Dr. **Bruno Fuchs** for providing me with the opportunity to pursue my PhD in his laboratory, for his continuous support, advice and trust in my work.

I am thankful to my thesis director Prof. **Dr. Beat Schäfer** for kindly accepting to be in my thesis committee and for their scientific suggestions, and directions during my PhD.

I would like to express my appreciation to my thesis members Prof. Dr. **Caroline Maake** and Prof. **Dario Neri**. I am thankful for their scientific expertise and their contribution of ideas and inspiration.

I am grateful to my supervisor Dr. **Sander Botter** for his constant guidance, availability, patience and help at any time throughout my PhD.

I would like to thank Prof. Dr. **Walter Born** for his help, his support, his valuable scientific input and all the scientific discussions we had together over the past years.

Special thanks goes to Dr. **Ana Gvozdenovic** and Dr. **Carmen Campanile** for their generous help, patience, guidance and their friendship throughout my PhD. They both had educated me in various biological and scientific aspects.

Many thanks also to all my current and former lab colleagues for their help and the friendly atmosphere in the lab, especially to **Bernhard**, **Alex**, **Olga, Joaquin and Alekhya** for their contribution to my work and for being great friends and cheering me up when times were tough.

A big thanks you also goes to Dr. **Giovanni Pellegrini**, for his profound knowledge in veterinary pathology and his scientific input on my thesis manuscripts, even in very busy times.

Special thanks to Dr. **Marco Eijken**, for his scientific input and for supporting my work.

I would also like to thank Dr. **Susanna Gräfe** for her support and help within the PDT project.

I would like to thank Dr. **Anna-Claude Couffin** and Dr. **Fabrice Navarro** for their help and input.

I would also like to thank all my friends, especially **Maëlis, Mirjam** and **Angie** for their friendship and support outside the lab.

I would like to express my deepest gratitude to my parents **Dorli** and **Werner** for their love, great support and for always believing in my work and me. A special thanks to my brothers Remo and Roger and my sister-in-law Tanja for their support, encouragement and all the good times we are having together.

Last but not least, I especially thank you, **Tojo**, for all your love, never-ending support and for always being by my side. Thank you for having faith and believing in me and for your patience in stressful and difficult times.

Thank you all.